Research in
AGRICULTURAL ENGINEERING

Czech Academy of Agricultural Sciences

VOLUME 57
Special Issue
PRAGUE 2011
ISSN 1212-9151

Research in AGRICULTURAL ENGINEERING

formerly ZEMĚDĚLSKÁ TECHNIKA since 1955 to 1999

An international peer-reviewed journal published by the Czech Academy of Agricultural Sciences and financed by the Ministry of Agriculture of the Czech Republic

Aims and scope: The journal of RAE publishes original research papers devoted to all scientific and applied aspects of Agricultural Engineering including those laying on the border with other scientific disciplines, for example mechatronics, IT, robotics, ecology, energetics, economy, ergonomic, applied physics, biochemistry, biotechnology, bionics and waste management. Special at attention is devoted to new technologies with respect to their environmental aspects and agricultural products quality control. Papers are published in English (British spelling).

Abstracts are comprised in:
- Agrindex of AGRIS/FAO database
- CAB Abstracts
- Czech Agricultural and Food Bibliography
- SCOPUS

Periodicity: 4 issues per year, volume 57 appearing in 2011.

Editorial Office

Research in Agriculture Engineering, Ing. Lucie Pešová, Executive Editor, Czech Academy of Agricultural Sciences, Slezská 7, 120 00 Prague 2, Czech Republic, phone: + 420 227 010 606, fax: + 420 227 010 116, e-mail: rae@cazv.cz

Subscription information

Subscription orders can be entered only by calendar year and should be sent to: Czech Academy of Agricultural Sciences, Slezská 7, 120 00 Prague 2, Czech Republic. Subscription price is 140 USD (subscribers from the Czech Republic can apply for special rates).

Electronic access

Full papers from Vol. *48* (2002), instructions to authors and information on all journals edited by the Czech Academy of Agricultural Sciences are available at http://agriculturejournals.cz/web/rae.htm.

Online Manuscript Submission

All manuscripts must be submitted to the journal website (http://agriculturejournals.cz/web/rae.htm). Authors are requested to submit the text, tables, and artwork in electronic form to this web address. Authors unable to submit an electronic version should contact by e-mail the Editorial Office.
Both the dates of the receipt of the manuscript and of the acceptance by the Managing Editorial Board for publishing will be indicated in the printed contribution.

ISSN 1212-9151 MK ČR E 6698

Research in **AGRICULTURAL ENGINEERING**

formely ZEMĚDĚLSKÁ TECHNIKA

Volume 57 **2011**

Research in AGRICULTURAL ENGINEERING

Volume 57, 2011, Special Issue

CONTENTS

Go to the website for information about Research in Agricultural Engineering:
http://www.agriculturejournals.cz/web/RAE.htm

Analysis of the relations between some physical indicators of market eggs

R. Gálik, Z. Poláková, Š. Bočo, M. Denker

Faculty of Engineering, Slovak University of Agriculture in Nitra, Nitra, Slovak Republic

Abstract

Gálik R., Poláková Z., Bočo Š., Denker M., 2011. **Analysis of the relations between some physical indicators of market eggs**. Res. Agr. Eng., *57 (Special Issue)*: S1–S6.

The paper discusses the relations between some physical indicators of market eggs of laying hens housed in conventional and enriched cage batteries. The measured results were evaluated by the multiple regression dependence method. They show that in the case of both the conventional as well as the enriched cages a statistically significant dependence exists between the eggshell deflection (dependent variable) and thickness, or the force needed for the eggshell destruction (independent variable). The respective P values are given in brackets ($0.002 < 0.05$; $0.03 < 0.05$; $1.16 \times 10^{-10} < 0.05$; $8.31 \times 10^{-4} < 0.05$); in the case of the conventional cage and enriched cage also a statistically significant dependence existed ($3.81 \times 10^{-91} < 0.05$; 3.86×10^{-81}; $1.27 \times 10^{-97} < 0.05$; $3.46 \times 10^{-57} < 0.05$) between the shell weight (dependent variable) and shell thickness, or egg weight (independent variable); in the conventional cage, statistical dependence also occurred between the eggshell weight and egg shape index, ($1.07 \times 10^{-6} < 0.05$), in the enriched cage this was on the verge of statistical significance ($0.062 > 0.05$); if in the conventional cage the eggshell thickness was increased by 1 mm, the shell deflection decreased by 0.08 mm, and if the force necessary for the eggshell destruction was increased by 1 N, the shell deflection decreased by 0.0003 mm; if in the conventional cage the shell thickness was increased by 1 mm, the shell weight increasee by 15.509 g and if the egg weight was increased by 1 g, the shell weight increased by 0.061 g. Our work brings further knowledge concerning the monitored characteristics and their mutual relations.

Keywords: conventional cage; enriched cage; physical indicators of market eggs

Alongside the efficient production of eggs, current rearing of laying hens also requires a gradual shift to new housing technologies, introduced by the European Union Directive 1999/74 EC, which says that as from January 1, 2012 only enriched cage systems should be used in the rearing of laying hens. In addition to new enriching elements, they have to comply with the requirement of a larger area per hen – from the current 550 cm^2 to 750 cm^2. The requirement to increase the area per hen decreases the number of hens in a battery, which results in the increase of the number of batteries – that is, the number of halls.

The results of experimental measurements of some foreign researchers, especially in the beginnings of the introduction of enriched cages, show that, as far as the quality of eggs is concerned, less favourable results were achieved by using the enriched cage technologies than those in the conventional cages (Appleby et al. 2002; Leyendecker et al. 2005). The authors mentioned reached lower values, for example, for the shell strength, egg weight, and shell weight in the enriched cages compared to the un-enriched ones. Similar results were also arrived at by Lichovníková and Zeman (2008). Walker et al. (1998) compared conventional cages

with enriched cages in terms of the weight of laid eggs. They found that the average weight of eggs in the conventional cages was 63.5 g, in the enriched cages 62.9 or 63.0 g. The lower weight of eggs from the enriched cages did the authors attribute to the fact that the hens rest on the perch or in dust bath during the dim light and at night while in the conventional cage they devote to feeding.

These facts demonstrated the need to compare the individual technologies, especially from the aspect of the physical features of eggs.

MATERIAL AND METHODS

The research was conducted under laboratory conditions on the Slovak University of Agriculture premises in Nitra, equipped with a three-floor classical (un-enriched) cage technology and with a three-floor (enriched) cage technology. The given batteries were placed in one hall, which ensured identical conditions for both technologies as regards the lighting, ventilation, or the warmth of animals, which influences the quality of the animal environment (KARANDUŠOVSKÁ et al. 2009; LENDELOVÁ, POGRAN 2009; POGRAN et al. 2009). The classical cages housed 18 laying hens (2 hens per cage), 33 hens were housed in the comfort cages (11 hens per cage).

In both rearing technologies, the laying hens were of the same hybrid (ISA Brown), the same age, and were fed with the same complete feed mixture. The egg samples intended for analyses (in the total amount of 30 pieces) were taken during the whole laying cycle (7 times in total), always 10 pieces from every floor and at the same time; the laying hens were weighed. The influence of different stabling systems on the weight of hens is dealt with in the work by GÁLIK et al. (2009). The following quantitative indicators of market eggs were analysed and evaluated:

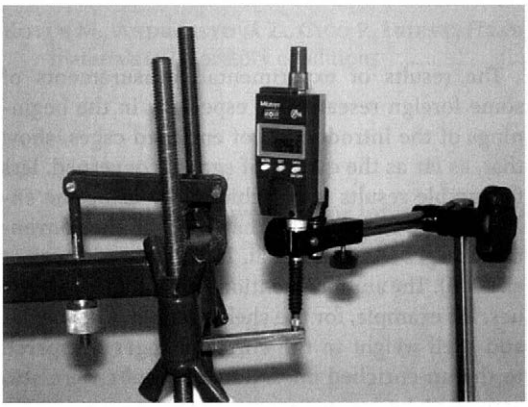

Fig. 1. Instrument for the measuring of eggshell deflection

Weight of eggs and weight of eggshell (g)

To determine the weight of eggs and that of eggshell, the laboratory scales Chirana P3-200, type 397, No. 1627-85 with the 0.1 g precision (Chirana Strašnice, Prague, Czechoslovakia) was used.

Thickness of eggshell (mm)

The eggshell thickness was measured after the removal of the undershell membrane by the slot gauge, type R-4-0247 (Somet CZ, Ltd., Hradec Králové, Czech Republic) on both poles as well as on the equator of the egg. It was expressed as an average of these three values.

ITV – Index of egg shape (%)

The egg dimensions were determined with an electronic digital slide calliper. The ITV was expressed as the quotient of the egg width and length in % (HALAJ 1999). It was assessed according to the following relation:

$$ITV = \frac{\text{width of egg (mm)}}{\text{length of egg (mm)}} \times 100 \quad (\%) \quad (1)$$

Force needed for eggshell destruction

The force needed for the eggshell destruction was determined with the egg crusher (Veit Elektronics, Ltd., Brno, Czech Republic). This portable instrument is powered by a battery. Its simple operation allows fast measuring of a large number of samples. The measured values may be read directly from the instrument display (or stored on a chip card). They may be consequently loaded into PC for further processing.

Deflection of eggshell (mm)

The eggshell deflection was determined with the instrument described in the work by GÁLIK et al. (2004), to which the digital gauge, type ID-N112, (Mitutoyo, Kawasaki, Japan), was added (Fig. 1). The

deflection was determined on the egg equator while using a non-destructive load (500 g) on the longitudinal axis of the egg (BAINOVÁ 2004).

The results measured were processed and evaluated using suitable statistical methods (POLÁKOVÁ 2007). The dependence of the values of the dependent variables (deformation of eggshell in mm, or weight of eggshell in g) on several independent variables (force needed for the destruction of eggshell, or the ITV, eggshell thickness, egg weight) was assessed through a multiple regression analysis method. The model formula used is as follows:

$$y = b_0 + b_1x_1 + b_2x_2 + b_3x_3 \quad (2)$$

where:

y – value of dependent variable

b_0 – intercept

$b_1...b_3$ – regression coefficient expressing the influence of the unit change of independent variable on the value of the monitored dependent variable

$x_1...x_3$ – value of independent variable

The calculations were done in Microsoft Excel.

RESULTS AND DISCUSSION

The aim of the analysis was to determine the functional relations between the eggs qualities, i.e.: the eggshell deflection, eggshell thickness and force needed for the eggshell destruction. Table 1 shows the results of the dependence of the dependent variable (eggshell deflection) on the independent variables (eggshell thickness and force needed for eggshell destruction). Thus, for example, in the case of the conventional cage [KK (whole)], the correlation coefficient R (0.328) shows statistical dependence; according to the determination coefficient R^2 (0.108), however, only 10.8% of the eggshell deflection variability can be explained through the regression model chosen.

In the case of the enriched cage, the correlation coefficient R has a markedly higher value (0.538), and according to the coefficient of determination,

Table 1. Results of multiple dependence between eggshell deflection and some physical indicators of market eggs

Cage	Dependent variable	Independent variable	R	R^2	P	Result	Model's equation
KK (top)	deflection	thickness	0.117	0.014	0.616	no dependence	$y = 0.048 - 0.024x_1 - 0.0002x_2$
		force			0.568	no dependence	
KK (centre)	deflection	thickness	0.390	0.152	0.055	no dependence	$y = 0.077 - 0.09x_1 - 0.0003x_2$
		force			0.173	no dependence	
KK (bottom)	deflection	thickness	0.616	0.379	0.000	dependence	$y = 0.117 - 0.197x_1 - 0.0003x_2$
		force			0.121	no dependence	
OK (top)	deflection	thickness	0.470	0.221	0.000	dependence	$y = 0.093 - 0.133x_1 - 0.0002x_2$
		force			0.265	no dependence	
OK (centre)	deflection	thickness	0.497	0.247	0.000	dependence	$y = 0.116 - 0.189x_1 - 0.0003x_2$
		force			0.095	no dependence	
OK (bottom)	deflection	thickness	0.655	0.429	0.000	dependence	$y = 0.11 - 0.168x_1 - 0.0004x_2$
		force			0.004	dependence	
KK (whole)	deflection	thickness	0..328	0.108	0.002	dependence	$y = 0.072 - 0.08x_1 - 0.0003x_2$
		force			0.030	dependence	
OK (whole)	deflection	thickness	0..538	0.289	1.16×10^{-10}	dependence	$y = 0.105 - 0.158x_1 - 0.0003x_2$
		force			8.31×10^{-4}	dependence	

KK – conventional cage; OK – enriched cage

Table 2. Results of multiple dependence between eggshell weight and some physical indicators of market eggs

Cage	Dependent variable	Independent variable	R	R^2	P	Result	Model's equation
KK (top)	eggshell weight	ITV	0.9899	0.960	0.734	no dependence	$y = -4.87 + 0.002x_1 + 16.098x_2 + 0.074x_3$
		eggshell thickness			2.30×10^{-35}	strong dependence	
		egg weight			1.51×10^{-35}	strong dependence	
KK (centre)	eggshell weight	ITV	0.966	0.932	3.64×10^{-5}	strong dependence	$y = -1.889 - 0.024x_1 + 15.82x_2 + 0.059x_3$
		eggshell thickness			1.38×10^{-34}	strong dependence	
		egg weight			3.46×10^{-29}	strong dependence	
KK (bottom)	eggshell weight	ITV	0.931	0.867	0.00071	strong dependence	$y = -0.878 - 0.0265x_1 + 15.335x_2 + 0.052x_3$
		eggshell thickness			3.63×10^{-26}	strong dependence	
		egg weight			3.08×10^{-19}	strong dependence	
OK (top)	eggshell weight	ITV	0.969	0.940	0.072	no dependence	$y = -3.096 - 0.0144x_1 + 16.042x_2 + 0.065x_3$
		eggshell thickness			1.19×10^{-35}	strong dependence	
		egg weight			7.45×10^{-22}	strong dependence	
OK (centre)	eggshell weight	ITV	0.923	0.852	0.682	no dependence	$y = -3.479 - 0.0028x_1 + 15.645x_2 + 0.059x_3$
		eggshell thickness			1.99×10^{-25}	strong dependence	
		egg weight			5.89×10^{-17}	strong dependence	
OK (bottom)	eggshell weight	ITV	0.952	0.907	0.430	no dependence	$y = -4.406 - 0.0068x_1 + 18.454x_2 + 0.062x_3$
		eggshell thickness			8.07×10^{-34}	strong dependence	
		egg weight			2.30×10^{-19}	strong dependence	
KK (whole)	eggshell weight	ITV	0.963	0.926	1.07×10^{-6}	strong dependence	$y = -2.277 - 0.0019x_1 + 15.509x_2 + 0.061x_3$
		eggshell thickness			3.81×10^{-91}	strong dependence	
		egg weight			3.86×10^{-81}	strong dependence	
OK (whole)	eggshell weight	ITV	0.953	0.908	0.062	no dependence	$y = -3.629 - 0.008x_1 + 16.784x_2 + 0.061x_3$
		eggshell thickness			1.27×10^{-97}	strong dependence	
		egg weight			3.46×10^{-57}	strong dependence	

KK – conventional cage; OK – enriched cage

through the given regression model, up to 28.9% of variability is explained by the eggshell deflection. By comparing the P values and the significance level $\alpha = 0.05$, it was determined that a statistically significant dependence exists between the deflection and eggshell thickness, as well as between the deflection and the force needed for the eggshell destruction.

The equation of the linear model of multiple dependence for KK is as follows:

$$y = 0.072 - 0.08x_1 - 0.0003x_2 \quad (3)$$

The regression coefficient for x_1 (value 0.08) reveals that: if in KK the eggshell thickness increases by 1 mm, the eggshell deflection decreases by 0.08 mm. The regression coefficient for x_2 (value 0.0003) says: if in KK the force needed for the eggshell destruction thickness increases by 1 N, the eggshell deflection decreases by 0.0003 mm. Table 2 shows multiple dependencies between the dependent variable (eggshell weight) and the independent variables: ITV (x_1), eggshell thickness (x_2) and egg weight (x_3). The correlation coefficient (for KK whole) R (0.963) shows a strong statistical dependence. The determination coefficient value (R^2) was 0.926 (92.6% of eggshell weight variability is explained by the selected regression model). By comparing the P values and the significance level $\alpha = 0.05$, it was found that a statistically significant depend-

ence occurs between the eggshell weight and the ITV, between the eggshell weight and eggshell thickness, as well as between the eggshell weight and egg weight.

The equation of the linear model of multiple regression is as follows:

$$y = -2.277 - 0.0019x_1 + 15.509x_2 + 0.061x_3 \quad (4)$$

From the regression coefficient values it follows that if the ITV increases by 1%, then the eggshell weight decreases by 0.0019 g, if the eggshell thickness increases by 1 mm, then the eggshell weight increases by 15.509 g, and if the egg weight increases by 1 g, then the eggshell weight increases by 0.061 g.

The most frequent indicators of the eggshell quality evaluation include its weight, thickness and strength. There are many works dealing with these issues and the possibility to compare the individual rearing methods, their advantages and shortcomings, which have become the objects of monitoring and comparison by many professionals in the field. The acquired overall view of these systems helps in the search for optimum distribution of the individual enriching elements, which gradualy brings the enriched cages to the level of conventional cages also from the aspect of the acquired utility. If we manage to decrease the number of non-standard eggs below the level achieved in the case of conventional cages, this system will prove to be a suitable substitution as regards its economic aspect as well as the aspect of welfare. However, the results achieved in the field are so far not unified. Thus, for example, according to KARKULÍN and CHMELNIČNÁ (2004), the enriched cage technology positively influenced the eggshell quality. A statistically evident difference ($P < 0.05$) was recorded between the technologies; in the force needed for the eggshell destruction, a statistically highly evident difference ($P < 0.01$) existed in the eggshell thickness. The eggshell weight was not influenced by the technology. In contrast to these results, it follows from the work of POKLUDOVÁ et al. (2008) that the housing technologies do not have any significant influence on the egg quality. A lower weight of eggs in the conventional cage technologies (as opposed to the enriched cage technologies and the housing on bedding) is equalised by a higher laying intensity. This was partly confirmed also by GÁLIK et al. (2009) who did not record any evident differences between the weight of laying hens and the weight of eggs of the hens housed in enriched or conventional batteries. In another work, however, GÁLIK et al. (2010) determined a statistically significant difference in the force needed for the eggshell destruction and a statistically not evident difference in the eggshell thickness and eggshell deflection between the enriched and un-enriched cage batteries. KARKULÍN et al. (2005) claim that there have been just a few experiments so far which could lead to concrete conclusions.

CONCLUSION

The analysis of the relations between some physical variables of consumer eggs shows that between the shell deflection (dependent variable) and the thickness of the shell, respectively the force needed to destroy the shell (independent variables), statistically significant dependence exists for the batteries of both conventional and enriched cages. If the shell thickness was increased by 0.1 mm, the deflection of the shell was reduced by 0.008 mm in the conventional cages and by 0.0158 mm in the enriched cages. If the force to destroy the shell was increased by 1 N, the deflection of the shell was reduced by 0.0003 mm in the conventional as well as in the enriched cages. Statistically significant dependence was also found between the shell mass (dependent variable) and egg shape index, shell thickness and egg weight (independent variables) in both the conventional and enriched cages. Between the shell weight and egg shape index statistical dependence close to the limit of significance was observed with the enriched cage. If the egg shape index increased by 1%, the shell weight was reduced by 0.0019 g in the conventional and by 0.008 g in the enriched cages. If the shell thickness increased by 0.1 mm, the shell mass increased by 1.550 g in the conventional and by 1.678 g in the enriched cages and if the egg mass increased by 1 g, the shell weight would increase by 0.061 g in the conventional as well as in the enriched cages. The results obtained are a contribution benefits to scientific knowledge, characteristics observed and their interrelationships.

References

APPLEBY M.C., WALKER A.W., NICOL C.J., LINDBERG A.C., FREIRE R., HUGHES B.O., ELSON H.A., 2002. Development of furnished cages for laying hens. British Poultry Science, *43*: 489–500.

BAINOVÁ M.M., 2004. New innovations in the assesment of eggshell quality – a Review. In: Proceedings of the XXII.

World's Poultry Congress. Istanbul, Turkey, WPSA Turkish Branch, 22: 8–9.

Council Directive 1999/74/EC. Laying down minimum requirements for minimum protection of laying hens. Available at http://eur-lex.europa.eu/LexUriServ/LexUriServ.do?uri=OJ:L:1999:203:0053:0057:EN:PDF

Gálik R., Karas I., Švenková J., Žitná M., 2004. Vývoj zariadenia na meranie pevnosti škrupiny vajec (Development of a device for measuring eggshell solidity). Acta Technologica Agriculturae, *7*: 11–14.

Gálik R., Poláková Z., Boďo Š., 2009. Vplyv rôznych technologických systémov ustajnenia na hmotnosť nosníc a produkovaných vajec (The influence of different stabling systems at the weight of hens and their eggs production). In: International Science Conference "Technika v podmienkach trvalo udržateľného rozvoja", May 20–22, 2009. Plavnica: 13–18.

Gálik R., Švenková J., Poláková Z., Boďo Š., 2010. Vplyv niektorých technologických systémov ustajnenia nosníc na vybrané ukazovatele kvality škrupiny vajec (Effect of technological systems for layng hens housing on selected indicators of eggshell quality). Acta Technologica Agriculturae, *13*: 1–5.

Halaj M., 1999. Posudzovanie vlastností a kvality konzumných vajec (Assessment of performance and quality of table eggs. In: Weis J., Halaj M., CHmelničná Ľ., Kopecký J., Chov hydiny (Poultry). Nitra, SAU in Nitra: 61–71.

Karandušovská I., Pogran Š., Knížatová M., 2009. Posudzovanie produkcie škodlivín v objektoch pre chov dojníc a hydiny (Assessment of production of pollutants in buildings for dairy and poultry). 1st Ed. Nitra, SPU in Nitra: 170.

Karkulín D., Chmeliničná Ľ. 2004. Vplyv rozdielnych klietkových technológií na kvalitu škrupiny konzumných vajec (Influence of different cage technologies on shell quality of market eggs). In: Možnosti a perspektívy zvyšovania produkcie v chove hydiny a malých hospodárskych zvierat. Nitra, SAU in Nitra: 27–32.

Karkulín D., Gálik R., Švenková J., Šesták M., 2005. Kvalita škrupiny konzumných vajec nosníc ustajnených v rozdielnych technológiách (Eggshell quality of table eggs from laying hens housed in different cage technologies). In: First International Scientific Poultry Days Section 3: Table Eggs Production. Nitra, SAU in Nitra: 14–17.

Lendelová J., Pogran Š., 2009. Technika prostredia a možnosti redukovania vplyvu klimatických extrémov v ustajňovacích objektoch (Environ technique and reduction possibility of climatic extrems effect in stables). Technika v technológiách agrosektora 2009 (CD-ROM). Nitra, SPU in Nitra: 137–142.

Leyendecker M., Leyendecker M., Hamann H., Hartung J., Kamphues J., Neumann U., Sürie C., Distl O., 2005. Keeping laying hens in furnished cages and an aviary housing system enhances their bone stability. British Poultry Science, *46*: 536–544.

Lichovníková M., Zeman L., 2008. Effect of housing system on the calcium requirement of laying hens and on eggshell quality. Czech Journal of Animal Science, *53*: 162–168.

Pogran Š., Šottník J., Karandušovská I., Knížatová M., Orság J., Mihina Š., 2009. Sledovanie rozdielov koncentrácií amoniaku počas zimného a letného chovu v ustajnení brojlerov (Monitoring of differences of ammonia concentrations during winter and summer feeding in broiler housing). Acta Technologica Agriculturae, *12*: 26–28.

Pokludová M., Hrouz J., Klecker D., 2008. Influence of particular technological systems on selected qualitative parameters of eggs. Available at www.old.af.mendelu.cz/mendelnet2003/obsahy/zoo/pokludova.pdf (accessed October 23, 2008).

Poláková Z., 2007. Návody na cvičenia z bioštatistiky (Instructions for Exercises in Biostatistics). Nitra, SAU in Nitra: 1–84.

Walker A.W., Walker A.W., Tucker S.A., Elson H.A., 1998. An economic analysis of a modified, enriched cage egg production system. British Poultry Science, Sp*39*: S14–15.

Received for publication December 8, 2010
Accepted after corrections May 25, 2011

Corresponding author:

doc. Ing. Roman Gálik, Ph.D., Slovak University of Agriculture in Nitra, Faculty of Engineering, Department of Production Engineering, Tr. A. Hlinku 2, 949 76, Nitra, Slovak Republic
phone: + 421 376 414 307, e-mail: Roman.Galik@uniag.sk

Using satellite navigation for seeding of wide-row and narrow-row crops

M. Macák, M. Žitňák, L. Nozdrovický

Faculty of Engineering, Slovak University of Agriculture in Nitra, Nitra, Slovak Republic

Abstract

Macák M., Žitňák M., Nozdrovický L., 2011. **Using satellite navigation for seeding of wide-row and narrow-row crops**. Res. Agr. Eng., *57 (Special Issue)*: S7–S13.

The present paper is aimed at the use of satellite navigation of field machinery during seeding, this operation belonging to the most important field practises. Our attention was focused on the determination of the accuracy of the satellite navigation system based on using the correction signal real-time kinematic and its correct application for planting a wide-row crop (sunflower) and seeding a narrow-row crop (spring barley). The aim of the field experiment was also to specify the level of the necessary accuracy of satellite navigation systems during planting and seeding. The length of seeding/planting equipment was confronted with the accuracy of navigation of individual passes, especially when turning on the headlands. In the conclusion, the importance is highlighted of the automated tractor headland control during satellite navigation of combined field machines in the crop production.

Keywords: precision farming; satellite navigation; accuracy; quality of seeding

In the context of increasing competitiveness on the open European market, the farmers have currently to face an important requirement – to increase the production efficiency of field products. Among the tools that can match such requirement, the field guidance systems are considered. Tillett (1991) nearly twenty years ago tried to classify automatic guidance sensors for agricultural field machines. Zuydam et al. (1994) have conducted test of an automatic precision guidance system used for guidance of cultivation implements. Fulton et al. (1999) analysed a variable-rate spinner spreader, equipped with DGPS and a variable rate control system to assess its distribution accuracy using a 13 by 13 matrix of collection pans and following the test procedures outlined in ASAE Standard S341.2. They performed uniform and variable rate tests to characterise the application variability of the spreader and test the effect of the rate changes via GPS control. From the collected data, a uniform and a variable rate application models were developed. The authors found that the models can be considered as an efficient tool for projecting the actual application rates for the uniform and variable-rate applications. The quality of the fertiliser application depends upon the accuracy of the guidance system used. Ehsani et al. (2002) studied important issues related to testing and comparing the guidance systems which they defined and explained, and a method of evaluating GPS guidance systems while following a straight line was introduced. According to their results, comparing the performance of the guidance systems with a real-time kinematic (RTK) GPS is the easiest method and probably the most accurate way of field-evaluating guidance systems. The advantage of this method is that it reflects the overall performance of a guidance system on the

The paper reflects the results obtained within the research, Project NFP No. 26220220014: "Application of the information technologies to increase the environmental and economical sustainability of the production agrosystem (Activity 3.1 Creation of the department of transfer of innovative technologies to the practice)" (OPVaV– 2008/2.2/01-SORO).

farm and the results can be used directly by the end user. It is possible to agree with FADEL (2004), who stated that, due to the environmental concerns in addition to economical considerations, the variable rate of fertilisers is widely applied in the agriculture. Granular fertilisers broadcasting is one of the most growing applications employing variable rate technologies (VRT) and GPS guidance technologies. Such systems are commercially produced. For the performance assessment ASAE Standard S341.2 can be used which provides a standard procedure for broadcasters performance testing. Anyway, this standard does not cover the testing of broadcast spreaders used within the variable-rate technology. According to GRIFFIN (2009), the use of the guidance systems to guide the farm machines during their work on the field brings several benefits including the reduction in overlap, increased working speed during the field operations, workday expansion, and appropriate placement of spatially sensitive inputs. During recent years, many researchers studied different effects of using the guidance systems in view of accuracy, economical efficiency, etc. LAWRENCE and YULE (2007), developed a model within a geographic information system (GIS) environment using the transverse spread pattern and GPS driving track during spreading to map the actual fertiliser application at any point in a paddock. The spreading vehicle required a GPS of sufficient accuracy to provide the proof of placement and guidance assistance to the driver. The method was used to assess the effects of the field size and shape on the actual application rate and application variation. MACÁK et al. (2009) developed a methodology for the evaluation of the accuracy of the satellite machine guidance for fertiliser application in the field conditions. According to MACÁK, ŽITŇÁK (2010), this methodology was practically used for the evaluation of satellite guidance accuracy with centrifugal and pneumatic fertiliser spreader, and minimal accuracy requirements were determined.

EHSANI et al. (2004) investigated the potential use of RTK GPS receiver for seed mapping with a high level of accuracy. Their hypothesis was based on the presumption that high-accuracy seed mapping can be potentially used in the weed control and plant-specific crop management. FINDURA and MAGA (2006) stated that the accuracy of the seeding machine passes during the seeding operation significantly affects the crop establishment and subsequently also the yield of the field crop. The use of the field guidance systems has some specific economical consequences, and therefore GRIFFIN et al. (2008) and GRIFFIN (2009) used a linear programming model to compare 5 types of the guidance system:

(1) a baseline scenario with foam, disk, or other visual marker reference,
(2) lightbar navigation with basic GPS availability (+/–0.3 m accuracy),
(3) lightbar with satellite subscription correction GPS (+/–0.1 m),
(4) automated guidance with satellite subscription (+/–0.1 m),
(5) automated guidance with a base station RTK GPS (+/–0.01 m).

The results obtained indicate that RTK automated guidance becomes the most profitable alternative when farm size is increased while maintaining the same equipment set. The results also indicate that the relative profitability ranking is sensitive to years to depreciate the technology.

The specific objectives of this research were:

- to verify the function of the navigation system Trimble EZ Guide 500 RTK (Trimble Navigation, Ltd., Sunnyvale, USA) based on using the correction signal RTK for planting a wide-row crop (sunflower) and seeding a narrow-row crop (spring barley),
- to test the effect of the length of the combined field machine (rotary harrow + seeding machine) on the accuracy of navigation during the field operation.

MATERIAL AND METHODS

The field experiments were conducted on the Cooperative farm in Vrable, district Nitra, Slovak Republic. The satellite navigation systems were used for the guidance of the tractor-machine set used in sunflower planting and spring barley seeding.

Characteristics of the machine used in the experiments

The experiments were focused on the measurement of the guidance accuracy during the field operation when the seedbed preparation was combined with the seeding. For this operation, we used a tractor John Deere 7820 (John Deere Tractor Works, Waterloo, USA) (with dual tyres on the rear axle) and combined machines (Table 1).

a) for sunflower planting:
rotary harrow Amazone KG 452 (Amazonen-Werke H. Dreyer GmbH & Co. KG, Hasbergen, Germany) with vertical tines driven by power take-off shaft and a horizontal compacting roller, precision planter Kuhn Planter 2 (Kuhn S.A., Saverne, France) with a unit allowing the application of granular fertilizer containing nitrogen, phosphorus and potassium and micro-granules,
b) for spring barley seeding:
rotary harrow Amazone KG 452 + tyre roller, drill seeder Amazone AD 452 (Amazonen-Werke H. Dreyer GmbH & Co. KG, Hasbergen, Germany).

The above combined machines were assembled directly on the farm.

The planter Kuhn Planter 2 and drill machine Amazone AD 452 (Table 2) were equipped with mechanical markers used only on the field headlands in order to obtain more accurate guidance for the next pass without skips as the field was cultivated in runs parallel to one another (one way pattern). The machine started to move at one boundary of the field and ended on the opposite side with turns being made on the headlands.

In ordinary conditions (using the satellite navigation system with the autopilot), there would have been no need to use markers. In our case, the markers were used due to insufficient experience of the operator.

Characteristics of the navigation system with autopilot used in the experiments

During seeding, the satellite navigation system Trimble EZ Guide 500 RTK (Trimble Navigation, Ltd., Sunnyvale, USA) with the autopilot was used. The system consisted of the following parts:

a) ightbar with the colour monitor and control unit EZ Guide 500,
b) receiver of the satellite and correction signals,

Table 1. Specifications of the tractor John Deere 7820

Parameter	Value
Engine power (ECE-R24) (kW)	147
Number of gears (F/R)	20/20
Number of cylinders/displacement (–/cm^3)	6/6,780
Max. forward speed (km/h)	50
Power-take-off shaft (rpm)	540/540E or 1000/1000E
Max. lift capacity of hydraulic (kN)	90

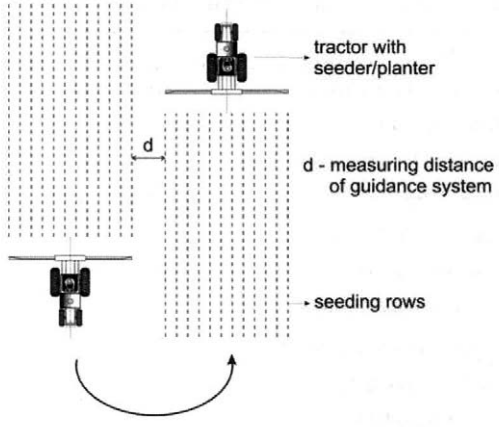

Fig. 1. Principles of measuring the navigation accuracy in the inter-rows by using the metric measure

c) control unit,
d) electric stepper motor EZ-Steer T2.

Principle of measuring the accuracy of the satellite navigation RTK during seeding

During experiments, we used a guidance system using the correction signal RTK with the accuracy ±2.5 cm. The method used for measuring the guidance accuracy should be highly accurate in order to reduce the measurement error. We tried to use a laser range-finder (distance meter) but after some experience we decided to use a new method. This method was based on measuring the distance between the outer rows of the crop after the crop emergency. The first planter/seeder pass was marked with a wooden peg. As we knew the number of the planter/seeder rows, it was sufficient to find the wooden peg marking the first pass. Then, the next passes were identified according to the number of the crop rows. In the inter-row area between the neighbouring passes, we measured the distance between the individual plants during the machine navigation. For the measuring, we used the metric measure (Fig. 1).

The required (theoretical) row spacing was given by agronomy requirements related to the given crop. The final values of the skips and overlaps were calculated using the difference between the measured values and the row spacing required for the given crop.

The row spacing for sunflower was 75 cm and for spring barley 12.5 cm. Statistical data processing

Table 2. Basic specifications of the used machines

Parameter	Value
Vertical rotary harrow	Amazone KG 452
Working width (m)	4
Requested tractor power (kW)	140
Type of drive	Tractor PTO
Machine weight (kg)	1,500
Precision planter	Kuhn Planter 2
Number of seeding units	6
Weight of planting unit (kg)	55
Hopper capacity (l)	25
Row spacing (cm)	38–80
Seeding drill	Amazone AD 452
Working width (m)	4.5
Number of rows (–)	36
Row spacing (cm)	12.5

was done using the analytical module spreadsheet MS Excel 2003 and also by software Statistica 6.0 (StatSoft CR, Ltd., Prague, Czech Republic).

RESULTS

Using the given methodology, we conducted the measurements of the guidance accuracy of the tractor-machine sets:

- tractor John Deere 7820 + rotary harrow Amazone KG 452 + horizontal compacting roller + planter Kuhn Planter 2 for sunflower precision planting,
- tractor John Deere 7820 + rotary harrow Amazone KG 452 + tyre roler + drill seeder Amazone AD 452 for spring barley seeding.

The guidance system Trimble EZ-Guide 500 with the correction signal RTK was used. For the evaluation of the guidance accuracy, the deviations were measured of the individual points from the ideal trajectory which was determined by the initial "zero pass". From the methodology point of view, the negative values represented the overlaps and the positive values represented the skips. For the correct evaluation of the results obtained, all data were *t*. In terms of a fair evaluation, all data obtained were converted to absolute values, which were further evaluated in a spreadsheet MS Excel 2003. The deviations measurements were done for two types of crops: sunflower (wide-row crop) and spring barley (narrow-row crop).

Bar graphs in Figs 2 and 3 present the distribution of the deviations during the sunflower planting and spring barley seeding. Table 3 present the basic descriptive statistics indicators, which were determined by statistical data analysis module in a spreadsheet MS Excel 2003.

During sunflower planting, the average value of the deviations was 2.76 cm (total number of measurements was 69). 52.2% of the values were found in the interval from 0 to 2.5 cm, and 88.5% of the values were found in the interval from 0 to 5 cm.

During spring barley seeding, the average value of the deviations was 2.62 cm (total number of measurements was 65). 66.15% of the values were found in the interval from 0 to 2.5 cm, and 89.23% of the values were found in the interval from 0 to 5 cm.

For both crops, maximal value of deviation found was 7.5 cm. Histograms of the measured deviations are shown in Figs 2 and 3.

According to the navigation system producer, the navigation accuracy is ±2.5 cm the producer guarantees such accuracy for parallel passes within 15 min. The average values of deviations found in our measurements were higher by 0.12–0.26 cm. It is possible to state that within the guaranteed range from 0 to 2.5 cm, only a few data were located which did not reach the statistically significant level. When analysing the range 0–5 cm, we achieved in both cases a high proportion of the measured deviations, which approached 90%. Thus, we can conclude that the satellite navigation using the autopilot works correctly in view of the basic agro-

Table 3. Basic parameters of descriptive statistics of measured deviations of the satellite navigation with the RTK correction signal

Statistical parameter	Calculated value	
	sunflower planting	spring barley seeding
Average (cm)	2.76	2.62
Error of average value (cm)	0.224	0.231
Median (cm)	2.5	2.5
Mode (cm)	1	1.5
Minimum (cm)	0	0
Maximum (cm)	7.5	7.5
Sum (cm)	191	170.5
Number of values	69	65

RTK – real-time kinematic

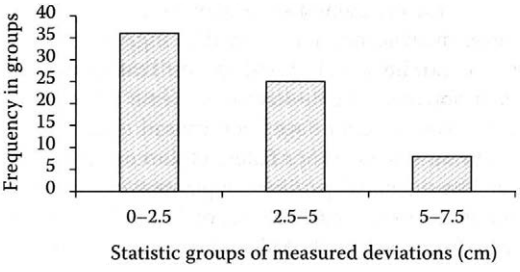

Fig. 2. Frequency distribution bar chart presenting the deviations of the satellite navigation with the RTK correction signal (planting of sunflower)

nomic requirements. In the next step, we analysed the insufficient proportion of the measured values within the range 0–2.5 cm and the reasons for such results. After the consultations with the production manager, we found out that as the main reason could be considered the action of the clearance of the clamping of the three-point hitch. There was also an adverse effect of the articulated joint between the rotary harrow and the planter/seeder as a combination for tillage and seeding. The angle of the swing of the low arms of the three-point hitch matched the requirements and the clearance of the three-point hitch clamping was small. For the total length of the combined machine (6.5 m), even a small angle of swing was sufficient to deflect the side seeding units for 5–8 cm.

As the field where the seeding experiments were conducted was almost completely flat (with maximal slope 0.5° in some marginal areas), the effect of the clearance of the three-point hitch clamping was not very evident. When working on the fields with a higher slope, the inaccuracy was much higher. The slope effect can be compensated by changing the driving direction so that the machine should be more inclined in the longitudinal direction than in the transverse direction. On the basis of the experience gained, we recommend not to use long combined machines when satellite navigation guidance systems with RTK are used. It is also necessary to reduce the mechanical clearance between the linked machines. The length of the combined machines (6.5 m), has also an adverse effect when starting a new pass on the field headland. Small skip areas having a triangular shape have occurred (Fig. 4). This phenomenon was best observed first of all in the case of spring barley but also in the case of the wide-row crop – sunflower. The length of skips varied from 6–32 m and their initial width on the side nearer to the field border varied from 25 to 75 cm. The skips where the seed was not applied occurred during the run-out of the machine when the machine after completing the turn on the headland was directed to the approximate direction for the next parallel pass.

During the machine start-up, it was necessary to engage the correct gear, to lower the rotary harrow to the requested depth, to engage the power-take-off (PTO), to lower the seeding units to the working position, to switch on the fan, and finally to activate the autopilot for it to start to guiding the machine accurately in the requested direction. All these operations had to be done during the machine movement, and it was necessary at the same time to navigate the tractor in order to reach the next parallel pass as accurately as possible. The machine operator tried to make all these operations easier by indicating the axis parallel to the next drive with a mechanical marker, which was mounted on the drill. The marker was activated manually from the cab on the headland in the distance of 20–40 m from the field boundary. Such solution was not sufficient from our point of view, thus the headland management system (HMS) was used which greatly reduces the operator's fatigue in row-cropping and tillage applications through the automatic sequencing of the tractor functions normally associated with headland turns. HMS was programmed to control the following tractor functions: mechanical front-wheel drive on/off, rear PTO on/off and hitch raise/lower.

In the case of HMS not being available on the tractor, it is necessary at the beginning to engage a lower gear to set the tractor in motion on a lower forward speed. This will give the operator more time to carry out all operations manually. The activation of the autopilot should be done as the first step as the machine must be correctly navigated

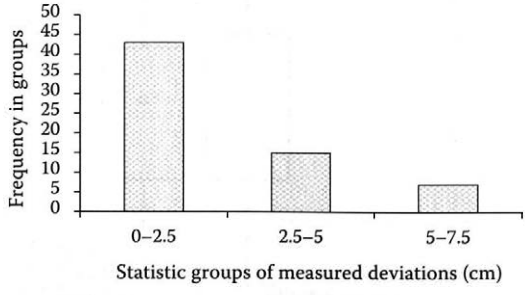

Fig. 3. Frequency distribution bar chart presenting the deviations of the satellite navigation with the RTK correction signal (seeding of spring barley)

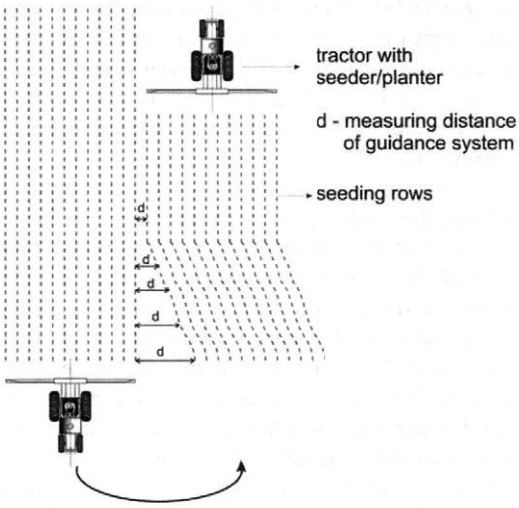

Fig. 4. Skips area of the field near the headland (the area of the field without seeding) – emerged crop stand of spring barley

from the field boundaries and the operator has time enough to control the tractor/machine functions in the correct order. In the next step, it is possible to increase the working speed to the level required.

In Fig. 5 are Box-and-Whisker diagrams to show the spread of the data. The diagrams show the quartiles of the data, using these as an indication of the spread of deviations (skips and overlaps) from the ideal machine trajectory when planting/seeding both crops. The diagrams also display the upper quartile, lower quartile, and inter-quartile ranges of the data set. It can be seen in the diagrams that among the data obtained, there were no extreme values (outliers), which could have been caused either by the measurement error or a failure of the correction and satellite signals. Regarding the planting of sunflower, the medium was on the level of 0 cm. As it can be seen from Fig. 5b, the value of median reached the level of 0.5 cm during spring barley seeding and it means that the difference between the seeding of both crops was small.

On the basis of the results obtained, we can state that, if there is the same number of deviations above and below the value of the median, we can confirm that the guidance navigation system has the same tendency to create skips and overlaps in the ideal trajectory.

The negative values represent the overlaps of the working widths while the positive values represent the skips. That means that if the row spacing was 12.5 cm and we measured 14.5 cm, the skip value was 2 cm.

In the case of spring barley seeding (Fig. 5b), the value of the lower quartile (25%) was at the level of –2.5 cm and that of the upper quartile (75%) was at the level of 2.5 cm. According to these data, we can state that there were 50% of the data within the range ±2.5 cm. In the case of sunflower planting (Fig. 5a), the values of the lower and the upper quartiles were on the level from –2.5–3.0 cm.

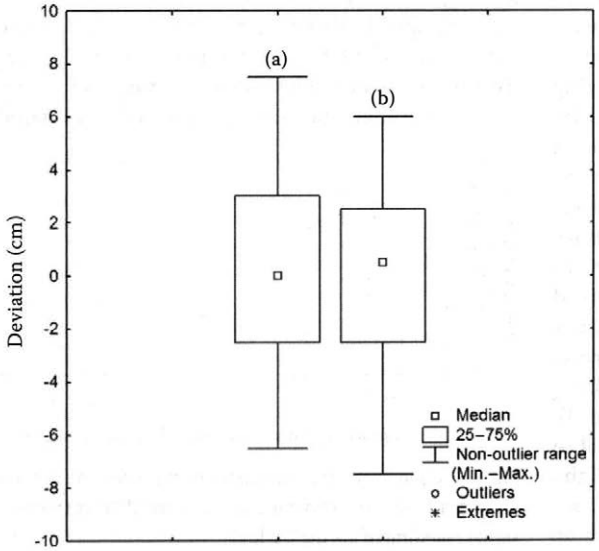

Fig. 5. Box-and-Whisker diagram of a deviations from ideal trajectory
(a) sunflower planting, (b) spring barley seeding

CONCLUSIONS

We can state that the use of the satellite navigation system with the RTK correction signal is suitable for the planting of wide-row crop (sunflower) and seeding of narrow-row crop (spring barley). The accuracy and work quality claimed by the manufacturer (deviation ±2.5 cm) were observed only with minor deviations. The average value of deviation was 2.76 cm with sunflower planting and 2.62 cm with spring barley seeding. The above deviations were caused due to the clearance in the articulated joint between the rotary harrow and seeder/planter, which created one unit – combined machine. In view of the agronomy requirements for wide-row crops planting and narrow crops seeding, the accuracy of the satellite navigation at the level of ±5 cm is sufficient.

On the basis of the results obtained, we recommend to join the seeder/planter only with a tractor. The creation of combined machines is connected with the occurrence of clearances in joints which cause the deviations in the machine trajectory, especially when working on the slope.

There may be cases needing to use a combined machine together with the satellite navigation with automatic machine control. From the point of view of the process technology, it is necessary in such cases to use a tractor with the automatic HMS. If the HMS in not available on the tractor, it is necessary to use the above mentioned procedure.

References

Ehsani M.R., Sullivan M., Walker J.T., Zimmerman T.L., 2002. A Method of Evaluating Different Guidance Systems. St. Joseph, ASAE Paper No. 021155.

Ehsani M.R., Upadhyaya S.K., Mattson M.L., 2004. Seed location mapping using RTK GPS. Transactions of the ASABE, *47*: 909–914.

Fadel M.A., 2004. Performance assessment of VRT-based granular fertilizer broadcasting systems. CIGR e-Journal, *6*: 1–12.

Fulton J.P., Shearer S.A., Chabra G., Higgins S.G., 1999. Field Evaluation of a Spinner Disc Variable-Rate Fertilizer Applicator. Toronto, ASAE Paper No. 991101.

Findura P., Maga J., 2006. Vplyv spôsobu sejby na tvorbu biomasy (Effect of seeding technology on the biomass creation). Acta Technologica Agriculturae, *3*: 75–78.

Griffin T., 2009. Whole-farm Benefits of GPS-enabled Navigation Technologies. St. Joseph, ASABE.

Griffin T.W., Lambert D.M., Lowenberg-Deboer J., 2008. Economics of GPS-enabled navigation technologies. In: Proceedings of the 9th International Conference on Precision Agriculture, July 21–23, 2008. Denver, USA.

Lawrence H.G., Yule I.J., 2007. A GIS methodology to calculate in-field dispersion of fertilizer from a spinning-disc spreader. Transactions of the ASABE, *50*: 379–387.

Macák M., Žitňák M., 2010. Efektívne využitie satelitnej navigácie v systéme presného poľnohospodárstva (Effective using of satellite guidance in precision farming system). 1st Ed. Nitra, SUA in Nitra: 124.

Macák M., Nozdrovický L., Krupička J., 2009. Vplyv fyzikálno-mechanických vlastností priemyselných hnojív na funkciu rozhadzovačov z pohľadu požiadaviek presného poľnohospodárstva (Effect of physical and mechanical properties of the fertilizers from the point of view of precision farming requirements). 1st Ed. Prague, Czech University of Life Sciences: 209.

Tillett N.D., 1991. Automatic guidance sensors for agricultural field machines: A review. Journal of Agricultural Engineering Research, *50*: 167–187.

Zuydam R., Van P., Sonneveld C., 1994. Test of an automatic precision guidance system for cultivation implements. Agricultural Engineering Research, *59*: 239–243.

Received for publication January 17, 2011
Accepted after corrections June 22, 2011

Corresponding author:

prof. Ing. Ladislav Nozdrovický, Ph.D., Slovak University of Agriculture in Nitra, Faculty of Engineering, Department of Machines and Production Systems, Tr. A. Hlinku 2, 949 76 Nitra, Slovak Republic
e-mail: ladislav.nozdrovicky@uniag.sk

Evaluation of efficiency of precision irrigation for potatoes

J. Jobbágy, J. Simoník, P. Findura

Faculty of Engineering, Slovak University of Agriculture in Nitra, Nitra, Slovak Republic

Abstract

Jobbágy J., Simoník J., Findura P., 2011. **Evaluation of efficiency of precision irrigation for potatoes.** Res. Agr. Eng., *57 (Special Issue)*: S14–S23.

The objective of the presented paper was to verify in practice the methods of precision irrigation, defined theoretically, under the employment of reel hose irrigation machines. The surface area of the field was 22 ha. The basic soil hydrological coefficients were measured in 19 monitoring points, specifically the field capacity and the wilting point. The field capacity ranged between 28.83% and 32.11% by vol., and the wilting point was in the interval between 8.40% and 12.40% by vol. At the conclusion, the soil moisture as a factor decisive for determining the irrigation rate was measured in these monitoring points. The irrigation rate ranged from 0 to 40 mm for the specific date of the soil moisture determination. During the whole growing season, five irrigation rates were applied according to the principles of precision irrigation. As compared to conventional water application, precision irrigation contributed to water saving in the amount of 478.56 m^3/ha. The electric power saving reached 249.68 kWh/ha. The cost saving was characterised by the value of 9.1 EUR/ha and this represented 23.8%. The results have shown that precision irrigation is a fully effective system of precision farming, although the procurement and implementation of new technology and software requires at first a significant financial cost. There is also an increased need for the education and skills of the operating staff.

Keywords: precision irrigation; soil hydrological coefficients; soil moisture

As compared to conventional farming, precision farming perceives the within-field conditions in a different manner. Precision farming takes into account the fact that the field as a whole together with the soil and its properties, the content of nutrients, soil moisture, etc. represents an environment that is spatially variable (Nozdrovický et al. 2008).

Precision irrigation, as part of precision farming, is at the beginning of investigation and represents water application in a specific place and at a specific rate. That concurrently takes into account a reduction in irrigation water consumption and contributes in this way to the fulfilment of a world-wide trend resulting from the shortage of this strategic element (Sourell 2003).

The implementation of precision irrigation requires additional equipment to control the irrigation rate, information on soil properties and on the condition of a crop stand. The potential of variable rate irrigation is in the increase of the yields, quality and economic rate of return (King et al. 2006).

The use of precision irrigation is restricted by the lack of basic knowledge on spatially variable crop and soil properties. The experiments resulted in a positive assessment as regards the implementation of precision farming in the management of irrigation (Sadler et al. 2002).

Fraisse et al. (1995) simulated variable rate irrigation with a subsequent verification of the results in practice.

Supported by the Scientific Grant Agency VEGA of the Ministry of Education of the Slovak Republic and the Slovak Academy of Sciences, Grant No. 1/0082/09.

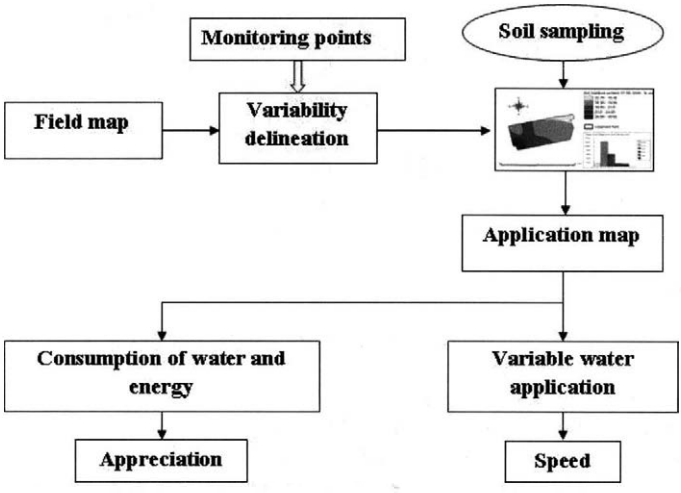

Fig. 1. Strategy of precision agriculture

Irrigation practice often uses the conventional method of irrigation. However, there are very few homogeneous fields in practice as regards the granulometric composition of soil. Therefore, a field must be divided into individual sub-units that are mutually independent in terms of the need for tillage, nutrition and irrigation (Sourell, Al-Karadsheh 2003).

Research connected with precision irrigation and soil hydrological coefficients was conducted, *inter alia*, at Idaho Agricultural Experiment Station (Kimberly, USA). The experiments were based on measuring the field capacity (25.0–44.6% by vol.), wilting point (10.0–18.4% by vol.), and available water capacity (13.9–28.4 cm/m) (King et al. 2006).

The mapping of spatial variability concerning the field capacity, wilting point, and reduced available water capacity was performed in 9 zones and subsequently used as an input parameter for the management of precision irrigation. In the first three zones was a pasture, the following three zones contained potatoes, and the last three zones contained maize. The values of the field capacity ranged between 10% and 37% by vol., those of the wilting point were in the interval between 3% and 11% by vol., and the values of reduced available water capacity ranged from 7–31% by vol. (Hedley et al. 2009).

Based on the research conducted abroad (Federal Agricultural Research Centre FAL, Braunschweig, Germany), the lowest costs amounting to 191 EUR/ha were achieved in the case of centre pivot irrigation with the total irrigated area of around 57.6 ha. During the irrigation season, the highest costs amounting to 911 EUR/ha were obtained with stationary drip irrigation. Mobile drip irrigation fell between these extremes with the cost amounting to 267 EUR/ha (Debrala, Sourell 2002).

Fig. 2. Moisture meter HH2 with Wet sensor

MATERIAL AND METHODS

The objective of the presented paper was to verify the elaborated methods of precision irrigation. The solution of the work followed the methodical procedure shown in Fig. 1. The field boundaries were determined using a hand-held GPS navigator – Garmin eMAP. The soil moisture was measured by HH2 Moisture Meter and WET Sensor (Delta-T Devices, Ltd., Cambridge, UK) (Fig. 2). The application maps were prepared after the determination of the soil moisture and soil hydrological coefficients. Irrigation was performed using reel hose irrigation machines distributed within the field. The map of spatially variable soil moisture contained the zones of delineated within-field variability.

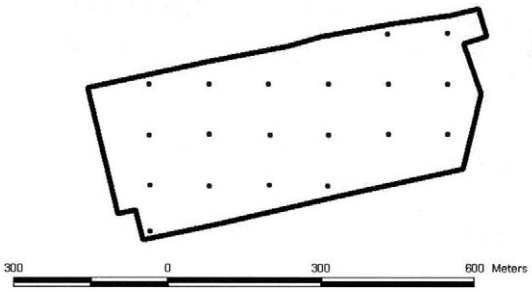

Fig. 3. Localised field and monitoring points

The tables of the irrigation schedule were produced after preparing the application map.

In conclusion, the crop yield was determined, and the use of precision irrigation was evaluated in terms of its economical benefits. The methodology suggested by the Department of Machines and Production Systems (Slovak University of Agriculture in Nitra) was used for determining the soil moisture. This methodology involves taking a crop sample from the area of 10 m^2 (in each monitoring point). The samples were placed into bags marked with a relevant numerical code.

The algorithm according to RATAJ (2005) was used to determine the operating costs. This algorithm enables to change the input parameters (irrigation water requirement, tractor insurance, diesel fuel price, electrical power price, water price, hour rate for an employee and field size) that are associated with the selected field and year in which the experiment is undertaken.

In terms of law, water for irrigation is provided free of charge but the price of services for the water supply is subject to payment. In our case, the agricultural holding had its own wells and pumps. The costs were computed for such case when the entity had not obtained water subsidies.

In the case of variable rate irrigation, the value of labour costs will be increased by the value of costs incurred by the employee who changes the irrigation rate.

Annual costs for the change of irrigation rate under variable rate irrigation (this equation shall apply if the work is performed by one worker):

$$ {}_{r}N_{zm} = {}_{h}N_{zp} \times 1.352 \times {}_{r}W_{zm} \quad (1) $$

where:

${}_{h}N_{zp}$ – hour rate of the employee for changing the irrigation rate (EUR/h)

1.352 – coefficient of insurance contributions

${}_{r}W_{zm}$ – total time of all changes in irrigation rates (h/year)

The time required for the change of the irrigation rate depends on:

- field size;
- number of irrigation machines;
- time required for one shift;
- time required for transport between irrigation machines;
- number of shifts during the whole irrigation period on all of the irrigation equipment used.

As compared to precision irrigation, conventional irrigation will show a change in the total cost. The following costs will be changed:

- variable costs per irrigation machines (higher annual employment of electric motor with the pump);
- costs of water (higher amounts of water consumed).

RESULTS AND DISCUSSION

By virtue of good experience gained over the years from cooperation, the agricultural holding Agrocoop Imeľ, Ltd. (Imeľ, Slovak Republic) was chosen for the experiments. This holding is situated in south-western Slovakia, in the district of Komárno. The area is characterised by a flat terrain, with a gradient ranging between 0° and 2°.

As regards the soil and weather patterns, the holding is classified as belonging to the maize production area. In terms of precipitation, the area can be included into arid, very dry area with an average long-term annual precipitation total of 547 mm (for the period from 1951 to 1980). The precipitation is not distributed uniformly. The average annual temperature is 9.9°C, the average temperature in the growing season is 16.6°C, and the precipitation in the growing season is 355 mm. The elevation of this area is 107–110 m a.s.l. The total area of agricultural land in this holding amounts to 1,822 ha, out of which arable land is 1,730 ha with the preponderant type of loamy sand to loamy soils. Potatoes take

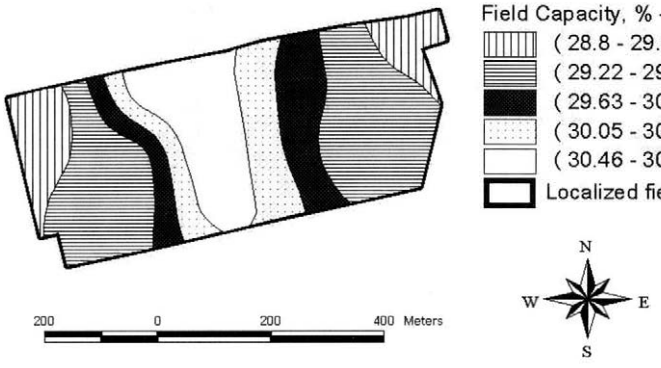

Fig. 4. Maps of field capacity

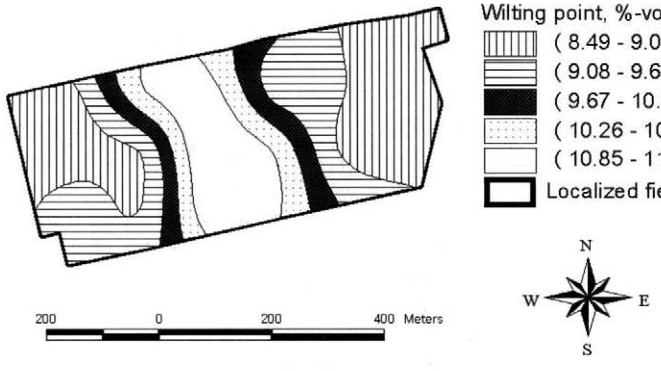

Fig. 5. Map of wilting point (BV)

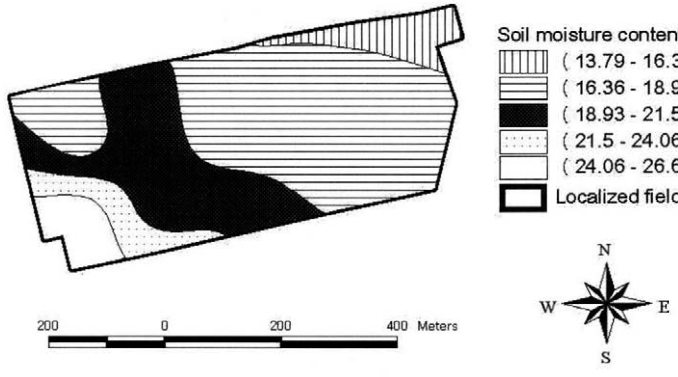

Fig. 6. Maps of soil moisture content (7. 6. 2006)

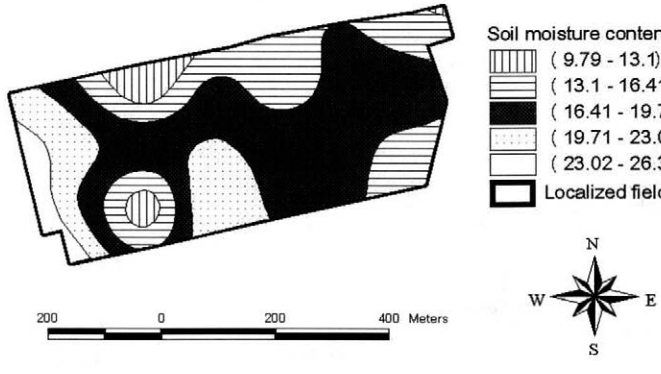

Fig. 7. Maps of soil moisture content (28. 6. 2006)

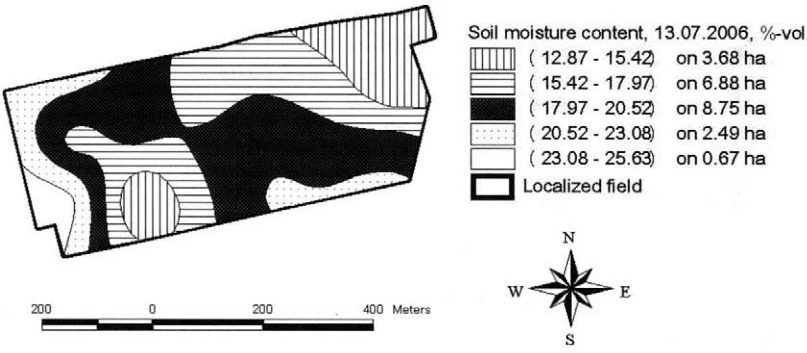

Fig. 8. Maps of soil moisture content (13. 7. 2006)

up a specific position in the crop production; this crop is grown on the area of about 200 ha.

The position of the field under investigation is shown in Fig. 3, with the surface area of 22 ha and with 19 monitoring points (output from the ArcView 3.2; Esri, NY, USA). The crop grown: potatoes – Victoria variety; soil: alkaline (pH 7.4).

Soil moisture and soil hydrological coefficients

The resulting map of the field capacity (FC) is shown in Fig. 4. The field capacity ranged between 28.80% and 30.88% by vol. The dominant interval was that from 29.22% to 29.63% on the area of 8.75 ha. As regards the wilting point (WP), its variation on the surface is displayed in Fig. 5 and ranged between 8.49% and 11.44% by vol. The interval from 8.49% to 9.08% occupied the area of 7.86 ha. All of the soil hydrological coefficients determined in percents by volume corresponded to the water content in millimetres in the soil layer of 10 cm.

Fig. 6 shows the spatial variability map of the soil moisture dated June 7, 2006. The soil moisture ranged between 13.79% and 26.63% by vol. The measured values of the soil moisture were in the range of limit values determined by the soil hydrological coefficients. The least represented were the intervals of the soil moisture ranging from 21.50%

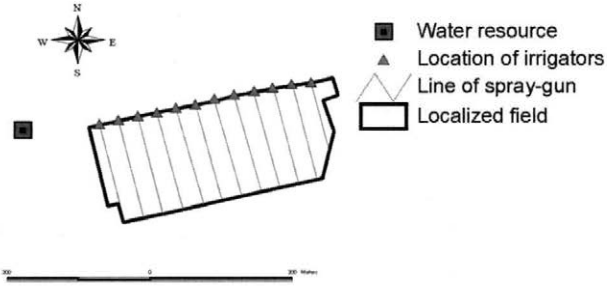

Fig. 9. Water resource and location of irrigators

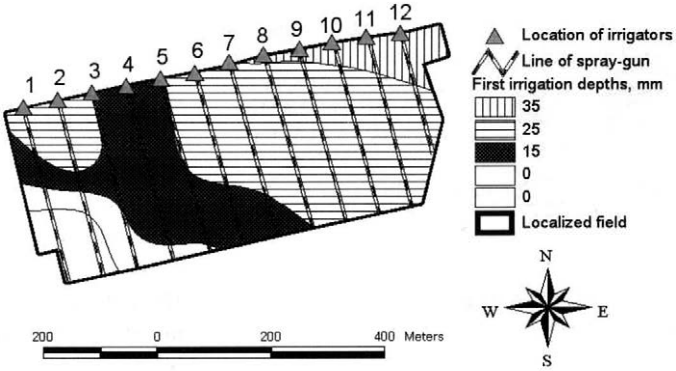

Fig. 10. First irrigation rate

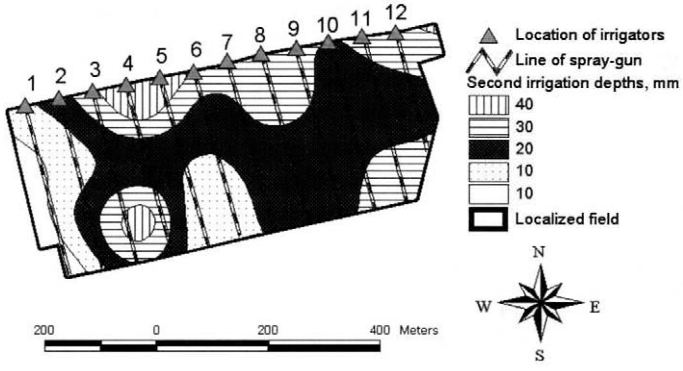

Fig. 11. Second irrigation rate

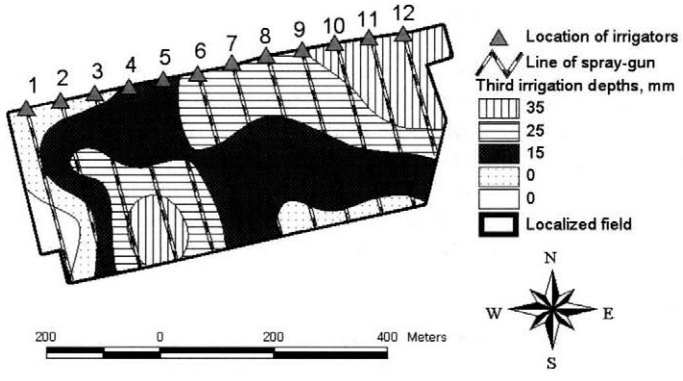

Fig. 12. Third irrigation rate

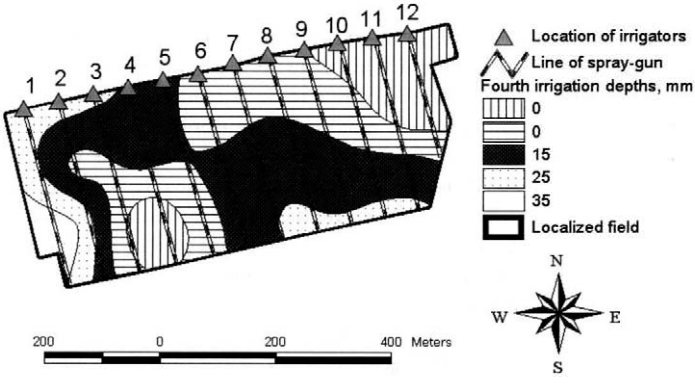

Fig. 13. Fourth irrigation rate

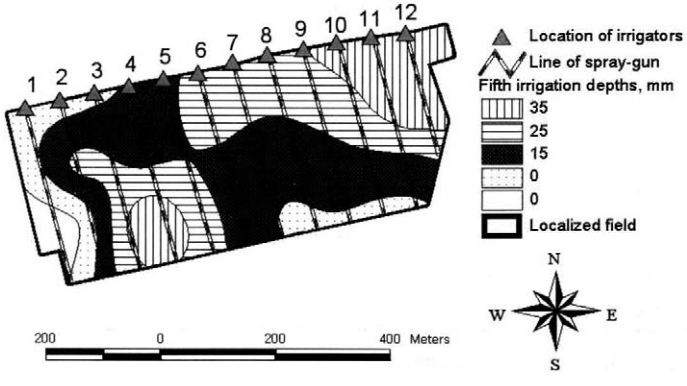

Fig. 14. Fifth irrigation rate

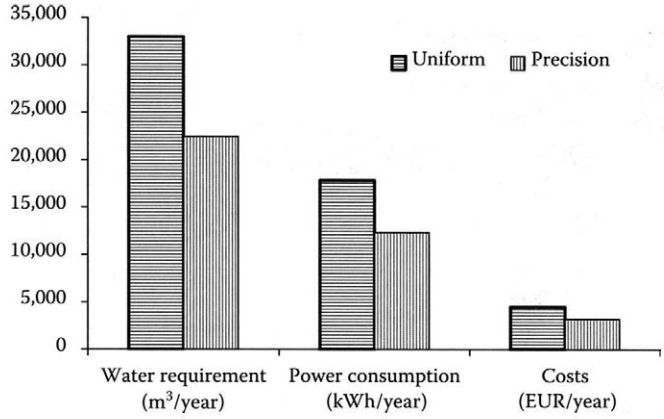

Fig. 15. Overall evaluation of the result

to 24.05% on the area of 1.4 ha (5.7% of the field) and from 24.06% to 26.63% on the area of 1.3 ha (5.5% of the field). The most represented was the interval from 16.36% to 18.93% on the area of 12.2 ha (55% of the field). Based on the resulting map of the soil moisture, it is possible to state that approximately 19.4 ha (88.18% of the field) require to be irrigated.

The subsequent date of soil moisture measuring was fixed on June 28, 2006. The resulting map is shown in Fig. 7. The soil moisture ranged from 9.79% to 26.32%. The most represented was the interval from 16.41% to 19.71% on the area of 10.8 ha (46.6% of the field). The least represented was the interval from 23.02% to 26.32% on the area of 0.8 ha (3.4% of the field). It is evident from the resulting soil moisture map that 100% of the field requires to be irrigated (22 ha) in the range from 10 to 40 mm at the graduated irrigation rates.

The spatial variability map of the soil moisture (dated July 13, 2006) was determined at repeated irrigation rate. The individual values of the soil moisture, as resulting from Fig. 8, ranged between 12.87% and 25.63% by vol. The measured values were in the range of limit soil hydrological coefficients. The most represented was the soil moisture interval from 17.97% to 20.52% on the area of 8.7 ha (39.3% of the field). The least represented was the interval between 23.08% and 25.63% on the area of 0.7 ha; this represents 3.18% of the field. The resulting map of the soil moisture revealed the need for irrigation water on 19.2 ha (87.27% of the field).

Preparing application maps and possibility to implement irrigation

The pumping station consisted of an electric motor with the output of 55 kW and pump flow of 144 m^3/h. According to the technical parameters of the irrigation machines monitored, the water flow of 26.6 m^3/h was determined for the use of nozzle diameter of 20.0 mm and nozzle pressure of 0.3 MPa. To achieve the required flow, only five irrigation machines could be connected to one pumping station. The spacing between the positions of the irrigation machines was 60 m (Fig. 9). One irrigation machine wetted a strip of the field covering a total area of 60 × 318 m. All of the 12 positions of irrigation machines were utilised.

Table 1. First position of irrigation machine

Irrigation machine	Zone 1			Zone 2			Zone 3			Zone 4		
	A	B	C	A	B	C	A	B	C	A	B	C
9	285	1,068	25	27	148	35	–	–	–	–	–	–
10	266	998	25	42	230	35	–	–	–	–	–	–
11	235	881	25	69	377	35	–	–	–	–	–	–
12	128	480	25	98	535	35	–	–	–	–	–	–

A – stage length (m); B – time of irrigation (min); C – irrigation rate (mm)

Table 2. Second position of irrigation machine

Irrigation machine	Zone 1			Zone 2			Zone 3			Zone 4		
	A	B	C	A	B	C	A	B	C	A	B	C
5	141	326	15	172	645	25	–	–	–	–	–	–
6	104	240	15	207	776	25	–	–	–	–	–	–
7	67	155	15	241	904	25	–	–	–	–	–	–
8	291	1,092	25	21	115	35	–	–	–	–	–	–

For abbreviations see Table 1

Table 3. Third position of irrigation machine

Irrigation machine	Zone 1			Zone 2			Zone 3			Zone 4		
	A	B	C	A	B	C	A	B	C	A	B	C
1	170	0	0	64	148	15	85	319	25	–	–	–
2	150	0	0	38	88	15	131	492	25	–	–	–
3	83	0	0	141	326	15	89	334	25	–	–	–
4	19	0	0	295	681	15	–	–	–	–	–	–

For abbreviations see Table 1

When determining the irrigation rate, the soil moisture map and the soil hydrological coefficients determined for the relevant part of the field were taken into account. Irrigation started on the spots where it was needed at the most – i.e. the spots with the lowest soil moisture contents.

The first irrigation rate ranged between 0 and 35 mm (zone rates of 35, 25, 15 mm; Fig. 10, Table 1–3). It was applied on the area of 19.4 ha (88.18% of the field). The irrigation rate of 35 mm was applied to the area of 1.6 ha. The area of 12.1 ha received the irrigation rate of 25 mm. The remaining part of the field obtained the irrigation rate of 15 mm (2.7 ha) and 0 mm.

The second irrigation rate ranged between 10 and 40 mm (zone rates of 40, 30, 20, 10 mm; Fig. 11). It was applied to the whole of the field (22 ha). The most represented was the irrigation rate of 20 mm on the area of 10.8 ha. The least represented was the irrigation rate of 40 mm (on the area of 1.1 ha). The irrigation rate of 30 mm was applied to the area of 6.1 ha.

Table 4. Cost of uniform and precision irrigation rate

Indication	Item	Value	
		uniform irrigation rate	variable irrigation rate
Annual cost			
$_rN_{mC}$	annual cost of irrigation (EUR/year)	2,011.35	1,709.83
$_rN_{eV}$	annual cost of water (EUR/year)	2,469.56	1,491.85
Sum (EUR/year)		4,480.92	3,201.68
Saving of cost (EUR/year)		1,279.23	
Unit cost			
$_jN_{mC}$	unit cost of irrigation (EUR/year)	18.28	15.54
$_jN_{eV}$	unit cost of water (EUR/year)	19.92	13.56
Sum (EUR/year)		38.2	29.1
Saving of cost (EUR/year)		9.1	

The area of 19.2 ha (87.27% of the field) received **the third irrigation rate** within the range from 0 to 35 mm (35, 25, 15 mm; Fig. 12). The figure shows that the irrigation rate of 35 mm (on the area of 3.6 ha), the irrigation rate of 25 mm (on the area of 6.8 ha), and the irrigation rate of 15 mm (the remaining area) were applied. Part of the area remained with no application of irrigation water (3.2 ha).

The fourth irrigation rate ranged between 0 and 35 mm (Fig. 13). The irrigation rate of 25 mm was applied to the area of 2.4 ha. The irrigation rate of 15 mm remained unchanged.

The last irrigation rate was applied to the area of 19.2 ha (87.27% of the field), that is, in the range from 0 to 35 mm (Fig. 14). The irrigation rate of 35 mm was applied to the area of 3.7 ha. The irrigation rate of 25 mm was applied to the area of 6.8 ha.

Crop yields and cost assessment

The yield of potatoes was determined according to the specified methodology. Only one variety (Victoria) with the average yield of 41.89 t/ha was grown in the field under investigation (22 ha).

In terms of irrigation accuracy, there are two basic methods for the application of the irrigation rate:

- conventional irrigation with a uniform rate applied to the whole field;
- precision irrigation with a variable rate applied to the whole field.

The method of applying irrigation significantly influences the size of the cost incurred.

When precision irrigation was implemented, it was possible to use only the machines available to the holding, namely: tractor Z 7211 (Zetor, Martin, Slovak Republic) and reel hose irrigation machines Bauer 90/300 (BAUER Gesellschaft, Voitsberg, Austria) with an on-board computer equipped with the basic software.

Cost calculation under precision irrigation and under uniform water application was done according to the introduced methodology. Moreover, variable rate irrigation requires to take account of the following input costs (they were neither taken into account in the work nor calculated):

- price of the program for the preparation of maps, for example ArcView 3.2;
- price of the GPS navigator, for example eMAP;
- costs for laboratory analyses, the determination of soil hydrological coefficients (FC, WP) in a laboratory;
- costs for the determination of the soil moisture, for example soil sample rings (for undisturbed soil sampling), HH2 Moisture Meter and WET Sensor;
- labour costs for the maps preparation.

A constant irrigation rate of 30 mm was considered under conventional irrigation.

The measurements were undertaken in the investigated field in the year 2006. The average diesel fuel price during this year was 0.83 EUR/l. The insurance for the tractor Z 7211 amounted to 42.62 EUR/year. The hourly rate for the tractor operator was 2.65 EUR/h, and the hourly rate for the irrigation operator was 2.65 EUR/h. The irrigation rate was changed by the irrigation operator, and his wage for this work amounted to 2.65 EUR/h. The cost for garaging the machine represented 2.16 EUR/m^2.

There were consumed 1,021.44 m^3/ha of water in the field of 22 ha in the experiment with precision irrigation. The electric power consumption to drive the pump was 560.9 kWh/ha. At a uniform irrigation rate, the consumption would be 1,500 m^3/ha of water. When applying such amounts of water (33,000 m^3), the planned electric power consumption was 17,832.65 kWh (810.58 kWh/ha). Water saving represented 478.56 m^3/ha (1,500 to 1,021.44; 31.9%). The electric power saving was 249.68 kWh/ha. The total cost for irrigation implementation was in the value of 1,709.83 EUR/year (with no energy subsidies, with no water cost). The unit cost amounted to 15.54 EUR/ha. The cost of consumed water was 1,491.85 EUR/year (without any consumed water subsidies). The unit cost of water reached 13.56 EUR/ha. Therefore, the total unit cost amounted to 29.1 EUR/ha. In the investigated agricultural holding, the total unit cost under uniform irrigation rate was 38.2 EUR/ha, thus showing the saving of 9.1 EUR/ha (23.8%; Fig. 15, Table 4). In favour of precision irrigation.

The obtained knowledge was confirmed by the research into precision irrigation conducted in the world. Hedley et al. (2009) identified preciously the performance indicators of variable rate irrigation; in their work, they described in detail the methods for soil conditions mapping with respect to soil hydraulic properties. That enabled to determine accurately the amount of the consumed water, water losses, nitrogen depletion from the soil depending upon concrete conditions of the selected fields. Water saving was from 9% up to 19% with an adequate reduction of energy consumption. It

follows that water saving in our experiments was higher.

Perry and Pocknee (2003) also achieved water saving when an agricultural crop was irrigated precisely. They transformed the application map into the Canlink 3000 control unit.

Hedley et al. (2009) evaluated the benefits of using variable rate irrigation for selected crops (dairy pasture, potatoes, maize grain). They reached water saving of 9% (dairy pasture), 13% (potatoes) and 19% (maize grain). That enabled to save the operating costs in the value of NZD 35 1/ha (potatoes), NZD 88 1/ha (pasture) and NZD 149 1/ha (maize). The maximum water saving was revealed in the location of maize.

CONCLUSION

The practical implementation of the presented methodology supported the possibility to apply precision irrigation. Experimental measurements confirmed the economic effectiveness of the suggested method. Under variable rate irrigation, the total cost was reduced by 9.1 EUR/ha and this represented the saving of 23.8% to the benefit of precision irrigation. The water saving amounted to 478.56 m^3/ha, the same expressing the value of 31.9%. The implementation of information technology in the given case enabled to process graphically the variability of input and output conditions needed for the implementation of precision irrigation in practice.

References

Derbala A., Sourell H., 2002. Development and evaluation of mobile drip irrigation with center pivot machine. In: Proceedings 8th International Congress on Mechanization and Energy in Agriculture, October 15–17, 2002. Kusadas, Turkey.

Fraisse C.W., Heermann D.F., Duke H.R., 1995. Simulation of variable water application with linear-move Irrigation systems. Transactions of the ASABE, *38*: 1371–1376.

Hedley C., Yule I., Tuohy M., Vogeler I., 2009. Key Performance Indicators for Variable Rate Irrigation Inplementation on Variable Soils. St. Joseph, ASABE.

King B.A., Stark J.C., Wall R.W., 2006. Comparison of site-specific and conventional uniform irrigation management for potatoes. Applied Engineering in Agriculture, *22*: 677–688.

Nozdrovický L., Rataj V., Galambošová J., Kollárová K., Macák M., Halva J., Tuček J., Koreň M., Smreček R., 2008. Presné pôdohospodárstvo. IMPL Ementácia s podporou informačných technológií a techniky (Precision Farming. Implementation with the Support of Information Technologies and Techniques). Nitra, SPU in Nitra: 168.

Perry C., Pocknee S., 2003. Precision pivot irrigation controls to optimize water application. In: Proceedings of the 2003 Irrigation Association Meeting, San Diego: 86–92.

Rataj V., 2005. Projektovanie výrobných systémov – Výpočty a analýzy (Projection of the Production Systems – Calculations and Analyses). Nitra, SPU in Nitra: 120.

Sadler E.J., Camp C.R., Evans D.E., Millen J.A., 2002. Spatial variation of corn response to irrigation. Transactions of the ASABE, *45*: 1869–1881.

Sourell H., 2003. Progressive irrigation technique for one certain und ecologically plant production. Landbauforschung Völkenrode Sonderheft, *258*: 107–108.

Sourell H., Al-Karadsheh E., 2003. Precision irrigation toward improving irrigation water management. ICID-CIID. Available at http://afeid.montpellier.cemagref.fr/mpl2003/AtelierTechno/AtelierTechno/Papier%20Entier/Sourell.pdf

Received for publicatrion December 6, 2010
Accepted after corrections June 6, 2011

Corresponding author:

Ing. Ján Jobbágy, Ph.D., Slovak University of Agriculture in Nitra, Faculty of Engineering, Department of Machines and Production systems, Tr. A. Hlinku 2, 949 76 Nitra, Slovak Republic
phone: + 421 376 414 796, e-mail: Jan.Jobbagy@uniag.sk

Drying medium – modelling and process evaluation

I. Vitázek, J. Havelka

Faculty of Engeneering, Slovak University of Agriculture in Nitra, Nitra, Slovak Republic

Abstract

Vitázek I., Havelka J., 2011. **Drying medium – modelling and process evaluation**. Res. Agr. Eng., *57 (Special Issue)*: S24–S29.

Natural gas is used as a heat source in the majority of modern drying plants in agriculture. The input gas is a mixture of natural gas and atmospheric air. With burning, the composition of this mixture changes. Drying medium is a mixture of hot combustion gases from natural gas and atmospheric air added. The thermic parameters of natural gas and atmospheric air are permanently constant. The authors present their method of the calculation of thermodynamic parameters of the drying medium. They elaborated two computer programmes in Q-Basic for the calculation related to the drying medium with temperatures in the range 100–200°C.

Keywords: natural gas; drying medium; computer program

Drying is a necessary process in agriculture for the final treatment of forages and grains.

In modern drying appliances, mixtures of combustion gases from natural gas with added atmospheric air are used as the drying medium.

The process of drying is explained in detail in specific literature by the authors Maltry and Pötke (1966), Valchař et al. (1967), Imre (1974), Pabis (1965, 1982). In this, Pabis (1965, 1982) presented his special knowledge gained in USA from Henderson. In the paper by Imre (1974), a computer program is given for the drying process modelling.

In their work, the authors try, to reach the most precise calculations of the drying medium parameters by using the gas mixtures thermodynamics according to Havelka et al. (1989) and Vitázek (2006), and precise parameters of individual gases coming from the tables by Ražnjevič (1969). The authors constat the best oldish description of fuel gases combustion by Kasatkin (1957).

Natural gas is used as a heat source in the majority of modern drying plants in agriculture. The source of the drying medium is a gas burner with a mixing chamber. The input gas mixture consists of natural gas and atmospheric air. With burning, the composition of this mixture changes as given by Vitázek (2008).

The quality parameters of natural gas are periodically published by SPP Bratislava (2010), Slovak Gas Industry in Bratislava. The quality parameters of atmospheric air and natural gas are permanently constant. Therefore, the authors state that one comprehensive elaboration suffices in many cases of research and practice.

The authors present here their method of the thermodynamic parameters calculation for the drying medium concerned. For this calculations, a computer program in Q-Basic was elaborated.

MATERIAL AND METHODS

The authors present the basic quality parameters of natural gas from the year 2009, the basic quality parameters of atmospheric air, stoichiometric relations for the oxidation of natural gas. With this knowledge,

Supported by the Scientific Grant Agency VEGA of the Ministry of Education of the Slovak Republic and the Slovak Academy of Sciences, Grant No. 1/0708/09.

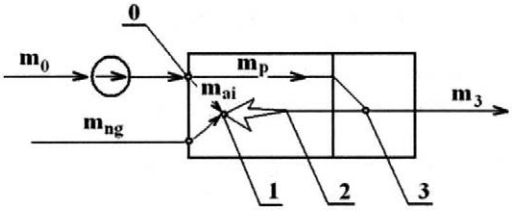

Fig. 1. Scheme of the mass flow in the burner chamber

they elaborated an analytical model of ideal burning of natural gas and of drying medium as a mixture of combustion gases with added atmospheric air.

For this analysis, they used the thermodynamics of ideal gases, thermodynamics of gas mixtures, and tables of quality parameters of individual gases as gived in the publication by Ražnjevič (1969).

They derived the relations for characteristic indexes of the drying medium analysed.

Model of drying medium

The scheme of the source of the drying medium, which is a gas burner with a mixing chamber, is shown in Fig. 1. The process of the drying medium creation is demonstrated in *i–x* diagram of wet air (wet gas) in Fig. 2. An air fan supplies atmospheric air m_0 in quality state, point 0. In the gas burner the first part of this air, stoichiometric part m_{0i}, is mixed with natural gas m_{ng}, state point 1. The quality of this mixture changes with burning into ideal combustion gases m_2, state point 2. These ideal combustion gases m_2 are mixed in the mixing chamber with the second part of the atmospheric air, added atmospheric air m_p, by which the final mixture is created, i.e. hot drying medium m_3, state point 3.

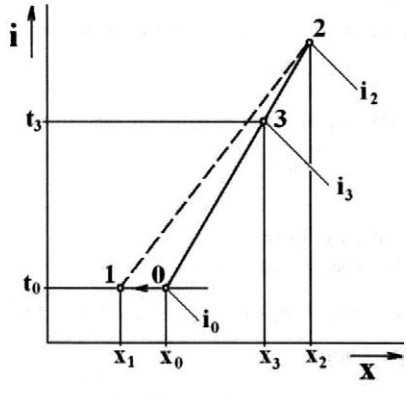

Fig. 2. Scheme of *i-x* diagram of wet air

Natural gas

SPP Bratislava published on the internet the average quality characteristics of natural gas in the year 2009.

Basic quality values:

Trade unit of natural gas:

1 m^3, t = 15°C, p = 101.325 kPa, φ = 0

Density	ρ_{ng} = 0.7048 kg/m^3
Relative density	ρ_{ng} = 0.5751
Heat value	Q_i = 9.563 kWh/m^3 = 34.427 MJ/m^3 = 48.98 MJ/kg
Heat of combustion	Q_s = 10.6077 kWh/m^3 = 38.188 MJ/m^3 = 54.32 MJ/kg

Average Molar concentrations (%):

Methan (CH_4)	x = 96.806
Etan (C_2H_6)	x = 1.4617
Propan (C_3H_8)	x = 0.6575
Carbon dioxyd (CO_2)	x = 0.2258
Nitrogen (N_2)	x = 0.8558

Average Mass concentrations:

Carbon	c = 0.7378
Hydrogen	h = 0.24279
Carbon dioxyd	co_2 = 0.006
Nitrogen	n_2 = 0.0145
Average value of Molar mass	M_{ng} = 16.56 kg/mol
Average value of Gas constant	r_{ng} = 502.04 J/kg K

Atmospheric air

Quality parameters from Chyský (1977). Atmospheric air serves as a source of oxygen for natural gas burning.

Average Mass concentrations:

Nitrogen	σ_{aN_2} = 0.75524
Oxygen	σ_{aO_2} = 0.23144
Carbon dioxyd	σ_{aCO_2} = 0.01282
Argon et add.	σ_{aAr} = 0.0005

RESULTS

Stechiometric relations

Ideal combustion of natural gas is described with basic chemical equations for the burning of 1 kg of natural gas.

$$C + O_2 = CO_2 \quad (1)$$

1 kg C + 2.6642 kg O_2 = 3.6642 kg CO_2

$$2\ H_2 + O_2 = 2\ H_2O \quad (2)$$
$$1\ kg\ H_2 + 7.9381\ kg\ O_2 = 8.9381\ kg\ H_2O$$

Mass of oxygen necessary for ideal combustion of 1 kg of natural gas:

$$m_{O_2 i} = 2.6642 \times c + 7.9381 \times h = 3.9049\ kg\ O_2 \quad (3)$$

The smallest mass of atmospheric air necessary for ideal combustion of 1 kg of natural gas:

$$m_{ai} = \frac{m_{O_2 i}}{\sigma_{aO_2}} = \frac{3.9049}{0.23144} = 16.8722 \quad kg \quad (4)$$

New gases produced by natural gas burning:

Carbon dioxyd $m_{CO_2} = 3.6642 \times c = 2.700\ kg\ CO_2$ (5)

Water steam $\Delta m_W = 8.94567 \times h = 2.1881\ kg\ H_2O$ (6)

The residual mass of intacted gases from natural gas after combustion of 1 kg of natural gas:

Carbon dioxyd $m'_{CO_2} = 0.00433\ kg\ CO_2$ (7)

Nitrogen $m'_{N_2} = 0.0142\ kg\ N_2$ (8)

Analytic model of combustion

Ideal combustion of 1 kg of natural gas: the air fan supplies atmospheric air m_0 from which a stechiometric part m_{ai} is completed with 1 kg of natural gas and the mixture changes by burning into ideal hot combustion gases.

Atmospheric air – mass flow:

Dry part mass $m_{0d} = m_{ai}$ (9)

Moist part mass $m_{0W} = m_{ai} \times x_0$ (10)

Whole mass $m_{0C} = m_{ai} \times (1 + x_0)$ (11)

Inflammable mixture of atmospheric air and natural gas:

Natural gas mass $m_{ng} = 1\ kg$

Dry part mass $m_{1d} = m_{0d} + m_{ng}$ (12)

Moist part mass $m_{1W} = m_{0W}$ (13)

Whole mass $m_{1C} = m_{1d} + m_{1W} = m_{ai} \times (1 + x_0) + 1$ (14)

Specific humidity $x_1 = m_{1W}/m_{1d}$ (15)

Ideal hot combustion gases:

Dry part mass $m_{2d} = m_{1d} - m_{O_2 i} + m_{CO_2}$ (16)

Moist part mass $m_{2W} = m_{0W} + \Delta m_W$ (17)

Whole mass $m_{2C} = m_{2d} + m_{2W}$ (18)

Specific humidity $x_2 = m_{2W}/m_{2d}$ (19)

Enthalpy of the inflammable gas mixture:

$$I_2 = (m_{ai} \times c_{pa} + m_{ai} \times x_0 \times c_{pW} + m_{ng} \times c_{png}) \times t_0 \quad (20)$$

Enthalpy of ideal hot combustion gases:

$$I_3 = I_2 + m_{ng} \times Q_i \times \eta_b \quad \rightarrow \quad i_3 = I_3 / m_{2C} \quad (21, 22)$$

Drying medium

Drying medium is a mixture of hot ideal combustion gases from natural gas m_2 and added atmospheric air m_p which is the second part of the atmospheric air flow supplied with the air fan. The calculation is given for 1 kg of natural gas.

Atmospheric air – mass flow:

Inflammable gas mixture – dry part mass

$$m_{0d} = m_{ai} + m_{pd} \quad (23)$$

Added atmospheric air – coefficient of added air

$$\alpha = m_{0d} / m_{ai} \quad (24)$$

Added atmospheric air – dry part mass

$$m_{pd} = m_{ai} \times (\alpha - 1) \quad (25)$$

Added atmospheric air – moist part mass

$$m_{pW} = m_{ai} \times (\alpha - 1) \times x_0 \quad (26)$$

Added atmospheric air – whole mass

$$m_{pC} = m_{ai} \times (\alpha - 1) \times (1 + x_0) \quad (27)$$

Hot drying medium:

Dry part mass

$$m_{3d} = m_{2d} + m_{pd} = m_{ai} \times \alpha - m_{O_2 i} + m_{CO_2} + m'_{CO_2} + m'_{N_2} \quad (28)$$

Moist part mass

$$m_{3W} = m_{2W} + m_{pW} = m_{ai} \times \alpha \times x_0 + \Delta m_W \quad (29)$$

Whole mass

$$m_{3C} = m_{3d} + m_{3W} \quad (30)$$

Specific humidity

$$x_3 = m_{3W} / m_{3d} \quad (31)$$

From this relations the authors derived the mass concentrations of individual gases in this hot drying medium

Nitrogen

$$\sigma_{3N_2} = (m_{ai} \times \alpha \times \sigma_{aN_2}) / m_{3C} \quad (32)$$

Oxygen

$$\sigma_{3O_2} = (m_{ai} \times (\alpha - 1) \times \sigma_{aO_2}) / m_{3C} \quad (33)$$

Carbon dioxyd

$$\sigma_{3CO_2} = (m_{ai} \times \alpha \times \sigma_{aCO_2} + m_{CO_2} + m'_{CO_2}) / m_{3C} \quad (34)$$

Argon et add.

$$\sigma_{3Ar} = (m_{ai} \times \alpha \times \sigma_{aAr}) / m_{3C} \quad (35)$$

Humidity

$$\sigma_{3W} = (m_{ai} \times \alpha \times x_0 + \Delta m_W) / m_{3C} \quad (36)$$

Drying medium – Molar mass

$$M_3 = 1 / (\sum \sigma_i / M_i) \quad (37)$$

Drying medium – Gas constant

$$r_3 = 8{,}314.4 / M_3 \quad \text{(J/kg K)} \quad (38)$$

Heat balance of the drying medium: on combustion of 1 kg of fuel gas the reaction heat is released – heat value Q_i – and the enthalpy of combustion gases compared to the ambient neighbourhood increases by:

$$\Delta I_3 = m_{ng} \times Q_i \times \eta_b = 1 \times Q_i \times \eta_b \quad \text{(kJ)} \quad (39)$$

Ražnjević (1969) tables for gas enthalpy are composed in such manner that the values $i_i = 0$ are assigned to the temperature $t = 0$°C. When using these tables, it is necessary to add a conversion amendment that represents the residual difference of enthalpy between the temperatures t_0 and 0°C:

$$\Delta I_{30} = \sum m_{3i} \times i_{3i} = \sum m_{3i} \times c_{pi} \times t_0 \quad \text{(kJ)} \quad (40)$$

The enthalpy of the combustion gases from 1 kg of fuel gas to 0°C is then:

$$I_3 = \Delta I_3 + \Delta I_{30} \quad \text{(kJ)} \quad (41)$$

and specific enthalpy:

$$i_3 = I_3 / m_{3C} \quad \text{(kJ/kg)} \quad (42)$$

By means of linear regression, the authors have obtained linear regression relations from Ražnjević (1969) tables for all individual gases in the given fuel gas for temperatures 100–300°C with excellent regression coefficient r as follows:

$$i_i = b_i \times t - a_i \quad (43)$$

The enthalpy of the gas mixture (hot drying medium) is

$$i_3 = \sum i_{3i} \times \sigma_{3i} = \sum b_i \times \sigma_{3i} \times t_3 - \sum a_i \times \sigma_{3i} \quad (44)$$

From this relation, the relation is derived for the temperature of the hot drying medium

$$t_3 = (i_3 - \sum a_i \times \sigma_{3i}) / \sum b_i \times \sigma_{3i} \quad (45)$$

The enthalpy $i_{3(1+x)}$ for the work with i–x diagram of wet air is the sum of the enthalpy of 1 kg of dry gases and that of x_3 kg of moisture with its specific heat of evaporation

$$i_{3(1+x)} = i_{3dg} + x_3 \times (2{,}500 + i_{3W}) \quad \text{(kJ/kg}_{dg}\text{)} \quad (46)$$

That is to be calculated using the relation:

$$i_{3(1+x)} = i_3 \times (1 + x_3) + x_3 \times 2{,}500 \quad \text{(kJ/kg}_{dg}\text{)} \quad (47)$$

Characteristic indexes

In this chapter, the measured natural gas consumption $\dot{V}_{ng}$ m^3/h is the basis for the calculations of the characteristic indexes.

Natural gas – Mass flow

$$\dot{m}_{ng} = \dot{V}_{ng} \times \rho_{ng} \quad \text{(kg/s)} \quad (48)$$

Atmospheric air (input volume flow)

$$\dot{V}_0 = (m_{ai} \times \alpha \times (1 + x_0) \times \dot{m}_{ng}) / \rho_0 \quad \text{(m}^3\text{/s)} \quad (49)$$

Gas burner performance

$$P = \dot{m}_{ng} \times Q_i \times \eta_b \quad \text{(W, kW, MW)} \quad (50)$$

Hot drying medium (output volume flow)

$$\dot{V}_3 = (m_{3C} \times \dot{m}_{ng} \times r_3 \times T_3) / p_a \quad \text{(m}^3\text{/s)} \quad (51)$$

Hot drying medium (volumetric concentrations of oxygen and carbon dioxide)

$$x_{3O_2} = \sigma_{3O_2} \times M_3 / M_{O_2} \quad (52, 53)$$

$$x_{3CO_2} = \sigma_{3CO_2} \times M_3 / M_{CO_2}$$

Hot drying medium (mass concentrations of individual gases)

$$\dot{m}_{3i} = m_{3C} \times \dot{m}_{ng} \times \sigma_{3i} \quad \text{(kg/s)} \quad (54)$$

Drying medium example

The authors present the drying medium parameters, calculated for the drying of cereals at about 120°C.

Given values:

Given coefficient of added air $\alpha = 26$

Average consumption of natural gas 10 m^3/h

Atmospheric air: $t = 15°C$, $p = 100$ kPa, $\varphi = 60\%$

Efficiency of gas burner $\eta_b = 98\%$

Calculated values:

Performance of the gas burner $P = 93.9$ kW

Atmospheric air, input volume flow 0.717 m^3/s

Drying medium, temperature $t_3 = 121.2°C$

Drying medium mass flow 0.866 kg/s

Drying medium volume flow 0.982 m^3/s

Drying medium enthalpy $i_{3(1+x)} = 153.3$ kJ/kg_{dg}

Program in Q-Basic

The authors elaborated two computer programs in Q-Basic for the modelling of a specific drying medium and evaluation of the measured process values in a drying appliance, for drying medium with temperatures 100–200°C. They enable a quick and precise calculation of the parameters for the given drying medium.

These programs consists of three parts:

1. Introduction part. The user introduces the basic parameters of the process. This is a very simple activity not requiring the knowledge of the theory and of the thermodynamic parameters of the gases;
2. Program for the realisation of calculations, in which all necessary parameter values are introduced coming from thermodynamic tables;
3. Calculation report. This is a particular report with all initial information and input values, and with the calculated characteristic values and indexes.

DISCUSSION

The authors divided the whole process of drying into two parts:

1. hot drying medium creation,
2. reduction of the moisture content in the dried material by means of evaporation.

In this work, the authors present a method for precise mathematical modelling of hot drying medium with temperature 100–300°C for drying agricultural products in food quality.

SPP in Bratislava presents perfect information on internet on the composition and thermodynamic parameters of the natural gas delivered. The authors used it in this work. The drying medium is a mixture of five individual gases: N_2, O_2, CO_2, H_2O, Ar + inert. gases. The authors used the enthalpy tables presented in the publication by Ražnjevič (1969). In this work, they used the relations from linear regression for temperatures 100–300°C, where all the regression coefficients were better than 0.999. The authors have used and presented special literature from recent time, which means all the time really significant.

The authors prepare a complex monograph "Theory of drying" in which they will present all their work done in this scientific branch.

CONCLUSION

The presented method enables precise calculations of the thermodynamic parameters of the hot drying medium consisting of a mixture of combustion gases from natural gas and added atmospheric air, in which the changes of the parameters with temperature are respected.

This calculation is very laborious. Therefore, practical use of this advantageous method is connected with a computer programme.

The presented method of the calculation of the thermodynamic parameters of the drying medium with natural gas is to be used with a great advantage in practice for the evaluation of the control measurements in drying plants and also for precise modelling of the drying medium parameters in the research into the drying processes. Using the computer program, this calculations are quick and precise.

References

Havelka J., Látal S., Navrátil S., 1989. Teplotechnika a hydrotechnika (Thermotechnics and Hydromechanics). Bratislava/Prague, Príroda/SZN: 352.

Chyský J., 1977. Vlhký vzduch (Wet Air). Prague, SNTL: 160.

Kasatkin A.G., 1957. Základní pochody a zařízení chemické technologie (Basic Processes and Appliances of Chemical Technology). Prague, SNTL: 415.

Imre L., 1974. Szárítási közikönyv (Manual of Drying). Budapest, Müszaki Könyvkiado: 1122.

MALTRY W., PÖTKE E., 1966. Technika poľnohospodárského sušiarenstve (Technics of Drying in Agriculture). Bratislava, SVPL: 340.

PABIS S., 1965. Suszenie plodów rolnych (Drying of Agricultural Products). Warszawa, PWRiL: 312.

PABIS S., 1982. Teoria konwekcyjnego suszenia produktov rolniczych (Theory of heat conduction drying of agricultural products). Warszawa, PWRiL: 229.

RAŽNJEVIČ J., 1969. Tepelné tabuľky a diagramy (Thermal Tables and Diagrams). Bratislava, ALFA: 340.

SPP Bratislava, 2010. Zloženie zemného plynu 2009 (Composition of natural gas 2009). Available at www.spp.sk (accessed March 10, 2010).

VALCHAŘ J., CHOC M., TUMA V., KOLÁŘ S., 1967. Základy sušení (Theory of Drying). Prague, ČVUT/SNTL: 396.

VITÁZEK I., 2006. Tepelné procesy v plynnom prostredí (Heat Processes in Gaseous Atmosphere). Nitra, SPU in Nitra: 98.

VITÁZEK I., 2008. Teplotechnika a hydrotechnika (Thermotechnics and Hydrotechnics). Nitra, SPU in Nitra: 104.

VITÁZEK I., HAVELKA J., 2010. Thermodynamics of combustion of fuel gases. In: ES 2010 Power System Engineering, Thermodynamics & Fluid flow. University of West Bohemia, Plzeň: 6.

Received for publication December 9, 2010
Accepted after corrections June 6, 2011

Corresponding author:

doc. Ing. IVAN VITÁZEK, CSc., Slovak University of Agriculture in Nitra, Faculty of Engeneering, Department of Transport and Handling, Trieda A. Hlinku 2, 949 76 Nitra, Slovak Republic
phone: + 421 376 414 756, e-mail: ivan.vitazek@uniag.sk

Comparison of numerical integration methods in strapdown inertial navigation algorithm

V. Cviklovič, D. Hrubý, M. Olejár, O. Lukáč

Faculty of Engineering, Slovak University of Agriculture in Nitra, Nitra, Slovak Republic

Abstract

Cviklovič V., Hrubý D., Olejár M., Lukáč O., 2011. **Comparison of numerical integration methods in strapdown inertial navigation algorithm**. Res. Agr. Eng., *57 (Special Issue)*: S30–S34.

The numerical mathematical theory provides a few ways of numerical integration with different errors. It is necessary to make use of the most exact method with respect to the computing power for a majority of microprocessors, because errors are integrated within them due to the algorithm. In our contribution, trapezoidal rule and Romberg's method of numerical integration are compared in the velocity calculation algorithm of the strapdown inertial navigation. The sample frequency of acceleration and angular velocity measurement was 816.6599 Hz. Inertial navigation velocity was compared with precise incremental encoder data. Trapezoidal method velocity error in this example was 1.23×10^{-3} m/s in the fifteenth-second measurement. Romberg's method velocity error was 0.16×10^{-3} m/s for the same input data.

Keywords: Romberg's method; trapezoidal rule; accelerometer; gyroscope; micro electro-mechanical systems (MEMS)

The utilisation of navigations has recently expanded to various scientific and engineering departments. We encounter the GPS system support most frequently, with it being increasingly available to general public. This system is used in such spaces, where the reception of the satellite signals is possible. However, there are some examples when we need to use navigation in closed spaces, for instance a storage house, where this signal is not available. In such cases, it is possible to use the advantages of inertial navigation, which does not require any input electric or magnetic signals, because the information about the position is obtained through the acceleration and gyro data from accelerometers and gyroscopes.

Two basic principles exist of inertial navigation. The first principle utilises gimbal suspension with a gyroscopically stabilised platform for balancing the sensors with predefined reference casing. Some advantages of the presented navigation include: a lower power strain of the sensor and a simpler calculation of the actual position. The navigation system without gimbal suspension is placed on a surface which is tightly connected to a vehicle (Titterton, Weston 2004).

We utilise the integrated circuit sensors in this principle, which causes inclination towards this technology. It concerns a combination of electronics and the 3D mechanical microelements, which convert the measured variable into an electrical signal. Consequently, this signal is quantified and sampled. The digital value is available on the output. The common title for this sensor subgroup is micro electro-mechanical systems (MEMS).

MATERIAL AND METHODS

The most important knowledge by inertial navigation is the acceleration value in a correct period (at the exactly defined moment). The acceleration is measured in each axis of the 3D Cartesian system. The accelerometer axes are consistent with the axes

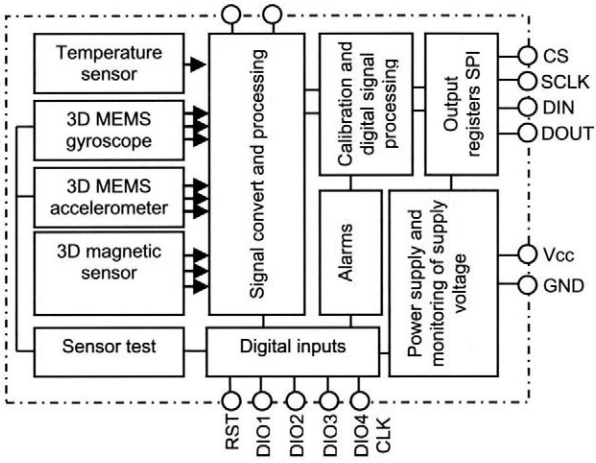

Fig. 1. Block diagram of the accelerometer ADIS16405 (Analog Devices 2009)
RST – device reset, DIO1-4 – digital general purpose pins, CLK – synchronisation pulse, GND – ground, Vcc – supply voltage, CS – chip select, SCLK – communication clock, DIN – data input, DOUT – data output

of the relative system by way of illustration. Thus we avoid complicated mathematics, which does not affect the position determination and the position error, if the information from the gyroscope and inclinometer are not taken into account.

In our example of inertial navigation, MEMS 3 axial inertial sensor ADIS16405BMLZ (Analog Devices, Inc., Norwood, USA) with digital output was used. Block diagram of the sensor is shown in Fig. 1. The capacitance sensors are sensitive parts of the accelerometers. In the case of the correctly calibrated sensor being in the rest position, the absolute value of the gravity acceleration is available at the output (Analog Devices 2009).

Acceleration is a second-order derivative of trajectory by time. The point position is calculated (can be expressed) by the position vector of the mass point:

$$\int_{r_0}^{r} d\vec{r} = \int_0^t \vec{v}_0 \times dt + \int_0^t (\vec{a}t) \times dt = \vec{v}_0 \int_0^t dt + \vec{a} \int_0^t t \times dt \qquad (1)$$

The position change is then the difference between the vectors:

$$\vec{r} - \vec{r}_0 = \vec{v}_0 t + \frac{\vec{a}t^2}{2} \qquad (2)$$

where:

$\vec{r}$ – position vector (m)
$\vec{v}$ – velocity vector (m/s)
$\vec{a}$ – acceleration vector (m/s^2)
t – time (s)
$\vec{v}_0$ – initial velocity vector (m/s)

It follows that the acquired information on the position is set by double integral acceleration, consequently the global position error will integrate in time. To minimise these errors, a properly configured Kalman's filter is used. All but one integrated methods bring errors into the calculations. The integrals for the actual position calculation cannot be calculated analytically, neither can they be defined by elementary functions. In some cases symbolic solutions exist, but this is more demanding than the numerical integration (Grewall et al. 2007).

By numerical integration, we may select from two basic alternatives. Either the interpolating polynomials are integrated or other integration methods are used. The interpolating upper (higher) degree polynomials are integrated with a greater error.

To calculate the definite integral of function $f(x)$ given by the functional values in the equidistant points the Newton-Cotes quadrature formulas are most frequently used. The best known applicable formulas are the trapezoidal rule and Simpson's rule. The outstanding feature of the trapezoidal rule is a slow convergence of the numerical process at relatively low accuracy and high error h^2 (Mošová 2003):

$$R_L = -\frac{(b-a)^3}{12n^2} f''(\xi) \qquad (3)$$

where:

$\xi \in \langle a, b \rangle$ – derivation of function in interval $\langle a, b \rangle$
R_L – method error
a, b – integral range
n – samples quantity in the interval $\langle a, b \rangle$

Simpson's rule approximates the selected function more precisely. The integral value of $f(x)$ is calculated in the node points. This method is characterised by a small error h^4. Geometrical interpretation is the sum of the areas above triplet of node points

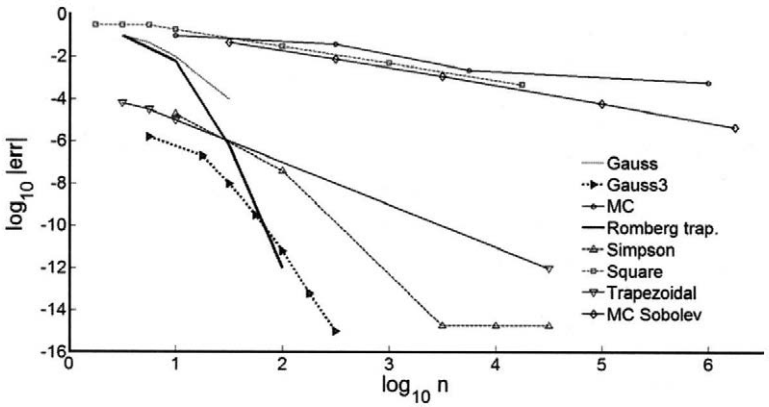

Fig. 2. Relative error comparison of the integration methods according to the amount of the points used (VICHER 2003)

with the common (collective) threshold point for the adjacent parabolas. The error of the calculation method is:

$$R_S = -\frac{(b-a)^5}{12n^4} f^{(4)}(\xi) \tag{4}$$

The precision of calculation depends on quantize step h. This is valid generally, not only for the trapezoidal and Simpson's rules. The calculations with the highest point count (amount) in the range $\langle a, b\rangle$ are the most exact. Since in this case is it needed to calculate the integrate area using algorithm in a microcontroller, the Romberg's method, that uses the calculation way of definite integral on the basis of trapezoidal rule, shows to be the most efficient and the most exact. Romberg showed by means of this method that it is possible to utilise the methods with greater errors for the formulation of more precise approximate integral value when using approximation for equal integration range with various partition steps. By combining the result with a higher error, the result with a lower error is reached (VICHER 2003).

With this method, we approximate first of all the integral in the interval $a \le x \le b$, that is split into $8N$ parts (N is integer, which is defined by the number of nodes) with step $h = (b - a)/8N$. With the aid of the node points $f(a + kh)$, where $k = 1, 2, \ldots, 8N-1$, non-precision approximation is obtained when using Eq. 5. According to Eqs 6 and 7, other approximations of the integral are calculated, by means of which the step value gradually decreases from $8h$ to h for value T_8.

$$T_1 = 8h\sum_{m=0}^{N-1} F_{8m} = (b-a)\overline{\sum_{m=0}^{N-1} F_{8m}} \tag{5}$$

$$U_1 = 8h\sum_{m=0}^{N-1} F_{8m+4} = (b-a)\overline{\sum_{m=0}^{N-1} F_{8m+4}} \tag{6}$$

$$U_2 = (b-a)\overline{\sum_{m=0}^{N-1} F_{8m+2} + F_{8m+6}} \tag{7}$$

$$U_4 = (b-a)\overline{\sum_{m=0}^{N-1} F_{8m+1} + F_{8m+3} + F_{8m+5} + F_{8m+7}} \tag{8}$$

$$T_2 = \overline{T_1 + U_1},\ T_4 = \overline{T_2 + U_2},\ T_8 = \overline{T_4 + U_4} \tag{9}$$

U and T are rough approximations of the calculated integral with the error rank h^2. Further, the more precise approximation using equations is sought (KAČEŇÁK 2001):

$$S_2 = T_2 + \frac{T_2 - T_1}{2^2 - 1} \tag{10}$$

$$S_4 = T_4 + \frac{T_4 - T_2}{2^2 - 1} \tag{11}$$

$$V_2 = U_2 + \frac{U_2 - U_1}{2^2 - 1} \tag{12}$$

$$V_4 = U_4 + \frac{U_4 - U_2}{2^2 - 1} \tag{13}$$

S and V are more precise approximations with error h^4. Thus the process continues up to calculated R, W with error h^6 and Q with error h^8. Consequent approximated value of the calculated integral is represented by parameter Q:

$$Q_8 = R_8 + \frac{R_8 - R_4}{2^6 - 1} \tag{14}$$

The final value Q is the result of the calculations whose results are written down into the scheme. As the Romberg's method is in reality the numerical calculation of the approximation results for different divided interval steps, it is possible to use another

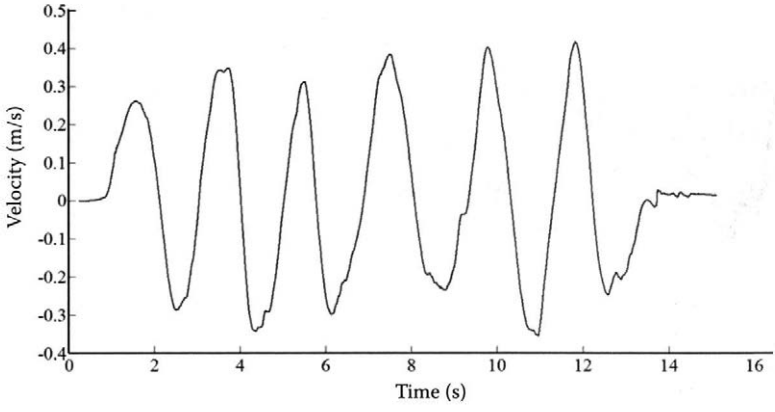

Fig. 3. Velocity course used for our example

approximation instead of the trapezoidal method, for example Simpson's rule. This method is simple but very precise. The errors comparison of the individual integration methods is showed in Fig. 2.

RESULTS AND DISCUSSION

Input acceleration and angular velocity data were measured for fifteen seconds. The velocity curve was optimised to exclude other errors (Fig. 3) and it was controlled by autonomous robot, whose navigation was based on incremental encoders. The calculations were evaluated by MATLAB application (MathWorks Inc., Natick, USA). The sample frequency of 816.6599 Hz and the properly selected course line of velocity for it enabled to minimise the error caused by the content of higher harmonic components in the signal (according to the criterion of SHANNON 1949). The acceleration course measured by ADIS16405BLMZ is shown on Fig. 4.

This change can be seen also on the final errors in their decrease. It is due to the selected type of approximation. It is not possible to describe the continuously modifying common phenomenon and changes by means of the trapezoidal method. The most exact results are obtained if concavity and convexity of the course change and when the positive and negative errors compensate each other.

Slightly better is the use of Simpson's rule in the Romberg's method that uses polynomial approximation, most frequently of the second rank. However, this calculation is more complicated because the final area can not be calculated from two values only, but from several measurements in the selected interval. The deviation course of the calculated velocity to real velocity for the Romberg's method and the trapezoidal approximation refers to the significant difference between the methods listed. The use of Romberg's method with trapezoidal approximation shows a significantly smaller deviation when compared with trapezoidal rule itself.

On Fig. 5, the velocity error course is shown. Romberg's method is caused by the trapezoidal approximation used. In the time interval between the fourteenth and fifteenth seconds the error decreases in Romb-

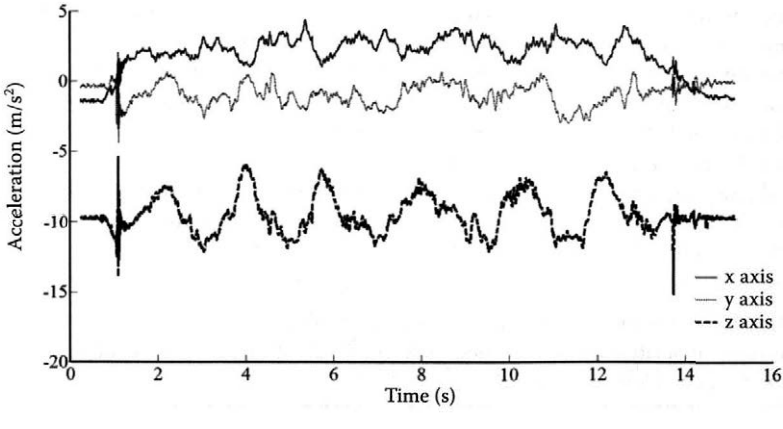

Fig. 4. Acceleration course used for our example

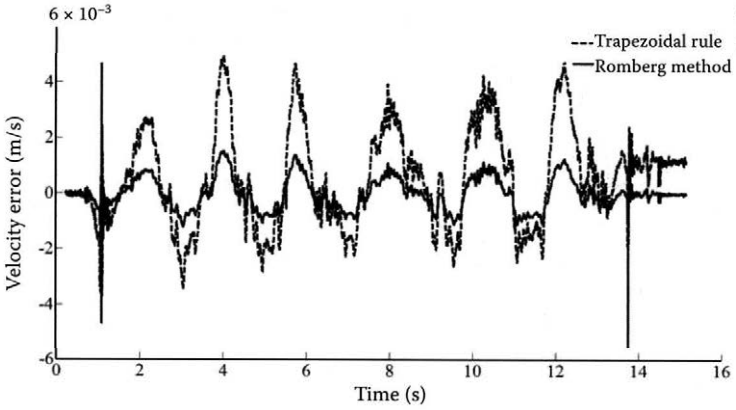

Fig. 5. Velocity error course according to time

erg's method. The trapezoidal rule is inaccurate for the use in the algorithm of strapdown inertial navigation systems. The trapezoidal method velocity error was in this example 1.23×10^{-3} m/s in the fifteenth-second measurement. Romberg's method velocity error was for the same input data 0.16×10^{-3} m/s.

CONCLUSION

The application of numerical integration methods to inertial navigation demands high attention and knowledge of various course specifications of the input values, from which the final integral is calculated. These values are the acceleration and time difference between the individual samples. Acceleration varies continuously, it does not jump. Therefore, it is preferable to use polynomial approximation in connection with an appropriate interpolation method. The reason resides in more precise description of the real functions by parabolas rather than lines. The intent of time belongs to the most exact values measured, therefore the projection of the time error is negligible.

The final actual position is defined by the acceleration calculation onto velocity and the velocity calculation onto trajectory. Acceleration is integrated two times together with the error, which accumulates in time. This error can be eliminated by filtering, but cannot be completely removed. Therefore, it is needed to pay attention to this problem, which should lead to general inertial navigation accuracy improvement. Navigation of higher quality may find very broad utilisation in the future, for example in the storehouses, where danger materials (substances) or heavy machine parts are used.

References

Analog Devices, 2009. MEMS Inertial Sensor ADIS16405. Available at www.datasheetcatalog.com (accessed November 25, 2009).

Grewall M.S., Weil L.R., Andrews A.P., 2007. Global Positioning Systems. Inertial Navigation, and Integration. John Wiley & Sons, Inc., New Jersey.

Kačeňák M., 2001. Rombergova metóda pre numerické integrovanie a jej implementácia v prostredí MATLAB. (Romberg's method for numerical integration and its implementation in the MATLAB application). Atca Montanistica Slovaca, *6*: 82–87.

Mošová V., 2003. Numerické metódy (Numerical methods). Olomouc, UP Olomouc.

Shannon C.E., 1949. Communication in the presence of noise. Available at www.stanford.edu/class/ee104/shannonpaper.pdf (accessed August 18, 2011).

Titterton D.H., Weston J.L., 2004. Strapdown Inertial Navigation Technology. 2nd Ed. The American Institute of Aeronautics and Astronautics, Reston, USA.

Vicher M. 2003. Numerická matematika (Numerical mathematics). Available at http://physics.ujep.cz/~mlisal/apl_nm/vicher_nm1.pdf (accessed August 18, 2011).

Received fo publication December 12, 2010
Accepted after corrections June 1, 2011

Corresponding author:

Ing. Vladimír Cvikovič, Ph.D., Slovak University of Agriculture in Nitra, Faculty of Engineering, Department of Electrical Engineering, Automation and Informatics, Tr. A. Hlinku 2, 949 76 Nitra, Slovak Republic
phone: + 421 376 415 783, e-mail: vladimir. cvikovic@uniag. sk

Operating parameters and emission evaluation of tractors running on diesel oil and biofuel

D. Müllerová[1], M. Landis[2], I. Schiess[2], J. Jablonický[1], M. Prístavka[1]

[1]*Faculty of Engineering, Slovak University of Agriculture in Nitra, Nitra, Slovak Republic*
[2]*Agroscope Reckenholz-Tänikon Research Station ART, Tänikon, Ettenhausen, Switzerland*

Abstract

Müllerová D., Landis M., Schiess I., Jablonický J., Prístavka M., 2011. **Operating parameters and emission evaluation of tractors running on diesel oil and biofuel**. Res. Agr. Eng., *57 (Special Issue)*: S35–S42.

This work is aimed at the evaluation of the operating parameters and emission of two tractors: Hürlimann H-488 DT and Hürlimann XB Max 100. The measurements were done on a test bench in the laboratory of the Agroscope Reckenholz-Tänikon Research Station ART, Ettenhausen, Switzerland during February 2010. The goal of this paper was to evaluate the operating parameters of the two models of tractors by using classical diesel oil and biofuel, as well as to evaluate the emission (greenhouse gases, dangerous exhaust gases and carcinogens), to make statistical analysis of the results and the conclusion about the samples used and the impact on engine parameters, environment and human health. From the results achieved, it is possible to state the following facts. In each way, the emissions of rape seed methylester (RME) and diesel are equivalent. The values of CO and HC and also particles are lower for RME. But NO_x values are lower for diesel oil. It is liquid that the newer engine of Hürlimann XB Max 100 decreases emission of CO, HC and NO_x significantly.

Keywords: environment; biofuels; tractors; parameters; greenhouse gases (GHG)

Presently, diesel oil and petroleum products belong to the most utilised fuels. Because of its uncoverability, the crude oil is often called 'the black gold'. Unfortunately, fossil fuels are not renewable or inexhaustible sources of energy. By the prognosis of Europe's energy portal, the real exhaustion of oil will be – 22nd of October 2047. The supply of natural gas is estimated to last up to the year 2068 (Europe's energy portal 2008). The society really depends on the gas and oil supply and their depletion may cause total collapse.

In the European Union, strategy was made for the utilisation of the renewable sources of energy whose use should grow until the year 2010 by up to 12%. The expanded utilisation of biofuels in transportation is also included in the strategy and the aim is the substitution of 20% of fossil fuels by biofuels until the year 2020 (Anonymous 2007).

The aim of this paper is to perform the operating parameters and emission tests to achieve the results on the changes of these parameters by specific fuels including alternative fuel. A lot of work has been done on different fuel characteristics. Scientists found out which alternative fuel could be the most appropriate to replace diesel oil. Considering the character of agricultural production, the transport in agriculture significantly affects the economic effectiveness of the agricultural production (Korenko, Žitňák 2008; Žitňák, Korenko 2008). The most used fuels tested are crude vegetable oils made from rape seed, sunflower seed, soybeans, palm fruit and their esters. The power and torque of the engine performance are

Fig. 1. Tractor Hürlimann H-488 DT

Fig. 2. Tractor Hürlimann XB Max 100

about 3–6% lower for biodiesel. Fuel consumption is about 5–12% higher for biodiesel. Also, a great smoke reduction (50%) and lower CO and HC take place with biodiesel. If biodiesel is used, NO_x values are higher. Generally, vegetable oils and their esters have a strong potential to be used as an alternative fuel. Esters provided good results even if they were blended with diesel oil (Checchio-Grotta et al. 2008). Rape seed methylester (RME) can be also used as fuel for diesel engine without the addition of various components or additives (Walter, Schäfer 1990).

MATERIAL AND METHODS

To measure the operating parameters, two models of agricultural tractors were used: Hürlimann H-488 DT and Hürlimann XB Max 100.

Hürlimann H-488 DT (Fig. 1)

Producer:	Hürlimann/Same (I.)
Engine:	S. L. H 1000.4 WT
Number of cylinders:	4
Capacity of cylinders:	4,000 cm^3
Bore/stroke:	105 mm/115.5 mm
Rated revolution:	2,500 1/min
Rated power:	65 kW
Injector pump:	Bosch/Kolbenpumpe PFR
Year:	1994
Runtime:	3,273 h
Emission class:	Stage 0

Hürlimann XB Max 100 (Fig. 2)

Producer:	Same-Deutz Fahr
Engine:	Deutz 2012, TCD 2012 L04 2V
Number of cylinders:	4
Capacity of cylinders:	4,038 cm^3
Bore/stroke:	101 mm/126 mm
Rated revolution:	2,300 1/min
Rated power:	72.5 kW
Injector pump:	Bosch Steckpumpen
Year:	2009
Runtime:	200 h
Emission class:	Stage III.A

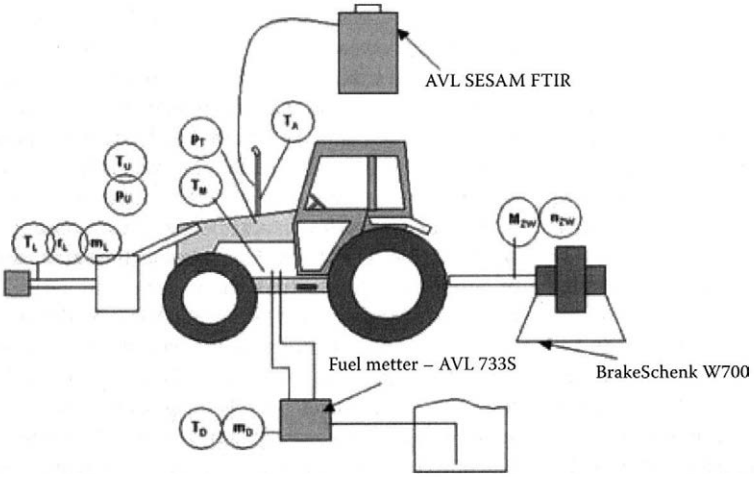

Fig. 3. Sight of the test bench

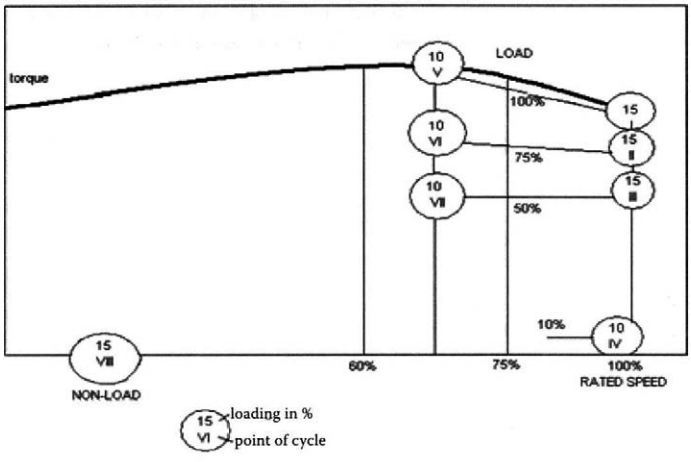

Fig. 4. Characteristics of 8-points cycle by ISO 8178-4 (2007), C_1

Specific: 100% biodiesel

The measurements were done on a test bench in Agroscope Reckenholz-Tänikon Research Station ART, Ettenhausen, Switzerland. The following measurement devices were used:

- Brake Schenck W700 (Schenck RoTec GmbH, Darmstadt, Germany) – measured torque and power, through output shaft;
- Filtermethod BOSCH (Bosch Rexroth Schweiz AG, Büttikon, Switzerland) – measured smoke, utilisation of filter layer with photo-element adapter, information in SZ Bosch (number/smoke places), smoke sonde on exhaust pipe;
- AVL 733S (AVL Graz, Graz, Austria) – measured fuel consumption, regulation (kg/h);
- Matter Engineering NanoMet C with particle counter CPC 3010D from TSI (Matter Aerosol AG, Wohlen, Switzerland) – measured particles in number/cm^3 in diluted exhaust gases, then calculated values (number/kWh);
- AVL SESAM FTIR 4 Fourier Transform Infra-Red gaseous analyser emission test system (AVL Graz, Graz, Austria) – measuring of limited and unlimited emission, values (ppm), calculated to g/kWh.

The measuring devices used were connected on the test bench. Fig. 3 is showing specific connection of the measuring devices with the parameters denoted.

Two different fuel samples were used for the measurement: diesel oil (SN 181160-1 2009) and RME (STN EN 14214 2009) – from EcoEnergie Etoy, produced in Switzerland. In Table 1, the analysis is given of the samples used. Obviously, there were just small differences between both samples. Oxidation stability of RME could be min 6 h but its value 5.2 h was good and should not have caused

Table 1. Analysis of used samples

Analysis	Abunit	Limit	Diesel oil[1]	Rape seed methylester (RME)[2]
Density by 15°C	kg/m^3	845.0	831.3	880.0
Carbon	mass. %	×	86.2	76.6
Hydrogen	mass. %	×	14.3	12.2
CFPP	°C	–20	–30	–17
Flamepoint	°C	×	67.0	×
Coldpoint	°C	–10	–10	×
Sulphur contain	mg/kg	10	7.4	×
Oxidability	h	min 6	×	5.2
Acid value	MgKOH/g sample	0.5	×	0.19
Water contain	ppm	500	×	256
Glycerol contain	%	0.02	×	0.0035

[1]Analysis by Intertek Caleb Brett, Switzerland (No. 109026/02); [2]Analysis by CleanPal, Ltd., Slovak Republic (No. 180110/D007)

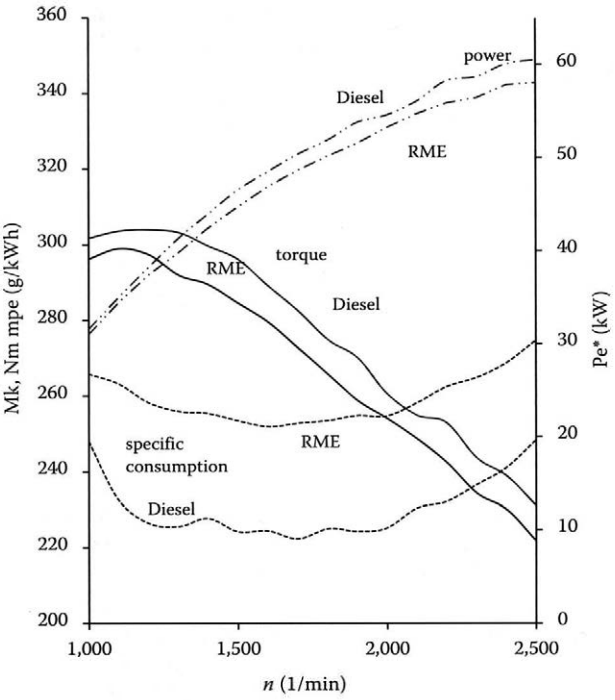

Fig. 5. External revolution curve for Hürlimann H-488 DT (for abbreviations see Fig. 6)

any problems. Also, the water and glycerol contents of RME were in the limits. They met the norm and both products could be used as engine fuel.

As the measuring method, the norm (EN ISO 8178-4 2007) was used. This norm is an international standard which is used for non-road engines. By the International Organization for Standardization (ISO), this norm specifies the test cycles for the measurement and the evaluation of gaseous and particulate exhaust emissions from reciprocating internal combustion engines, and is applicable to engines for mobile, transportable and stationary uses (Fig. 4).

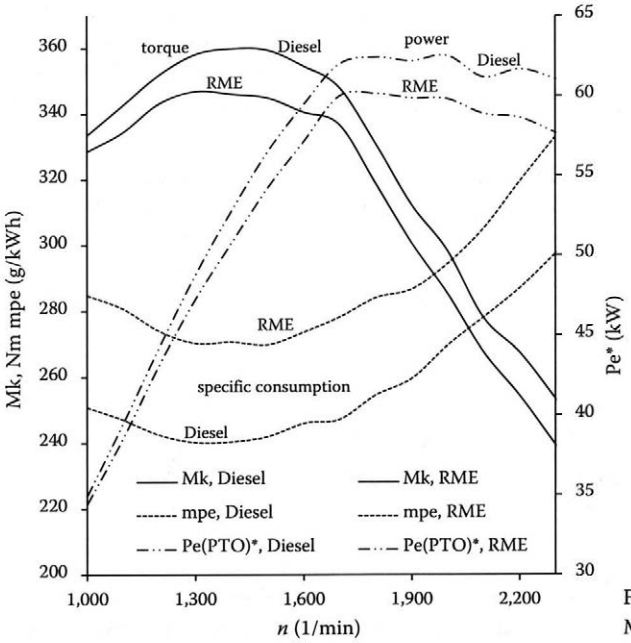

Fig. 6. External revolution curve for Hürlimann XB Max 100

Table 2. Values of limited emission

	Particle	CO	NO_x	HC
	number/kWh		g/kWh	
Hürlimann H-488 DT				
Diesel	3.93E+14	1.8	11.13	0.77
RME	3.33E+14	1.61	12.42	0.6
Hürlimann XB Max 100				
Diesel	4.31E+14	1.05	5.09	0.19
RME	2.66E+14	0.91	5.92	0.13

*average value, based on PTO (power take-off) power; RME – rape seed methylester

RESULTS AND DISCUSION

In Fig. 5 is presented the external revolution curve for Hürlimann H-488 DT, while the results obtained for Hürlimann XB Max 100 are presented in Fig. 6. Generally, there was no significant difference in the external revolution curve between both tractors but there were slight differences between diesel oil and RME characteristics:

- power and torque were lower with RME compared to diesel by about 5% at the rated power,
- fuel consumption was higher with RME by about 10% compared to diesel.

This was caused by the lower thermal capacity of methylester (37.3 MJ/kg) in comparison with the thermal capacity of diesel oil (42.5 MJ/kg). It was lower for RME by about 12%.

However, the fuel density should be also referred to, being with methylester (0.88 g/cm^3) and with diesel oil (0.82 g/cm^3), thus methylester density being higher by about 7%. This is also the reason for increasing fuel consumption and decreasing the power, and all this has to be taken into account if the individual results are compared. Based on these facts, the fuel tested may be marked as convenient for the motor engines.

Measurement of limited emission

Measurements were done with both tractors for limited emission which comprised – CO, HC, NO_x and particle by EN ISO 8178-4 (2007). In Table 2, the average values are given for each fuel based on

Table 3. Values of unlimited emission (in ppm)

Hürlimann H-488 DT	carbon dioxide	nitric oxide	nitrogen dioxide	nitrous oxide	ammonia	methane
Diesel	55,867	845	40	0.5	0.13	0.52
RME	56,769	890	43	0.66	0.21	1.27
	1.3-butadiene	hydrogen cyanide	aromatics HC	sulphur dioxide	formaldehyde	acetaldehyde
Diesel	0.97	0.57	2.1	4.6	8.1	2.7
RME	1.98	0.57	1.19	1.40	9.95	0.57
Hürlimann XB Max 100	carbon dioxide	nitric oxide	nitrogen dioxide	nitrous oxide	ammonia	methane
Diesel	64,426	378	16.9	0.43	0.12	0.1
RME	66,040	431	16.8	0.57	0.13	0.1
	1.3-butadiene	hydrogen cyanide	aromatics HC	sulphur dioxide	formaldehyde	acetaldehyde
Diesel	0.44	0.59	0.77	5.0	2.23	0.49
RME	0.90	0.45	1.19	2.9	2.08	0.73

RME – rape seed methylester

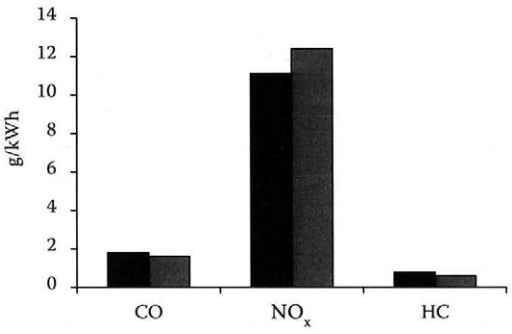

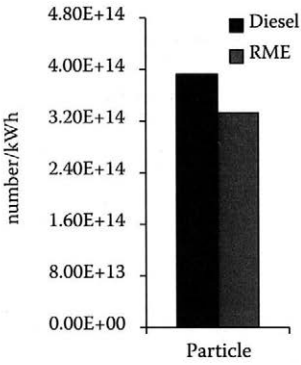

Fig. 7. Limited emission values for Hürlimann H-488 DT

power take-off (PTO) power. The graphic description for Hürlimann H-488 DT is in Fig. 7 and for Hürlimann XB Max 100 in Fig. 8.

Also, statistical analysis was carried out of limited emission using software Statistics (StatSoft, Tulsa, USA). Based on the results achieved, the method of regulatory diagram was chosen for average and standard deviations. This diagram works with the data measured on the output of the process. Standard deviation is a more effective indicator of the process variability, especially for larger subgroups. But it is more difficult for the calculation and less sensitive in the detection of determinable causes of instability introduced by the individual unusual values in the subgroups (Hrubec 2001).

Measurement of unlimited emission

Measurements were also done of unlimited emission which can be measured by AVL SESAM FTIR 4: CO_2, NO, NO_2, N_2O, NH_3, CH_4, C_4H_6, HCN, AHC, SO_2, HCHO and MECHO. In Table 3, the average values are shown for each fuel based on PTO power.

Measurement of smoke

The values of smoke in the exhaust gases are usually considerably lower with RME than with diesel oil. For the older tractor Hürlimann H-488 DT, the value of smoke was by more than 50% lower with RME than with diesel oil. From Fig. 9, it is evident that the newer tractor Hürlimann XB Max 100 had about 90% lower value of smoke than the tractor Hürlimann H-488 DT at maximal torque (MaxD). These values approached zero by using RME or diesel oil. The value of the emitted smoke was also determined at 95% and 70% of the rated revolution.

As for the operating parameters of the engine run on vegetable oils methylester as given by Walter and Schäfer (1990), the consumption and power are similar to the conventional fuel and there is not needed for the engine modification. Methylester can be used as fuel without using additives. Also according to Krahl et al. (1992), there is no need for the engine modification. Based on our results, we can confirm these theories and our results can be integrated into the existing information system. We have identical attitude to the emitted smoke measurements. As given by Sahoo et al. (2009), by us-

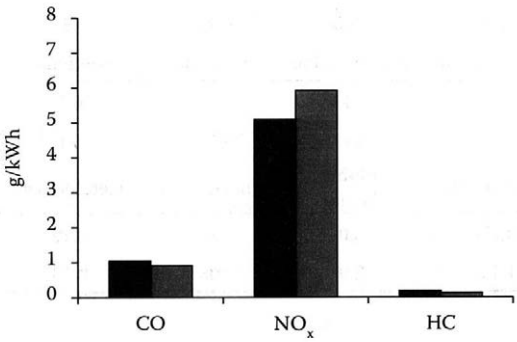

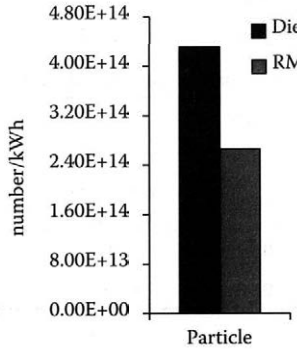

Fig. 8. Limited emission values for Hürlimann XB Max 100

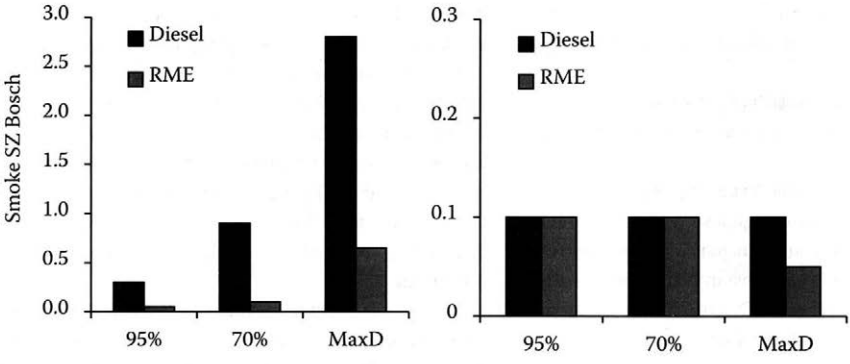

Fig. 9. Measurement of smoke (MaxD – maximal torque)

ing biofuel and full blends containing it, a significant emitted smoke reduction is reached. In our case, the reduction was up to 50%. By the biofuel utilisation, we also achieved limited emission reduction (CO, HC and particles), but also an increase of NO_x emission, similarly as presented by THUNEKE and EMBERGER (2007), THUNEKE et al. (2009). This evaluation can be affirmed by our results published. The significant unlimited emissions reduction can be monitored in the sphere of aromatic hydrocarbons, formaldehyde, sulphur dioxide, and hydrocyanic acid by using biofuel. These results agree with the publication by WÖRGETTER and WURST (1990).

CONCLUSION

The measured values are based on PTO power, thus they can not be evaluated by the Emission Standards for Off-Road Vehicles. If these measurements had been done on the engines, both tractors would have met the emission norm for CO and HC of RME and diesel. The values of NO_x were higher by about 21% for both fuels with Hürlimann H-488 DT, and by about 25% with Hürlimann XB Max 100 than the determined emission limit.

The values of unlimited emission for both fuels are equivalent. The tractor which used RME revealed not only higher values of NO_x (NO, NO_2 and N_2O) but also by almost 50% higher values of ammonia, methane, and 1.3-butadiene which are considered dangerous substances. With the newer tractor Hürlimann XB Max 100, higher values of NO_x, 1,3-butadiene, and acetaldehyde were obtained with RME use but the difference was not too great. On the other side, lower values were observed with RME for sulphur dioxide and acetaldehyde with Hürlimann H-488 DT, and for sulphur dioxide, hydrogen cyanide, and formaldehyde with Hürlimann XB Max 100. Nevertheless, the values of unlimited emission are negligible, except carbon dioxide where higher values could be seen for RME with both tractors. Statistical analysis shows the standard deviation from the determined value by the norm for emission – CO, HC and NO_x. From the graphs, it is evident that a higher value of the standard deviation occurred in the 4th point. That means at maximal revolution without loading.

The purpose of this work was to evaluate the operating parameters of two models of tractors by using classic diesel oil and biofuel. It is possible to state that the differences between these two tractors are inherent in their engines construction, the year of production, and specification (Hürlimann XB Max 100 is specified as 100% biodiesel). On the evaluation of the emission [greenhouse gases (GHG), dangerous exhaust gases and carcinogens] it can be declared that it is very important to study not just the limited but also unlimited emissions which can be very dangerous, although it was discovered in this work that the values of unlimited emission did not exceed the lethal limit.

References

ANONYMOUS, 2007. Stratégia vyššieho využitia obnoviteľných zdrojov energie v SR (The strategy of higher utilization of renewable sources of energy). Available at www.economy.gov.sk/strategia-vyssieho-vyuzitia-oze-6320/128005s

CHECCHIO-GROTTA D.C., LOPES A., FURLANI C.E.A., DA SILVA R.P, DOS REIS G.N., CORTEZ J.W., 2008. Filtered ethyl ester biodiesel from residual soybean oil: performance of an agricultural tractor in the disk harrow operation. Acta Scientiarum: Technology, *30*: 135–138.

EN ISO 8178-4, 2007. Piestové spaľovacie motory. Meranie emisií výfukových plynov. Skúšobné cykly na rôzne použitie

motora (Reciprocating internal combustion engines. Exhaust emission measurement. Steady-state test cycles for different engine).

Europe's energy portal, 2008. Available at http://www.energy.eu/

Hrubec J., 2001. Riadenie kvality (Control of Quality). Nitra, SPU in Nitra: 202.

Korenko M., Žitnák M., 2008. Využitie strojov pri zbere a doprave balíkov slamy na energetické účely. (Machines utilization during harvest and transport of straw bales for energetic purposes) In: Perspective in Education Process at Universities with Technical-Orientation in Visegrad Countries: International Science Conference. Nitra, SPU in Nitra: 275–279.

Krahl J., Vellguth G., Bahadir M., 1992. Determination of the exhaust-gas emissions of agricultural tractors running on rape seed oil methylester in comparison with diesel fuel. Landbauforschung Volkenrode, *42*: 247–254.

Raslavicius L., Bazaras Z., 2009. The analysis of motor characteristics of D-RME-E fuel blends during on-field tests. Transport, *24*: 187–191.

Sahoo P.K., Das L.M., Babu M.K.G., Arora P., Singh V.P., Kumar N.R., Varyani T.S., 2009. Comparative evaluation of performance and emission characteristics of jatropha, karanja and polanga based biodiesel as fuel in a tractor engine. Fuel, *88*: 1698–1707.

SN 181160-1, 2009. Mineralölprodukte – Qualitätsrichtlinien für Dieseltreibstoff (Petroleum products – Quality guidelines for diesel fuel).

STN EN 14214, 2009. Motorové palivá. Metylestery mastných kyselín (MERO) pre naftové motory. Požiadavky a skúšobné metódy (Automotive fuels. Fatty acid methyl esters (FAME) for diesel engines. Requirements and test methods).

Thuneke K., Emberger P., 2007. Exhaust gas emission characteristics of rapeseed oil fuelled tractors – investigations at a test stand. In: Engineering Solutions for Energy and Food Production: The 65th Conference on Agricultural Engineering, November 9–10, 2007. Hanover, VDI Wissensforum: 47–52.

Thuneke K., Gassner T., Emberger P., 2009. Rapsölkraftstoff – Traktoren am Prüfstand und im Feldeinsatz. (Rape Seed Oil as Fuel – Tractors on the Test Bench and on the Field). Straubing, Technologie- und Förderzentrum, Bayerisches Staatsministerium für Ernährung.

Walter H., Schäfer H., 1990. Rape Seed Oil Fatty Acid Metylester as a Fuel for Commercial Vehicles Diesel Engines. ATZ Automobiltechnische Zeitschrift, 92.

Wörgetter M., Wurst F., 1990. Emission beim Einsatz von Rapsölmethylester in Traktoren. Der Förderungsdienst, Heft 6: 154–163.

Žitňák M., Korenko M. 2008. Výkonnosť a energetická náročnosť dopravných prostriedkov pri zbere a doprave balíkov slamy. (Performance and energetic demandingness of vehicles during harvest and transport of straw bales) In: Vozidlá 2008: Nové trendy v konštrukcii a exploatácii vozidiel. Nitra, SPU in Nitra: 181–185.

Received for publication December 7, 2010
Accepted after corrections April 14, 2011

Corresponding author:

Ing. Daniela Müllerová, Slovak University of Agriculture in Nitra, Faculty of Engineering, Department of Transport and Handling, Tr. A. Hlinku 2, 949 76 Nitra, Slovak Republic
phone: + 421 907 562 864, e-mail: mullerova.daniela@gmail.com

The comparison of biodegradable hydraulic fluid with mineral oil on the basis of selected parameters

R. Majdan, J. Kosiba, J. Tulík, D. Kročková, V. Šinský

Department of Transport and Handling, Faculty of Engineering, Slovak Agriculture University in Nitra, Nitra, Slovak Republic

Abstract

Majdan R., Kosiba J., Tulík J., Kročková D., Šinský V., 2011. **The comparison of biodegradable hydraulic fluid with mineral oil on the basis of selected parameters.** Res. Agr. Eng., *57 (Special Issue)*: S43–S49.

The paper presents a comparison of two fluids quality. The first one was mineral oil type UTTO which is commonly used in the transmission and hydraulic systems of agricultural tractors. The second one tested was biodegradable hydraulic fluid type ERTTO which could replace the toxic mineral oil. Both fluids were tested under the same test conditions using a special test device. The selected parameters of the hydrostatic pump were evaluated. The tests were evaluated according to the parameters describing the technical state of the hydrostatic pump as follows: flow efficiency, decrease of flow efficiency and cleanliness level of the fluid tested. This additional measurement verifies the test results. On the basis of the results achieved, we can state that the biodegradable hydraulic fluid exerts no harmful influence on the technical state of the hydrostatic pump. Therefore, the biodegradable fluid tested can be applied to the agricultural tractor. Has been demonstrated that the selected parameters are suitable for the evaluation of hydraulic fluid during its working performance. Therefore, these parameters will be used in the next examination of the fluid under operational conditions of an agricultural tractor.

Keywords: cleanliness level; hydrostatic pump; flow efficiency; agricultural tractor

The durability and reliability of hydraulic systems depend among others on the hydraulic fluid used. Hydraulic fluids are used for the transmission of energy and control the hydraulic components. Another significant role is the lubrication in the operational system. In practice, it is often needed to integrate new and often contradictory properties of hydraulic fluids resulting from the increasing use of hydraulic systems in more and more extreme conditions, e.g. temperature, pressure, military engineering, space research etc. (Jobbágy et al. 2003; Petranský et al. 2003; Tkáč et al. 2005).

This article presents a comparison between biodegradable hydraulic fluid and mineral oil. The tests were realised in the laboratory of the Department of Transport and Handling of the Faculty of Engineering, Slovak University of Agriculture in Nitra.

MATERIAL AND METHODS

The tests were carried out as follows:

- test was realised on a special test device according to the standard STN 11 9287 (1983) and the work published by Radhakrishanan (2003),
- hydraulic pump was loaded with cyclically changing pressure from 0.1 MPa to the nominal pressure of the hydraulic pump 20 MPa during the test,

Supported by the Scientific Grant Agency VEGA of the Ministry of Education of the Slovak Republic and the Slovak Academy of Sciences, Grant No. 1/0462/09.

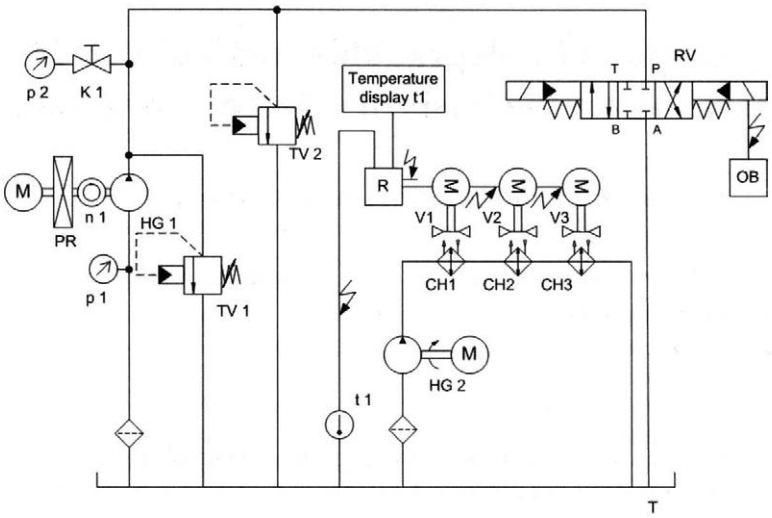

Fig. 1. Test device for realisation of laboratory durability test of hydrostatic pumps (TKÁČ et al. 2008)
M – electric motor, n 1 – rpm sensor, HG 1 – tested hydrostatic pump, TV 1 – two stage pressure relief valve, TV 2 – two stage sequence valve for adjusting nominal pressure in the hydrostatic pump outlet, p 1 – pressure gauge of pressure in the inlet, p 2 – pressure gauge of pressure in the outlet, K 1 – spherical plug valve, PR – gear box, OB – control block, T – tank, RV – tree-positions, four-port slide valve with closed center which is operated electro-hydraulically, CH 1, CH 2, CH 3 – coolers, V 1, V 2, V 3 – fans, HG 2 – hydrostatic pump for cooler, t 1 – temperature sensor for tank, R – thermostatic regulator which controls switching on of cooling fans

- the criteria of quality of the tested fluids comprised the flow efficiency, decrease of flow efficiency and fluids contamination (SLOBODA, SLOBODA 2002; MIHALČOVÁ, AL HAKIN 2008, 2009),
- fow efficiency was calculated from the flow characteristics measured,
- flow characteristics and the selected parameters were determined every 250,000 cycles until ending the test after 10^6 pressure load cycles.

Mineral oil MOL Traktol NH Ultra

MOL Traktol NH Ultra is a UTTO-type (Universal Tractor Transmission Oil) lubricant which can also be used in the gears and hydraulic systems of the tractors fulfilling the requirements generated by heavy loads in a wide range of the operating temperature. The fluid was made by the company Slovnaft, Ltd. (Bratislava, Slovak Republic). The product is suitable for use in wet brakes as well a long drain lubricant for cog-wheel gears, equalising gears, Power-Shift transmissions, wet break- and hydraulic control systems of agricultural and forest off-road machines and tractors. This oil belongs to the group of universal tractor oils UTTO. The technical parameters are listed in Table 1.

Table 1. Technical parameters of mineral oil MOL Traktol NH Ultra

Parameter	Value
Kinematic viscosity under 100°C (mm^2/s)	10.7
Kinematic viscosity under 40°C (mm^2/s)	60
Specific weight under 15°C (g/cm^3)	0.888
Viscosity class	SAE 80W
Performance level	API GL-4

Biodegradable hydraulic fluid MOL Traktol ERTTO

The hydraulic fluid is of an ERTTO-type (Environmentally Responsible Tractor Transmission

Table 2. Technical parameters of biodegradable fluid MOL Traktol ERTTO

Parameter	Value
Kinematic viscosity under 100°C (mm^2/s)	10.38
Kinematic viscosity under 40°C (mm^2/s)	47.89
Viscosity index VI (–)	213
Congealing point (°C)	–39

Table 3. The evaluation of mineral oil test

Cycle count	Rotation speed (n = 1,500 rpm)			
	flow Q (dm^3/min)	flow efficiency η (%)		decrease of flow efficiency Δ η (%)
0	35.98	0.959	95.9	0
250,000	36.46	0.972	97.2	–1.33
500,000	36.85	0.983	98.2	–2.42
750,000	36.91	0.984	98.4	–2.58
1,000,000	36.05	0.961	96.13	–0.19

Oil) and is biodegradable tractor oil. The fluid was made by the company Slovnaft, Ltd. The oil is made from vegetable natural oil and special additives. The oil is destined for use in the gearbox and hydraulic circuit of agricultural and construction machines. Primary biodegradation per CECL-33-A-93 is 90% within 28 days and test method OECD 301 B is 65%. The technical parameters are listed in Table 2.

The test device designed to tests of hydrostatic fluids

The designed test device (Fig. 1 shows the schema) enables to test the hydraulic fluids on the ground of the evaluation of the technical state of the hydrostatic pump which is tested with the fluid. In this case, the load of the hydrostatic pump and fluid is realised by cyclic pressure loading under pressure changing from p = 0.1 MPa to the nominal pressure p = 20 MPa, frequency f = 1.1 Hz, and velocity of pressure increasing v = 340 MPa/s. Radhakrishanan (2003) also presented this type of fluid test. The cyclic pressure loading is technically realised by the cyclic change of the slide valve position RV. This valve changes its state from the central position to the left position. The nominal pressure on the pump outlet is limited by the sequence pressure valve TV 2. The test device was designed according to the works published by Tkáč et al. (2001, 2003, 2006), Horka et al. (2005).

The calculation of flow efficiency decrease

The standard STN 11 9287 (1983) determines the way of the test evaluation. The fluid must be evaluated by flow efficiency decrease of the hydrostatic pump as follows:

$$\Delta\eta_{pr} = \frac{\eta_{pr0} - \eta_{prm}}{\eta_{pr0}} \times 100 \quad \% \tag{1}$$

where:

$\Delta\eta_{pr}$ – the flow efficiency decrease (%)

η_{pr0} – the flow efficiency at 0 cycles (start of the fluid test)

η_{prm} – the flow efficiency after 10^6 cycles (end of the fluid test)

Then, the flow efficiency is expressed by the Eq.:

$$\eta_{pr} = \frac{Q_2}{V_G \times n} \times 100 \quad \% \tag{2}$$

where:

Q_2 – flow of hydrostatic pump (dm^3/min)

V_G – geometrical volume of hydrostatic pump (dm^3)

n – nominal rotation speed of hydrostatic pump (1/min)

Table 4. The evaluation of biodegradable fluid test

Cycles count	Rotation speed (n = 1,500 rpm)			
	flow Q (dm^3/min)	flow efficiency η (%)		decrease of flow efficiency Δ η (%)
0	36.549	0.975	97.5	0
250,000	37.035	0.988	98.8	–14
500,000	36.634	0.977	97.7	–0.2
750,000	35.337	0.942	94.2	3.2
1,000,000	33.958	0.906	90.4	7.3

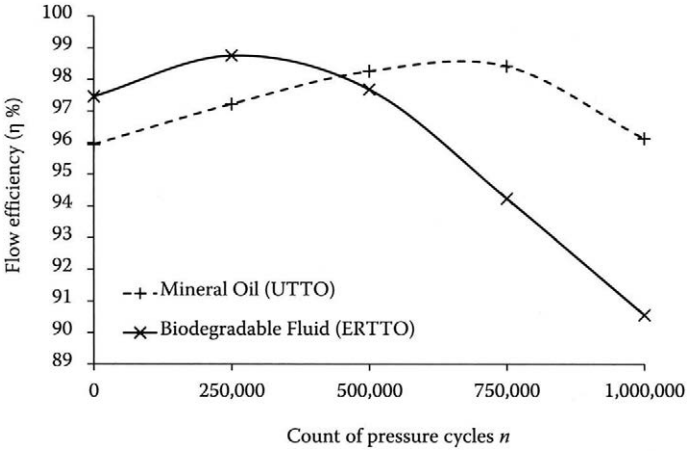

Fig. 2. The comparison between the biodegradable fluid (ERTTO) and the mineral oil (UTTO) on the basis of flow efficiency

RESULTS AND DISCUSSION

Test of mineral oil MOL Traktol NH Ultra

Table 3 shows the calculated flow rate, flow efficiency, and decrease of flow efficiency coming from mineral oil test at the rated speed n = 1,500 rpm. All values have been calculated from the measurements of the flow rate characteristics of the hydraulic pump UD 25 (Jihostroj Ltd., Velesin, Czech Republic). The flow rate characteristics were measured every 250,000 cycles during the fluid test.

Test of biodegradable hydraulic fluid

In Table 4 are the calculated values of flow rate, flow efficiency, and flow efficiency decrease of biodegradable fluid at the rated speed of the hydraulic pump n = 1,500 rpm. All values have been calculated from the measurements of the flow rate characteristics of the hydraulic pump type UD 25. The flow rate characteristics were measured every 250,000 cycles during the fluid test.

The comparison of biodegradable fluid with mineral oil

In Fig. 2 can be seen the comparison between the biodegradable fluid and mineral oil based on the tests performed with the test device (Fig. 1). The value of the flow efficiency of the biodegradable oil was decreased after the test as compared to the value measured before the test, while with the mineral oil no decrease was recorded.

In the case of the mineral oil test, the flow efficiency at the end of the test (η = 96.1%) was higher than at the beginning (η = 95.9%). Fig. 2 shows that no decrease of the flow efficiency occurred (dashed

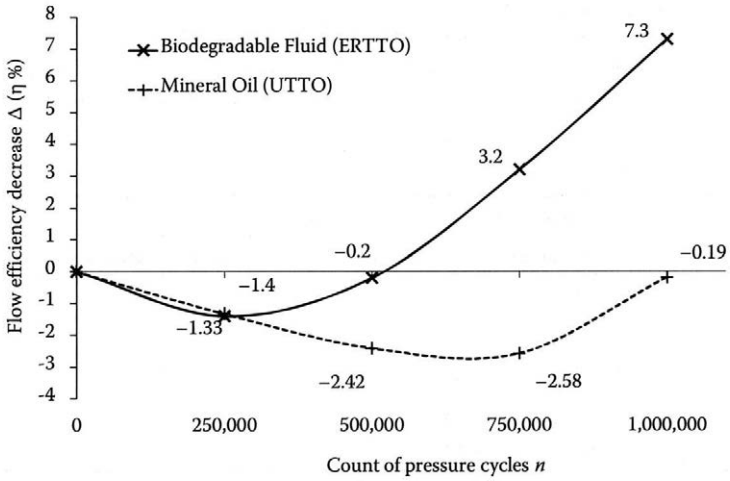

Fig. 3. The Comparison between the biodegradable fluid (ERTTO) and the mineral oil (UTTO) on the basis of flow efficiency decrease

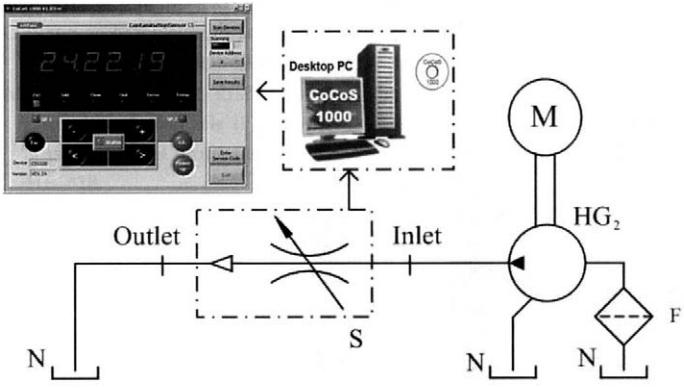

Fig. 4. The device CS 1000 intended for the measurement of fluid cleanliness level in the test device
N – tank of test device, S – contamination sensor, F – filter, HG_2 – pump which transports fluid through contamination sensor, M – electric motor

line). During the mineral oil test, the hydraulic pump was just running-in, which is expressed by the negative values listed in Table 3 and Fig. 3.

In the case of the biodegradable fluid, the flow efficiency at the end of the test (η = 90.4%) was lower than at the beginning (η = 97.464%). Fig. 2 shows this flow efficiency decrease (solid line). During the test of the biodegradable fluid, the hydraulic pump was only running-in to 500,000 cycles, which is expressed by the negative values listed in Table 4 and Fig. 3.

The cleanliness level of biodegradable fluid

The cleanliness level was measured with the help of the device type CS 1000 (Fig. 4; Hydac GmbH, Sulzbach, Germany), which enables to evaluate the fluids according to ISO 4406 (1999).

During the machine operation, all the particles resulting from wear and tear are collected in the fluid. The standard ISO 4406 (1999) evaluates the fluid pollution on the basis of three quantitative classes measurements. The classes are destined by the numbers of particles bigger that 4 μm, 6 μm and 14 μm. The classes are depicted in the form of columns in the graphs (Figs 5 and 6). Biodegradable fluid contamination is shown in Fig. 5.

The cleanliness level of mineral oil

Mineral oil contamination is shown in Fig. 6. In this case, the same test device was used for the evaluation of the cleanliness level by the standard ISO 4406 (1999).

CONCLUSION

This article presents a comparison between a new type of biodegradable hydraulic fluid ERTTO and the conventionally used mineral oil type UTTO. These

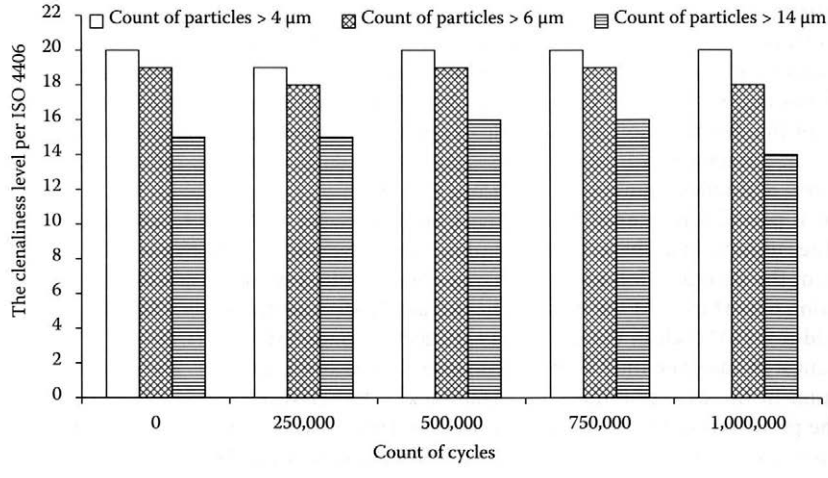

Fig. 5. Cleanliness level of biodegradable fluid evaluated as per ISO 4406 (1999)

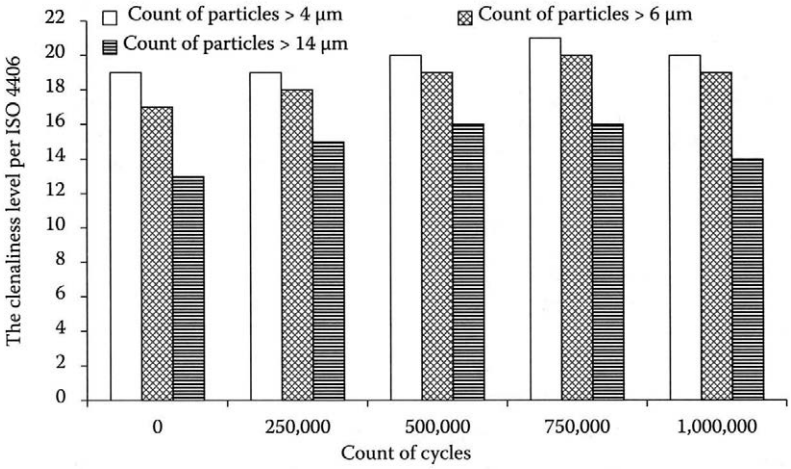

Fig. 6. Cleanliness level of mineral oil evaluated as per ISO 4406 (1999)

fluids have been evaluated on the basis of the technical state of the tractor hydraulic pump type UD 25 used during the test. The evaluation parameters were the flow efficiency and decrease of the flow efficiency; these were calculated based on the measured and statistically processed values of the flow rate. All results were transposed to graphs and tables.

The flow characteristics inform us about the process of deterioration during the tests of both fluids. In the case of the biodegradable fluid test (Figs 2 and 3), it is obvious that the flow on the output of the hydrostatic pump rose to 500,000 cycles. The parameters of the hydrostatic pump were improving. It is possible to explain it by the running-in at the beginning of the test. After 750,000 cycles, the flow started to decline, and at the end of the test the flow declined under the rated one measured within 0 cycles (new hydrostatic pump). The described development of the hydrostatic pump deterioration was confirmed also by the thermo-visual and fluid contamination measurements.

The particles arising from wear and tear are captured in the oil. The oil may also serve as the indicator for the evaluation of the deterioration process. Figs 5 and 6 describe the process of hydrostatic pump deterioration in view of fluid contamination evaluation. The number of particles rose until the end of the running-in. The running-in is characterised by the speeding-up of the deterioration process and a higher production of particles. At the end of the biodegradable fluid test (10^6 cycles), the decline in the particles count was observed only with big particles above 14 μm. In the case of mineral oil test, the decline of the particle count was found with particles above 14 μm and 6 μm.

On the fluids comparison, we can state that the mineral oil has better attributes than the biodegradable oil. While during the mineral oil test the hydraulic pump was just running-in, during the biodegradable oil test we recorded 7.3 per cent decrease of the flow efficiency (Fig. 3). This value is lower than maximum limit 20 per cent given by the standard STN 11 9287 (1983). Therefore, the biodegradable fluid tested can be applied to the agricultural tractor.

As mentioned above, all the parameters selected describe the deterioration process of the hydrostatic pump with which the fluid test was realised. Therefore, these parameters will be used to observe the application of the new biodegradable fluid under conditions of the agricultural tractor operation.

References

ISO 4406, 1999. Hydraulic fluid power – Fluids – Method for coding the level of contamination by solid particles.

Jobbágy J., Petranský I., Simoník J., 2003. Tlakové režimy v hydraulike traktorov ZTS v súprave s poľnohospodárskym náradím (The pressure states in hydraulic of tractor ZTS in set agricultural implements). In: International Student's Scientifics Conference, April 1–2, 2003. Nitra, SAU in Nitra: 94–101.

Horka M., Žarnovský J., Kováč I., 2005. Diagnostika hydraulického návesného systému traktorov UR II (Diagnostic of hydraulic semi trailer system of the tractor UR II). In: Hydraulické Mechanizmy Mobilnej Techniky, October 19–21, 2005. Dudince, SAU in Nitra: 36–41.

Petranský I., Drabant Š., Ďuďák J., Žikla A., Grman I., Jablonický J., 2003. Pressure in the hydraulic system of three point hitch of tractor equiped with electrical and mechanical control. Research in Agricultural Engineering, *49*: 37–43.

Mihalčová J., Al Hakim H., 2008. Tribotechnical diagnostics in waste oil operation I – Methods of evaluation of wear particles in oils. Chemické listy, *102*: 358–362.

Mihalčová J., Al Hakim H., 2009. Tribotechnical diagnostics of used oils II – Methods of assessment of physicochemical properties of oils. Chemické listy, *103*: 416–418.

Radhakrishanan M., 2003. Hydraulic Fluids. New York, American Society of Mechanical Engineers: 267.

Sloboda A. jr., Sloboda A., 2002. Využitie tribotechnickej diagnostiky z pohľadu bezpečnosti prevádzky pre núdzový hydraulický okruh lietadla (The use of tribotechnical diagnostic from view of safe operation for emergency hydraulic system of aeroplane). Acta Mechanica Slovaca, *3*: 107–113.

STN 11 9287, 1983. Jednotný systém hydrauliky všeobecného strojárstva. Hydrostatické zubové generátory a motory pre tlaky p|idx(n)| 16, 20 a 25 MPa. Technické požiadavky (Unified system of industrial hydraulic components. Hydrostatic gear generators and motors for p|idx(n)| 16, 20 and 25 MPa. Technical requirements).

Tkáč Z., Škulec R., Hujo Ľ., Jablonický J., 2001. Skúška traktora s biologicky odbúrateľným olejom Ekouniverzal (The test of tractor with biodegradable fluid Ekouniverzal). In: III. Student's Scientifics Conference, September 19–20, 2001. Prague, Czech Agricultural University: 127–132.

Tkáč Z., Petranský I., Varga D., Hujo Ľ., Bolla M., 2003. Hydraulický a prevodový systém traktora ZTS 8011 pri práci s bioolejom (The hydraulic and transmission system of tractor type ZTS 8011 under operation with biodegradable oil). Hydraulika a pneumatika, *5*: 32–35.

Tkáč Z., Jablonický J., Abrahám R., Klusa J., 2005. Measurement of pressure in hydraulics system of the ZTS 160 45 tractor. Research in Agricultural Engineering, *51*: 140–144.

Tkáč Z., Drabant Š., Žikla A., Abrahám R., 2006. The tests of the ZTS 122 45 tractor with biodegradable oil. In: Automotive Industry – Carrier of Technological Progress, October 4–6, 2006. Kragujevac, Faculty of Mechanical Engineering in Kragujevac: 12–17.

Tkáč Z., Drabant Š., Majdan R., Cvíčela P., 2008. Testing stands for laboratory tests of hydrostatic pump of agricultural machinery. Research in Agricultural Engineering, *54*: 183–191.

Received for publication January 18, 2011
Accepted after corrections October 31, 2011

Corresponding author:

Ing. Radoslav Majdan, Ph.D., Slovak Agriculture University in Nitra, Faculty of Engineering, Department of Transport and Handling, Tr. A. Hlinku 2, 949 76 Nitra, Slovak Republic
phone: + 421 904 198 433, e-mail: radoslav.majdan@gmail.com

Influence of welding method on microstructural creation of welded joints

P. Čičo[1], D. Kalincová[2], M. Kotus[1]

[1]*Faculty of Engineering, Slovak University of Agriculture in Nitra, Nitra, Slovak Republic*
[2]*Faculty of Environmental and Manufacturing Technology, Technical University in Zvolen, Zvolen, Slovak Republic*

Abstract

Čičo P., Kalincová D., Kotus M., 2011. **Influence of welding method on microstructural creation of welded joints**. Res. Agr. Eng., *57 (Special Issue)*: S50–S56.

This paper is focused on the analysis of the welding technology influence on the microstructure production and quality of the welded joint. Steel of class STN 41 1375 was selected for the experiment, the samples were welded by arc welding including two methods: a manual one by coated electrode and gas metal arc welding method. Macro and microstructural analyses of the experimental welded joints confirmed that the welding parameters affected the welded joint structure in terms of the grain size and character of the structural phase.

Keywords: thermal field; arc welding; coated electrode; gas metal arc welding GMAW (method); metallographical analysis

Welding is a production technology of non-demountable joints of two materials, whose principal mechanical or structural attributes succumb to the changes of the temperature influence from molten weld metal. The welded joint becomes heterogeneous part of the construction. Manufacturing degradation is brought into the parent material by welding; therefore, the individual welded joints have to be controlled by the standard STN EN ISO 15614-1 (2005) for the proposal of the welding way and parameters.

The tests of the joint welding, following this standard, are divided into non-destructive and destructive. The integrity, mechanical properties, and structure are mostly controlled. Every welding method is characterised by specific effects on the parent material in terms of the heat generated the welding process. The impact of the thermal changes resides in the changes of the properties in the welded joints zone. These depend on the chemical composition, material thickness, joint shape, welding conditions, but also on the physical characteristics of the welded materials (heat conduction, specific heat, etc.).

Heat input, heat field and heat cycle

Heat source causes changes of the joint materials temperature depending on the time and location in relation to the heat source in welding. The temperature distribution depending on time is called heat field. It can be calculated by means of differential equations of the heat conductance in solid bodies.

Rosenthal (1946) and Rykalin (1957) suggested its calculation for point linear movement of the source by Eq. (1) of the heat conductance in solid state.

Supported by the Scientific Grant Agency VEGA of the Ministry of Education of the Slovak Republic and the Slovak Academy of Sciences, Grant No. 1/0511/08.

$$\frac{\delta^2 T}{\delta x^2}+\frac{\delta^2 T}{\delta y^2}+\frac{\delta^2 T}{\delta z^2}=\frac{1}{a}\frac{\delta T}{\delta t} \quad (1)$$

where:

x, y, z – coordinates of the location

T – temperature (K)

$$a=\frac{\lambda}{\rho \times c} \quad (2)$$

whre:

λ – coefficient of heat conductance

$\rho \times c$ – volume heat capacity (J/m^3 K)

Thermal changes caused by electrical arc welding are characteristic by high speed of heating and cooling and the temperature gradient depending on the distance from the weld. The temperature changes of one spot of the welded joint depending on time characterise the heat cycle of the welding, that is the time change of temperature (Fig. 1) (Brziak et al. 2003). The structure formation of the welded joint significantly relates to the welding method selection because the given heat input increases proportionally with voltage and welding current which depend on the way of welding.

Different combinations of voltage and current (e.g. U = 24 V, I = 82 A) are used in manual electrical arc welding as compared to the welding method gas metal arc welding (GMAW) (e.g. U = 18–35 V, I = 120–380 A). There are also differences in the welding speed.

The thickness of the welded materials affects the speed of the weld cooling and also the transformational processes in austenitic structure of the heated heat affected zone (HAZ) of the parent material. Therefore, the final structure of the welded joint as a unit depends on whether the heat dissipation is two or three dimensional. The cooling speed of the welded sheet metal at two-dimensional heat dissipation (Fig. 2) depends on the thickness. The cooling speed at three-dimensional heat dissipation (Fig. 2) does not depend on the thickness of the sheet metal. The time of cooling $t_{8/5}$, which is calculated by means of Uwer and Degenkolbe (1976) equation for the individual ways of welding, is very important within the structural formation in HAZ.

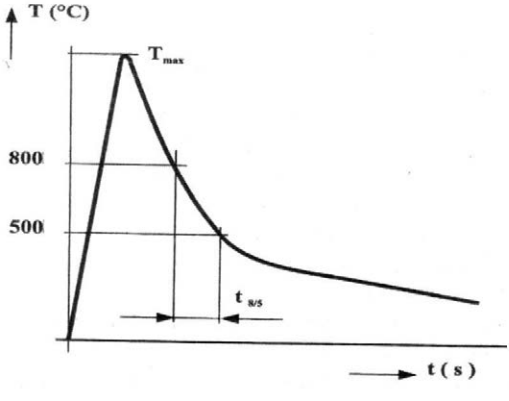

Fig. 1. Heat cycle of welding (Brziak et al. 2003)

For example, for three-dimensional heat dissipation:

$$t_{8/5}=K_3 \times Q \times \left(\frac{1}{500-T_0}-\frac{1}{800-T_0}\right) \times F_3 \quad (3)$$

where:

F_3 – factor of the weld shape

K_3 – proportional coefficient of heat dissipation

Q – heat input

T_0 – parent material temperature

$t_{8/5}$ – time of cooling

The boundary between two-dimensional and three-dimensional heat dissipation is formed by the so called transition thickness.

Structure of welded joint

Primary crystallisation of low-carbon and medium-carbon steel appears at a larger degree or a smaller degree peritecticly. The fact that secondary crystallisation can also develop in the dendrites and can get within the dendrites to boundary movement immediately after their formation leads to connections, which are not observable at the first sight. The structure of HAZ welded steel connects to phase balance in system Fe-Fe$_3$C. Fig. 3 illustrates the scheme of the heat field created in the joint vicinity at welding. Significant heat intervals 1–7 effective for low-carbon steel are derived from Fe-Fe$_3$C diagram. According to the initiate scheme for low-carbon steel welding, the following zones are distinguished in the heat impacted area (Štifner 2004):

Weld metal – its structure formats by cooling of the melt at a temperature of about 1,500°C, crystals of columnar type are formatted preferentially in the

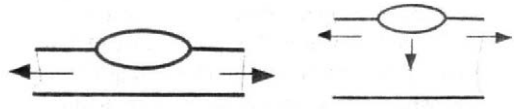

Fig. 2. Scheme of two-dimensional (left) and three-dimensional (right) heat dissipation

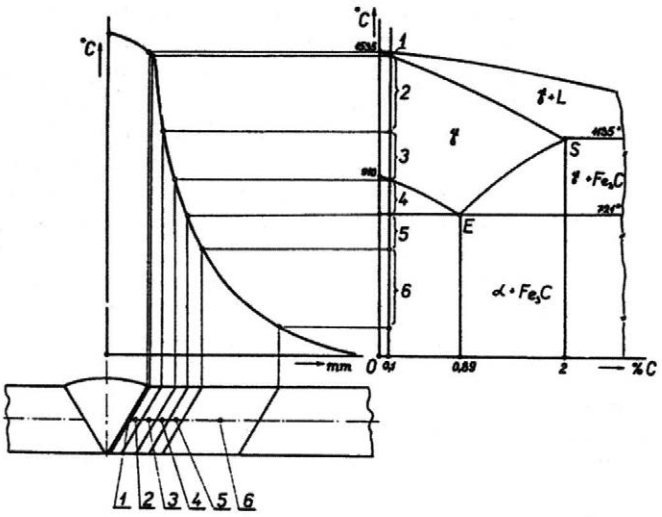

Fig. 3. Scheme of heat field of welded joint (ŠTIFNER 2004)

line of the heat dissipation. The welded metal has the structure of cast steel.

1. Partial melting-down zone – is a sharp-edged boundary between the welded metal and overheat zone. Partial melting-down zone usually presents more significant Widmannstätten structure.
2. Overheat zone – corresponds to the overheated material up to temperatures of the solid (1,050°C). The overheated coarse-grained austenitic structure and coarse-grained ferrite-perlitic structure after recrystallization are formed in realisation of more dimensional joints in this zone. Ferrite is commonly disengaged along the boundaries of the initial austenitic grains Widmannstättenicly.
3. Normalisation zone – includes the zone of temperatures above A_{c3} max 100–150°C. Complete austenitic initial structure is formed in the zone of normalisation annealing and according to the speed of cooling, the final structure is formed: ferrite-perlitic structure at slow cooling, bainitic at accelerated cooling, bainitic-martensitic at quick cooling, and martensitic at very quick cooling.
4. Incomplete recrystallization zone – heating of the ultimate material between A_{c1} and A_{c3} in low-carbon steel in the range of 725–900°C can cause very interesting changes of microstructure. Temperatures closely under A_{c1} create spheroidal perlite while those above A_{c1} cause in ferrite-perlitic steel the melting of perlite and subsequently also ferrite. Spheroidal perlite (in the case of a higher content of carbon and quick cooling hardening can occur in this zone) is formed by cooling.
5. Recrystallization zone – recrystallization can occur only on precondition that the welded material is in work hardening state. The zone of the heat recrystallization is in range from 500–725°C. Quantitative picture analysis of the welded joint structure (MARTINKOVIČ, ŠUGÁR 1994) could help with more detailed description of the phenomena that run the structure formation at welding.
6. Blue brittle zone – the temperature reaches up to 500°C. The heating of the parent material does not cause microscopic changes at the above mentioned temperature. However, significant sub-microscopic changes may occur.

The object of the experiment is the comparison of the microstructure of welded joints manufactured by two welding methods.

MATERIAL AND METHODS

Characteristics of sample and filler materials

The welding of the samples was carried out by following the standard STN EN ISO 15614-1 (2005), which determines the welding procedure. The material of the samples was low-carbon, fine-grained steel of class STN 41 1375 (1989). Chemical composition and mechanical properties of the parent material are shown in Table 1. The sample dimension were t = 8 mm, b = 350 mm, a = 150 mm.

The data presented in Tables 1–3 have been given by the producer.

Sample No. 1 – welded by manual arc welding method: Filler material – basic electrode EB-121 (ESAB Slovakia, Bratislava, Slovakia) with the diameter of 2.5 mm. Its chemical composition is shown

Table 1. Chemical composition and mechanical properties of steel STN 41 1375

C (%)	P (%)	S (%)	N (%)	Fracture limit	Yield limit
max 0.17	max 0.045	max 0.045	max 0.09	340–470 MPa	215 MPa

Table 2. Chemical composition of electrode EB-121

C (%)	Mn (%)	Si (%)	P (%)	S (%)	N (%)
0.05	0.80	0.40	–	–	–

Table 3. Parameters of welding wire OK Autrod 12.58

C (%)	Mn (%)	Si (%)	Gas	R_m (MPa)	R_e (MPa)
0.10	1.10	0.65	M21	515	420
			C1	485	375

in Table 2. The electrode is one of those most used for the welding of significantly stressed components of energy pipes of devices, transport, pressure vessels, shipping and building constructions of up to R_m = 480 MPa. Welding parameters: U = 24 V, I = 82 A.

Sample No. 2 – welded by GMAW method: Filler material – welding wire OK Autrod 12.58 (ESAB Slovakia, Bratislava, Slovakia), with the diameter of 1.2 mm. Chemical composition and mechanical properties are shown in Table 3. The wire is used for welding of the most common non-alloy and fine-grained structural steel with the yield strength limit of up to 380 MPa. It is suitable for the welding of constructions, pressure vessels, shipping components, and also parts from galvanised sheet metal. It allows welding by high-voltage current (spray transfer) and also by short arc in all positions. Welding parameters: U = 30 V, I = 220 A.

The drafts of the ample shape and location of sampling for the tests according to STN EN 15614-1 (2005) are illustrated in Fig. 4.

RESULTS AND DISCUSSION

Figs 5 and 6 illustrate the documented macrostructure of the monitored samples.

The boundary of the melting-down was not very noticeable; the root was overheated but the weld exceed was not sufficient in sample No. 1 (Fig. 5). The boundary of the melting-down was sharper; the sample root was not overheated in sample No. 2 (Fig. 6).

Figs 7 and 8 illustrate the documented microstructure of the welded metal sample.

The structure of sample No. 1 was more coarse-grained than that of sample No. 2. This was caused by acicular ferrite (AF), fine acicular ferrite (CAF) was bordered by more coarse ferrite at the boundaries of the initial austenitic grains, which grew along the heat dissipation (Figs 7 and 8).

Figs 9 and 10 illustrate the comparison of the boundary zones of the samples melting-down.

The boundary of the sample No. 1 melting-down was not so noticeable as with sample No. 2.

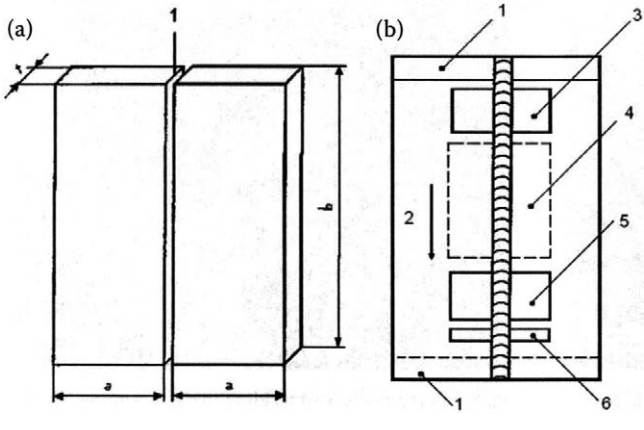

Fig. 4. (a) Sample disc with butt joint with re-weld; (b) example of sampling for test according to standard (6 – spot of sampling for microscopic analysis)

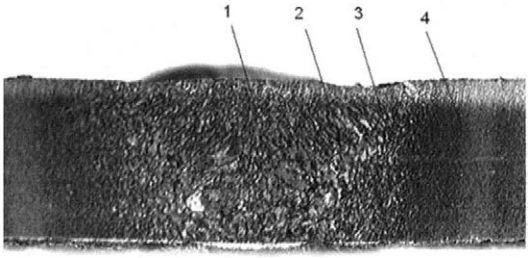

Fig. 5. Sample No. 1 (Mag. 12.5×)
1 – weld metal, 2 – melting-down boundary, 3 – HAZ, 4 – HAZ

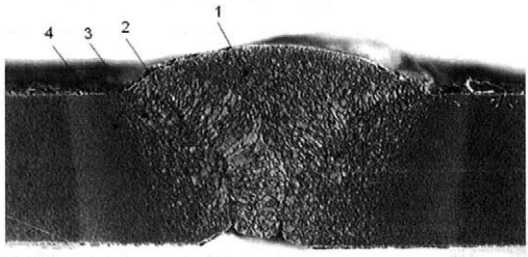

Fig. 6. Sample No. 2 (Mag. 10×)

Figs 11 and 12 illustrate the documented high-heated zone affected after transformation.

The microstructure of this part of HAZ was formed by upper bainite (UB) and acicular ferrite (AF) along the boundary of austenitic grains after austenite disintegration, which had locally Widmannstättenic character. In sample No. 1, this zone was more coarse-grained than in sample No. 2. The roughness of austenitic grain in HAZ heated in the zone of high temperatures formats the more coarse structures after its transformation at cooling, which was noticed in lower values of the mechanical attributes, particularly ductility in this part of joint.

Figs 13 and 14 illustrate the documented zones affected by the heat closely above A_{c3}. The structure was more fine-grained than with high-heated HAZ, and was formed by acicular ferrite (AF, CAF) and lower bainit (LB).

Sample No. 1 shows also non-metallic inclusions.

Figs 15 and 16 show the comparison between the sample zones after heating at a temperature below A_1, where the structural changes were not noticed to origin state (in comparison with the original state).

The structure of the parent sample material was fine-grained, ferrite-perlitic. The divergences in the grain size related to small inhomogeneity of the plate sheet metal, from which the samples were taken. The results of the structural analysis of micro-scratch pattern samples of welds made by manual electrical arc welding and GMAW method and the evaluation of macro-scratch pattern of welds correspond to the knowledge of the welding method used.

The amount of heat brought into the weld in the course of manual electrical arc welding is higher than that GMAW method. The welding speed in manual electrical arc welding is lower, therefore a greater volume of the weld metal, deeper penetration, a wider zone of the overheated material, and higher heat inertia of the heated material volume are noticed. Cooling is slower and that formats grain coarsening with the related mechanical attribute decrement of the material in the welding zone. From this point of view, we can assess GMAW method as positive. The range of HAZ is about 20% to 30% narrower with GMAW method by using optimal parameters of welding at manual electrical arc welding and GMAW.

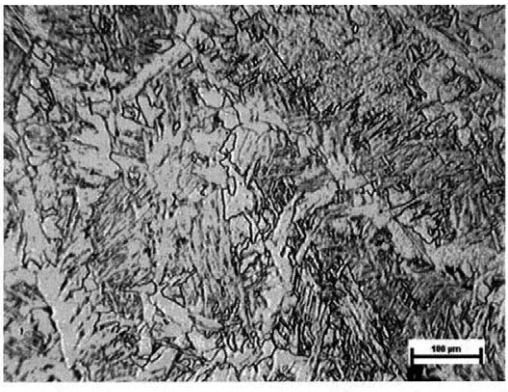

Fig. 7. Microstructure of welding metal – Sample No. 1

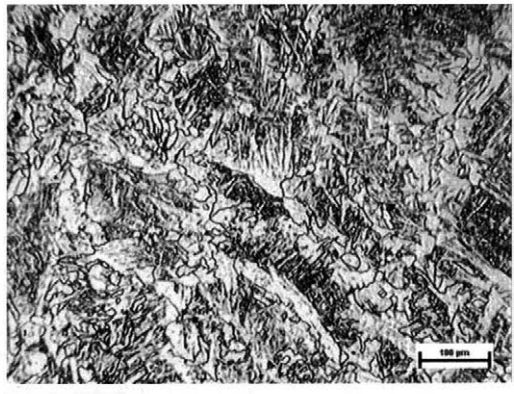

Fig. 8. Microstructure of welding metal – Sample No. 2

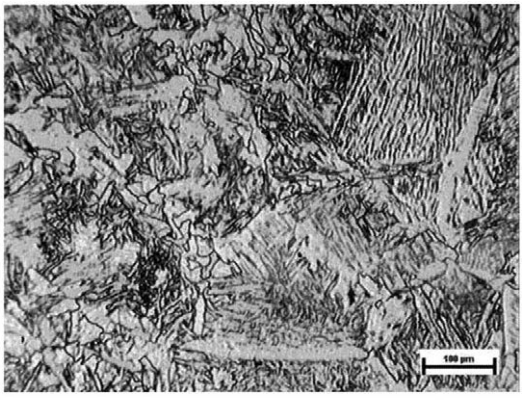

Fig. 9. Microstructure of melting-down boundary – Sample No. 1

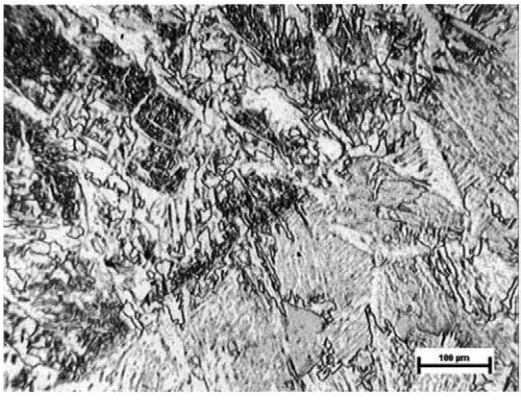

Fig. 10. Microstructure of melting-down boundary – Sample No. 2

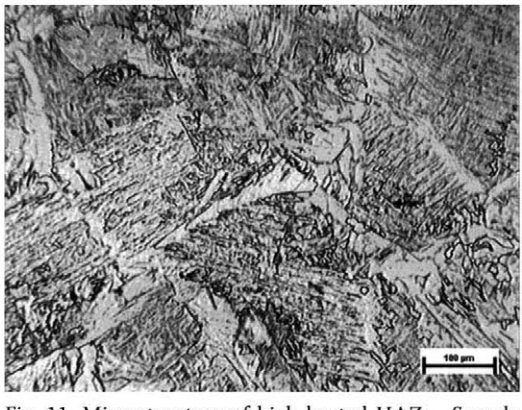

Fig. 11. Microstructure of high-heated HAZ – Sample No. 1

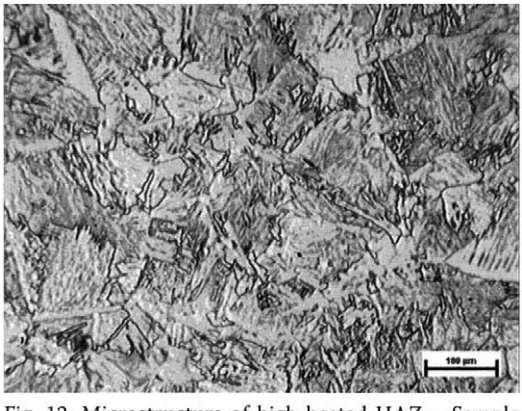

Fig. 12. Microstructure of high-heated HAZ – Sample No. 2

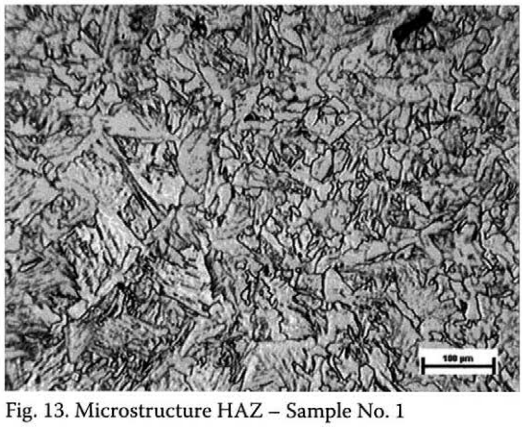

Fig. 13. Microstructure HAZ – Sample No. 1

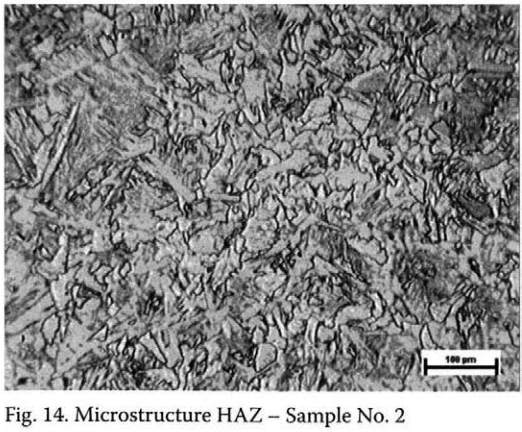

Fig. 14. Microstructure HAZ – Sample No. 2

The boundary of melting-down at manual arc welding is not noticeable and geometric, which is caused by the character of the manual electrical arc welding, electrode diameter, and movement of the electrode spike, possibly due to electric arc blowing. In consideration of the controlled electric arc in GMAW method and better geometry in the process kinematics, the geometry of the weld bead is symmetrical, the welded metal bound, and the welds geometry univocally definable.

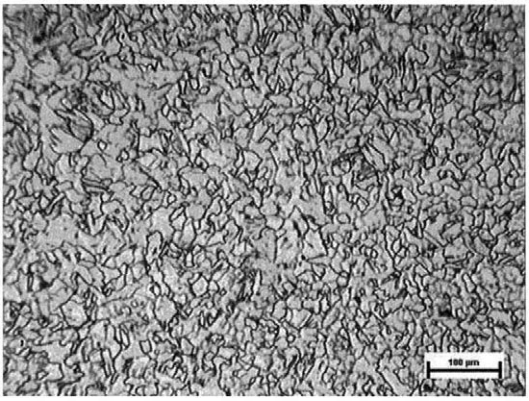

Fig. 15. Microstructure HAZ – Sample No. 1

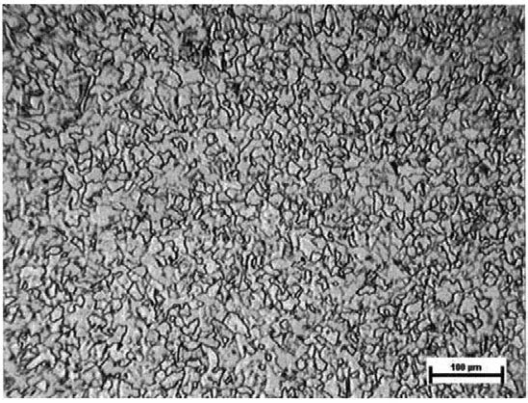

Fig. 16. Microstructure HAZ – Sample No. 2

CONCLUSION

The paper was focused on the analysis of the effects of welding technologies on the welded joint microstructure quality and formation. The samples tested came from the material class STN 41 1375 (1989) and were welded using the technologies of the manual electrical arc welding and of GMAW. The analyses of macro and microstructures of the welded joints confirmed that the technologies and technological parameters of welding influence the structure of the welded joint and range of the material affected by welding. From this point of view, the differential approach to the selection of progressive welding method is very important, particularly considering the heat input and other factors positively affecting the results of the welding process.

References

Brziak P., Bernasovský P., Mráz Ľ., Piussi V., Grgáč P., Mráz Ľ., Hrivňák I., Kálna K., Pecha J., Országhová J., Blaškovitš P., Balla J., Meško J., Országh V., 2003. Materiály a ich správanie sa pri zváraní – 2. kniha učebných textov pre kurzy zváračských inžinierov (Materials and their Behaviour at Surfacing Welding – 2nd Study Book for Courses of Welding Engineers). 2nd Ed. Bratislava, Welding Research Institute, PI SR.

Martinkovič M., Šugár P., 1994. Automation of materials structure analysis. In: DAAAM Symphosium. Maribor, Slovenia, DAAAM International Vienna: 269–270.

Rosenthal D. 1946. Theory of moving sources of heat and its application to metal treatments. Transactions of the ASME, *68*: 849–866.

Rykalin N.N. 1957. Berechneung der Wärmevorgänge beim Schweissen (Calculation of Heat Impact at Welding). Berlin, VEB Verlag Technik.

STN 41 1375, 1989. Oceľ 11 375 (Steel 11 375).

STN EN ISO 15614-1, 2005. Stanovenie a schválenie postupov zvárania kovových materiálov. Skúška postupu zvárania. Časť 1: Oblúkové a plameňové zváranie ocelí a oblúkové zváranie niklu a niklových zliatin (Specification and qualification of welding procedures for metallic materials. Welding procedure test. Part 1: Arc and gas welding of steels and arc welding of nickel and nickel alloys).

Štifner T., 2004. Kovové materially (Metallic materials). Available at www.stifner.sk/skola/doc/afm/texty_AFM_2004.doc (accessed November 22, 2008)

Uwer D., Degenkolbe J., 1976. Temperaturzyklen beim Lichtbogenschweissen. Journal de la Soudure/Zeitschrift für Schweisstechnik, *4*: 73–88.

Received for publication December 11, 2010
Accepted after corrections May 5, 2011

Corresponding author:

Ing. Martin Kotus, Ph.D., Slovak University of Agriculture in Nitra, Faculty of Engineering, Department of Quality and Engineering Technologies, Tr. A. Hlinku 2, 949 76 Nitra, Slovak Republic
e-mail: martin.kotus@uniag.sk

Measurement of titanium surface roughness created by non-conventional cutting technology

J. Rusnák[1], M. Zeleňák[2], J. Valíček[2], M. Kadnár[1], S. Hloch[3], P. Hlaváček[2], M. Kušnerová[2], R. Čep[4], J. Kadnár[5]

[1]*Faculty of Engineering, Slovak University of Agriculture in Nitra, Nitra, Slovak Republic*
[2]*Faculty of Mining and Geology, VŠB-Technical University of Ostrava, Ostrava, Czech Republic*
[3]*Faculty of Manufacturing Technologies, Technical University of Košice, Košice, Slovak Republic*
[4]*Faculty of Mechanical Engineering, VŠB-Technical University of Ostrava, Ostrava, Czech Republic*
[5]*Faculty of Materials Science and Technology, Slovak University of Technology in Bratislava, Bratislava, Slovak Republic*

Abstract

Rusnák J., Zeleňák M., Valíček J., Kadnár M., Hloch S., Hlaváček P., Kušnerová M., Čep R., Kadnár J., 2011. **Measurement of titanium surface roughness created by non-conventional cutting technology**. Res. Agr. Eng., *57 (Special Issue)*: S57–S60.

The paper evaluates the surface roughness quality of the titanium samples created by abrasive waterjet (AWJ) and by CO_2 laser beam cuttings. The introduction describes the principle of the mechanical (contact) method as well as the roughness parameters used for the experiment results evaluation. The following parts summarise the experimental conditions and the measurement methodology. The emphasis of this work is laid on the comparison of machined surfaces final quality for the selected traverse speeds.

Keywords: surface properties; metrology; titanium alloy; roughness measurement

The surface quality control is a very important part of the surface preparation in all types of technologies that are used for their creation (Valíček et al. 2009). Since 1930, when topography meters were invented, great progress has been made in both the methods and measuring equipment. The digital methods implemented in 1960s have enabled the surface evaluation by 3D method (Bumbálek et al. 1989).

MATERIAL AND METHODS

The standardisation of the surface roughness is both a technical and an economic task. Thus, its importance is increasing with the requirements for the precision, efficiency and reliability of the machine components and equipment. All the requirements mentioned depend on many parameters of roughness, mechanical characteristics of the functional surfaces

Supported by Student Grant Competition, Project No. SP2011/78, SP/201058, Czech Science Foundation, Grant No. 101/09/0650, Ministry of Education, Youth and Sports of the Czech Republic, Project No. MSM 6198910016, Regional Research Center of Materials and Technology, Project No. CZ.1.05/2.1.00/01.0040, Institute of Clean Technologies for Extraction and Utilization of Energy Resources, Project No. CZ.1.05/2.1.00/03.0082.

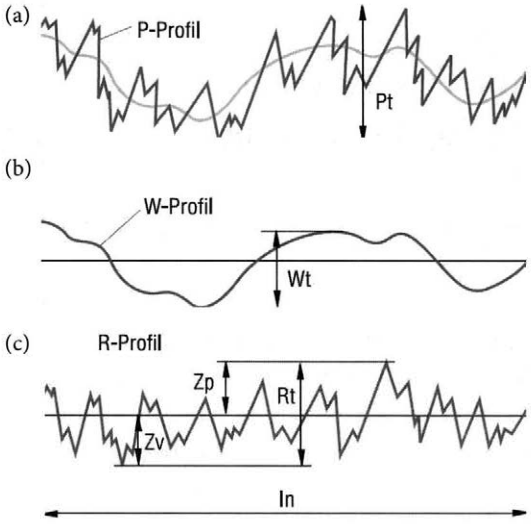

Fig. 1. The profiles according to ČSN EN ISO 4287 (1999) (a) *P* – profile, (b) *W* – profile, (c) *R* – profile

and the method of assembling. The main reason is to improve the lifetime and operational characteristics of the engineering products (Bumbálek et al. 1989).

According to the ČSN EN ISO 4287 (1999) standard, the following surface profiles are distinguished; the basic surface profile *P* (Fig. 1a), the surface waviness profile *W* (Fig. 1b) and the surface roughness profile *R* (Fig. 1c). The basic profile is an ideal smooth surface. The waviness profile is characterised by low frequencies and high amplitudes of the surface roughness. The roughness profile is characterised by high frequencies and low amplitudes of the surface roughness.

The middle arithmetic aberrance of the *Ra* profile is the primary parameter of the surface roughness. It is the average arithmetic value of absolute profile aberrances in the length range. It reflects the time and dimensional dependence of the surface roughness and is determined by the following Eq. 1:

$$Ra = \frac{1}{l_p}\int_0^{l_p} |y(x)|\,dx \quad \text{or} \quad Ra \approx \frac{1}{n}\sum_{i=1}^{n} |y(x_i)| \qquad (1)$$

where

l_p – measured length (m)

$y(x)$ – profile dependence (Bumbálek et al. 1989)

$y(x_i)$ – coordinates of n points (Bumbálek et al. 1989) in the length range, $i = 1, 2... n$

The mechanical (contact) method is currently the most used method mainly in engineering (Fig. 2). Its advantage is the direct measurement and the possibility of its use for all surface types (Hlaváček et al. 2009). The analogue recording of the surface topography which is the result of this method can be transformed into digital recording. The values measured by this method are also used in other types of methods (for comparison, etc.). The method also allows measuring the geometric profile of the surface repeatedly and identically (Zeleňák et al. 2009). However, the pressure generated on the prick sensor causes elastic and plastic deformation in the surface layer. The total deformation depends on the surface hardness. Thus, the prick sensor damages the measured surface which influences not only the evaluated surface but also the whole measuring.

As the initial material for the experimental purposes, unalloyed titanium was used with the specification ASTM B265-99 (1999), supplied in the annealed condition. The chemical and mechanical parameters of the titanium are given in Table 1.

Fig. 3 illustrates the cutting heads of the abrasive waterjet (AWJ) and CO_2 laser beams. The technological parameters for the cuttings are given in Table 2.

The surfaces created by AWJ and CO_2 laser beam cutting technologies were measured with a contact profilometer Surftest SJ 401 (Mitutoyo America Corporation, Aurora, USA) (Fig. 4). Each sample was measured in 19 depth traces. The results of the surface irregularities from each trace were obtained, analysed and statistically processed. The measurement was performed on five consecutive fundamental lengths (l_r = 2.5 mm) and the average value of the surface profile roughness *Ra* was determined from the results obtained.

RESULTS AND DISCUSSION

The comparison of the roughness parameters obtained by the AWJ and CO_2 laser cutting technologies (Fig. 5) shows that the AWJ technology achieved five times lower *Ra* values than were those obtained with CO_2 laser cutting, thus indicating that the AWJ

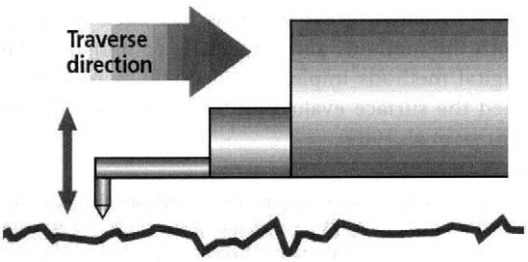

Fig. 2. The principle of sensor contact profilometer

Table 1. Chemical a mechanical parameters of ASTM B265-99

Fe	C	O	H	N
0.2% max	0.08% max	0.18% max	0.015% max	0.03% max
Yield strength 0.2%		Yong's module		Elongation %
172–310 MPa		103 GPa		25–37

Table 2. Experimental parameters of abrasive waterjet (AWJ) and CO_2 laser beam cuttings

AWJ				CO_2 laser			
Technological parameter	Sign	Unit	Value	Technological parameter	Sign	Unit	Value
Liquid pressure	p	MPa	370	pressure of inert gas	p_g	MPa	1.7
Water orifice diameter	d_o	mm	0.3	power	P	W	3,500
Focusing tube diameter	d_f	mm	0.8	traverse speed	v	mm/min	350, 450, 550
Focusing tube length	l_a	mm	76	standoff distance	z	mm	1.5
Abrasive mass flow rate	m_a	g/min	250	diameter of beam	d	mm	2
Standoff distance	z	mm	4	output speed of gas	v_p	mm/min	800, 500, 500
Traverse speed	v	mm/min	350, 450, 550	type of inert gas	N_2	–	nitrogen
Abrasive size	–	MESH	80	frequency	f	Hz	0

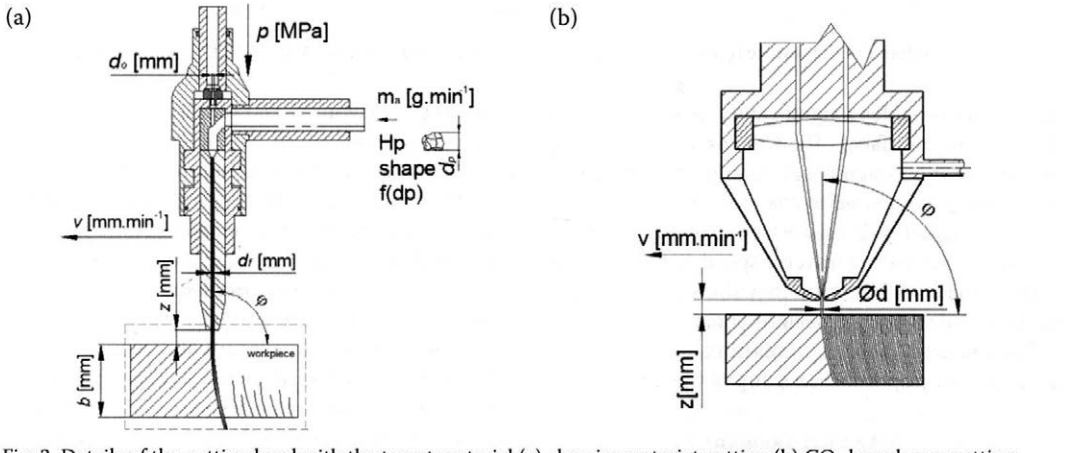

Fig. 3. Details of the cutting head with the target material (a) abrasive waterjet cutting (b) CO_2 laser beam cutting

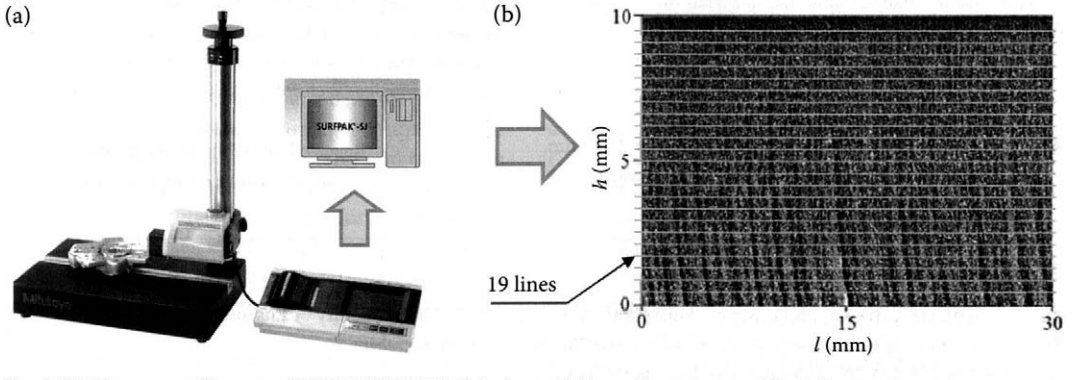

Fig. 4. (a) Contact profilometer SURFTEST SJ 401, (b) photo of the surface measured in 19 lines

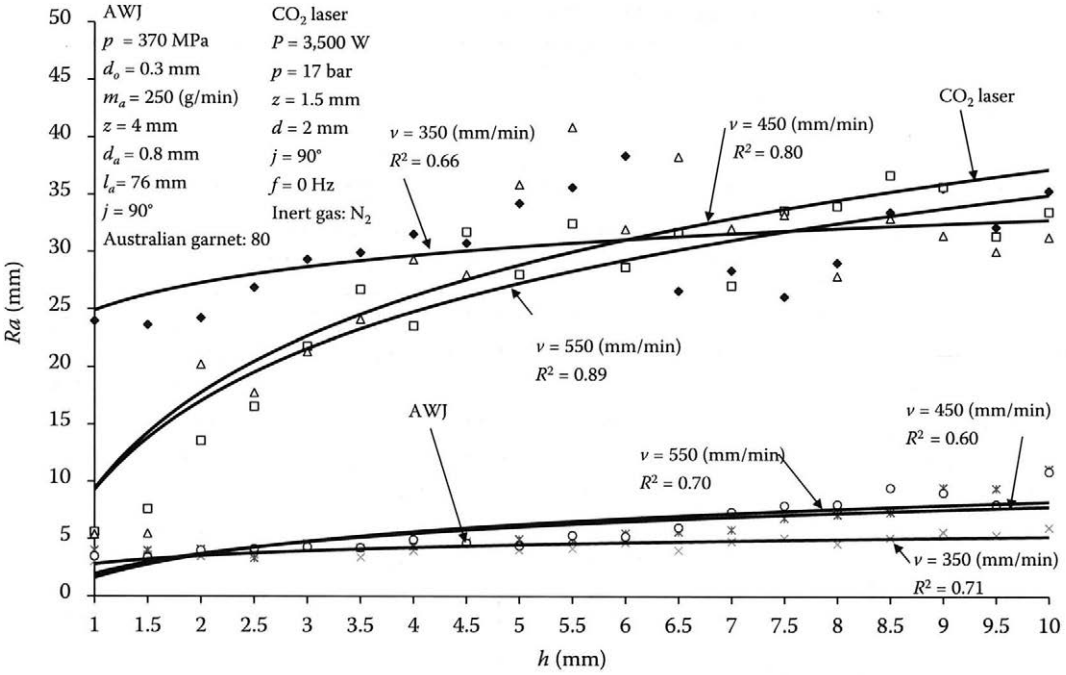

Fig. 5. The dependence of the surface roughness parameter *Ra* on the depth of cut *h* for AWJ and CO_2 laser beam cuttings

technology provides a significantly higher quality of the machined surfaces. The CO_2 laser beam cutting technology shows significant differences in the curve behaviour as compared to AWJ technology.

According to Fig. 5, the surface roughness increases with the increasing traverse speed. The behaviour of the curve in AWJ technology shows minimal differences and smooth behaviour at particular speeds, which indicates good optimisation of the cutting process and an appropriate setup of the input.

Acknowledgement

We would also like to thank the Moravian-Silesian Region 01737/2010/RRC for financial support.

References

ASTM B265-99, 1999. Standard Specification for Titanium and Titanium Alloy Strip, Sheet, and Plate. Available at http://www.astm.org/Standards/B265.htm

Bumbálek B., Obvody V., Ošťádal B., 1989. Drsnost povrchu (Surface Roughness). Prague, SNTL.

ČSN EN ISO 4287, 1999. Geometrické požadavky na výrobky (GPS) – Struktura povrchu: Profilová metoda – Termíny, definice a parametry struktury povrchu (Geometrical product specifications (GPS) – Surface texture: Profile method – Terms, definitions and surface texture parameters).

Hlaváček P., Valíček J., Hloch S., Greger M., Foldyna J., Ivandić Ž., Sitek L., Kušnerová M., Zeleňák M., 2009. Measurement of fine grains copper surface texture created by abrasive waterjet cutting. Strojarstvo, *51*: 273–380.

Valíček J., Hloch S., Kozak D., 2009. Study of Surface Topography Created by Abrasive Waterjet Cutting. Slovanski Brod, Strojarski Fakultet u Slovanskom Brodu.

Zeleňák M., Valíček J., Hloch S., Hreha P., Čepová L., 2009. Analogy of abrasive waterjet technology with classical technologies. Technologické inžinierstvo, *6*: 84–87.

Received for publication December 7, 2010
Accepted after corrections April 7, 2011

Corresponding author:

doc. Ing. Milan Kadnár, Ph.D., Slovak University of Agriculture in Nitra, Faculty of Engineering, Departnemt of Machine Design, Tr. A. Hlinku 2, 949 76 Nitra, Slovak Republic
phone: + 421 376 414 107, e-mail: milan.kadnar@uniag.sk

Material machining for friction knots of moving parts for agricultural machines

J. Žitňanský, J. Žarnovský, R. Mikuš, I. Kováč, Z. Andrássyová

Faculty of Engineering, Slovak University of Agriculture in Nitra, Nitra, Slovak Republic

Abstract

Žitňanský J., Žarnovský J., Mikuš R., Kováč I., Andrássyová Z., 2011. **Material machining for friction knots of moving parts for agricultural machines.** Res Agr. Eng., *57 (Special Issue)*: S61–S68.

The study deals with the effect of the cutting parameters such as the cutting speed, feed and cooling on the quality of machined surfaces in the process of hole drilling for the sliding bearings used in agricultural technique. This effect has been studied on various metals such as copper, brass, dural and leaded bronze, which are commonly used for their friction knots of the moving parts for agricultural machinery. The results suggest the use in the design of collection parts, scything strips, as well as lifting equipment of agricultural technique, where particular linear and rotary movements of the friction parts are slow, as well as for the design of appropriate drilling procedures.

Keywords: friction knot; sliding bearing; cutting speed; cooling; quality of machined surfaces

Quality and efficiency of the agricultural equipment machining depend on the methods, devices and parameters that affect the work piece and so change its initial properties into those required. Finishing processes are also included, affecting the required shape, precision and surface of the component (Audy 2008, 2009).

Various machining procedures are used. Drilling process is one of the most used manufacturing techniques. Precision of the holes made and quality of machined surfaces after drilling can be additionally increased by subsequent roughing or reaming. The selection of the convenient drilling procedure can influence the manufacturing economics, machined surface quality, productivity and total technological cost of machining (Stephenson, Agapiou 2006). This effect is studied for various metals such as copper, brass, dural, and leaded bronze, which are commonly used for the preparation of the friction knots for the moving parts of agricultural machinery.

MATERIAL AND METHODS

Single-circuit detector Utilcell-M120 was used for obtaining the data on the changes of cutting forces in the process of drilling (Fig. 1). The crush element of this detector is made of beryllium-copper alloy made by the Utilcell Co., Barcelona, Spain.

The cutting force measured is the force acting on the arm, therefore it was recalculated for the real cutting force of the drill – following the equation:

$$F_z = \frac{2F_{nam} \times L}{D} \quad \text{(N)} \tag{1}$$

where:

F_z – real cutting force (N)
F_{nam} – measured force (N)
L – distance between the detector and drill axis (mm)
D – diameter of the drill (mm)

Detector of temperature – a thermoelectric segment operates on the basis of Seebeck feature. Two

Supported by the Scientific Grant Agency VEGA of the Ministry of Education of the Slovak Republic and the Slovak Academy of Sciences, Grant No. 1/0813/10.

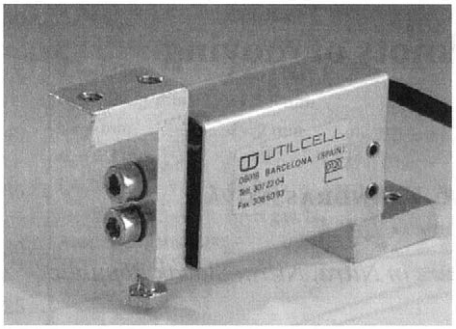

Fig.1. Detector of cutting force Utilcell M120 (Utilcell 2007)

line wires of different metals are linked on one end. If the ends of the circuit made have different temperatures, it incurs the proportional tension of temperature difference between them. The thermoelectric segment used in this study consists of two line wires of copper and of constantan (Stephenson, Agapiou 2006). The most accurate information about the temperature flow in the process of drilling can be obtained by measuring the temperature always at the level of the cutting spot. This position can be adjusted by displacement of the fixing holder on zero-sequence withdrawable part of the spindle. The position of the temperature detector is illustrated in Fig. 2.

Sample preparation

The samples were made of soft metals such as copper, dural, brass and leaded bronze for the effect assignment of the machining material type and cutting conditions on the process of drilling. Three samples were made of each metal, one for each particular rotation. All samples were in the shape of cylinder with the dimension Ø 30 × 30 mm. The precise measuring of temperatures was ensured by convenient surface quality. The samples were made by lathe-turning. The drilling was conducted without any cooling fluid.

Drill Poldi HSS 02 Ø 16 mm STN 22 1140 (1977) was used as the cutting tool; it had been made of high-alloy high-speed steel (Anonymous 2003).

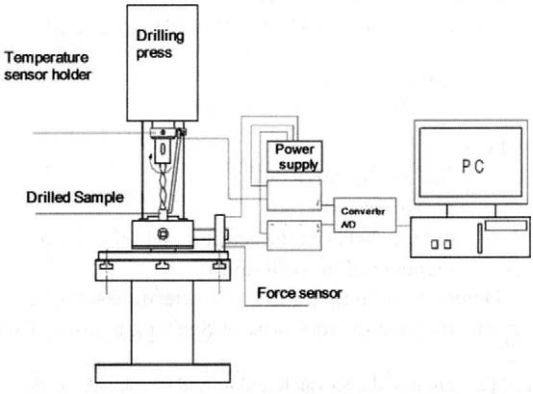

Fig. 2. Scheme of measuring device structure

Procedure of measuring

The rotation of 85 1/min was used for the first measuring. The feed was constant for the whole measuring process. Four snapshots were taken with thermography video camera throughout drilling. The first snapshot was taken when the drill reached the scope by whole cutting edge. The rest of snapshots were taken at periodical intervals. The last snapshot was taken in the position of close run out of the drill from the sample. Next two samples were measured at higher rotations of 150 1/min and 265 1/min. This procedure was repeated with other materials (Bátora, Vasilko 2000).

RESULTS AND DISCUSSION

Particular samples were measured within the parameters illustrated in Table 1.

The data on the average temperatures on the work-piece surface and cutting forces are illustrated in the following tables (Tables 2–5). The measured values were selected according to the gradation of the drilling tool track (Anonymous 2007).

Table 2 shows the data on the average temperatures on the work-piece surface and cutting forces for dural. The flow of the cutting forces in the dependence on the rotation change of dural is illustrated in Fig. 3.

Table 3 shows the data on the average temperatures on the work-piece surface and cutting forces for leaded bronze. The flow of the cutting forces in the dependence on the rotation change of leaded bronze is illustrated in Fig. 4.

Table 1. Applied parameters of drilling

	Rotation (1/min)	Feed (mm)	Cutting speed (m/min)
Sample 1	85	0.1	4.27
Sample 2	150	0.1	7.54
Sample 3	265	0.1	13.32

Table 2. Applied measured average temperatures and cutting forces for dural

Tool track (mm)	Sample 1		Sample 2		Sample 3	
	temperature (°C)	cutting force (N)	temperature (°C)	cutting force (N)	temperature (°C)	cutting force (N)
0	22.9	0	28.5	14	32.0	0
3	27.8	3,489	36.1	3,099	37.4	3,465
6	35.4	4,524	40.1	3,994	43.3	4,490
9	42.0	3,277	49.7	4,110	50.3	3,576
12	48.5	3,609	54.1	3,133	56.5	3,821
15	51.0	3,446	58.9	3,677	61.8	3,301
18	54.7	4,750	58.9	2,912	65.3	3,215
21	57.7	3,754	61.8	3,056	69.2	3,162
24	59.5	3,735	64.1	3,508	73.6	3,191
27	59.5	4,096	67.0	3,277	76.3	3,499
30	51.6	1,554	54.7	4,009	54.7	10

Table 4 shows the data on the average temperatures on the work-piece surface and cutting forces for brass. The flow of the cutting forces in the dependence on the rotation change of brass is illustrated in Fig. 5.

Table 5 shows the data on the average temperatures on the work-piece surface and cutting forces for copper. The flow of the cutting forces in the dependence on the rotation change of copper is illustrated in Fig. 6.

Measured values of hardness

Table 6 shows the measured hardness of dural with all three samples measured. Hardness *Ra* in the dependence on the rotation of dural is illustrated in Fig. 7.

Table 7 shows the measured hardness of leaded bronze with all three samples measured. Hardness *Ra* in the dependence on the rotation of leaded bronze is illustrated in Fig. 8.

Table 8 shows the measured hardness of brass with all three samples measured. Hardness *Ra* in the dependence on the rotation of brass is illustrated in Fig. 9.

Table 9 shows the measured hardness of copper with all three samples measured. Hardness *Ra* in the dependence on the rotation of copper is illustrated in Fig. 10 (Žitňanský, Žarnovský 2010).

Geometry of drilled hole

The calculated values of ovality for each material studied are clearly shown in Table 10. Ovality was studied in the working plane A-A and B-B.

The basic prerequisite for the most suitable cutting parameters detection in drilling coloured met-

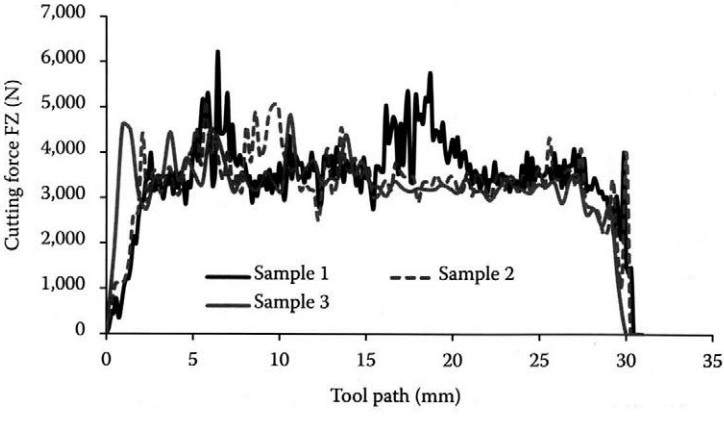

Fig. 3. Flow of cutting forces in dependence on rotation change – dural

Table 3. Applied measured average temperatures and cutting forces for leaded bronze

Tool track (mm)	Sample 1		Sample 2		Sample 3	
	temperature (°C)	cutting force (N)	temperature (°C)	cutting force (N)	temperature (°C)	cutting force (N)
0	25.0	5	27.8	14	33.4	0
3	31.3	2,228	30.6	4,822	34.0	2,517
6	37.4	4,919	34.7	4,331	39.4	4,822
9	44.6	5,149.5	40.1	5,414	44.0	5,727
12	48.5	4,519	44.6	4,851	47.8	4,456
15	52.8	4,875	49.1	5,342	53.4	5,188
18	57.7	4,837	53.4	5,438	57.7	5,101
21	62.4	5,106	57.1	4,938	61.2	5,987
24	67.0	5,433	63.6	5,313	66.4	5,082
27	70.3	5,554	68.1	5,482	74.7	5,756
30	64.1	3,268	54.1	703	57.1	1,319

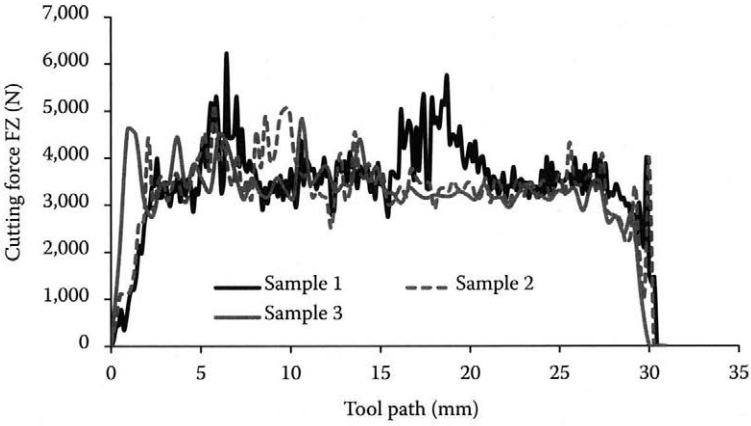

Fig. 4. Flow of cutting forces in dependence on rotation change – leaded bronze

Table 4. Applied measured average temperatures and cutting forces for brass

Tool track (mm)	Sample 1		Sample 2		Sample 3	
	temperature (°C)	cutting force (N)	temperature (°C)	cutting force (N)	temperature (°C)	cutting force (N)
0	25.0	5	29.9	5	34.0	10
3	28.5	2,777	32.0	3,605	36.1	3,629
6	34.0	4,822	36.1	3,908	38.7	4,558
9	37.4	4,548	38.1	4,774	41.4	5,390
12	43.3	5,130	40.7	4,822	45.9	4,173
15	45.9	5,188	44.6	4,663	48.5	5,299
18	51.0	4,923	46.6	5,304	50.3	5,607
21	53.4	4,769	52.8	4,938	55.9	6,083
24	57.1	5,741	57.1	5,650	57.1	4,933
27	52.2	6,155	63.0	5,193	61.8	6,507
30	50.3	6,222	58.9	6,271	62.42	5,385

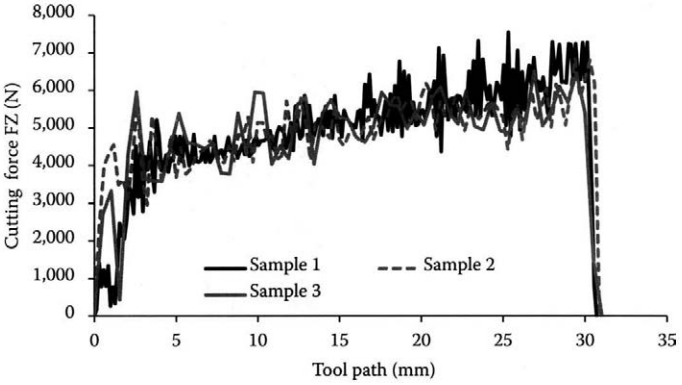

Fig. 5. Flow of cutting forces in dependence on rotation change – brass

Table 5. Applied measured average temperatures and cutting forces for copper

Tool track (mm)	Sample 1		Sample 2		Sample 3	
	temperature (°C)	cutting force (N)	temperature (°C)	cutting force (N)	temperature (°C)	cutting force (N)
0	31.3	10	36.7	10	39.4	14
3	32.0	4,842	44.6	8,167	41.4	9,879
6	46.6	12,143	60.1	13,343	47.2	10,835
9	55.9	11,583	73.1	12,232	58.9	14,196
12	67.0	12,076	84.9	12,623	67.0	13,936
15	69.2	11,766	92.0	12,698	76.8	14,687
18	79.9	15,621	98.7	13,109	80.9	14,365
21	80.4	12,604	100.3	13,643	93.9	11,599
24	79.4	10,974	86.9	12,574	95.6	11,798
27	77.3	14,916	89.7	14,324	84.4	14,324
30	69.8	683	72.0	154	74.7	2,233

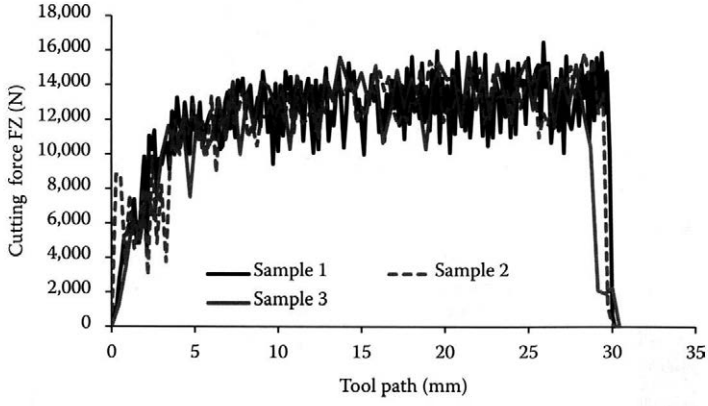

Fig. 6. Flow of cutting forces in dependence on rotation change – copper

als for friction knots of agricultural equipment was quality monitoring of the surfaces thus machined on the experimental samples. Quality of drilled holes was evaluated in accordance with the surface hardness, geometric precision, and conformity of the machined hole proportion with the drill diameter used. A rapid increase in cutting forces out of consideration to the average cutting force level was accomplished with dural samples drilling. It stayed around this value henceforth. The high-

Table 6. Measured values of hardness – dural

Parameter (μm)	Sample 1	Sample 2	Sample 3
Ra	2.02	1.33	1.72
Rq	2.45	1.61	2.03
Rt	12.4	7.3	9.4
Rv	8.7	5.5	7.3
Rz	6.1	3.9	5.1
Rp	4	2.5	3.7

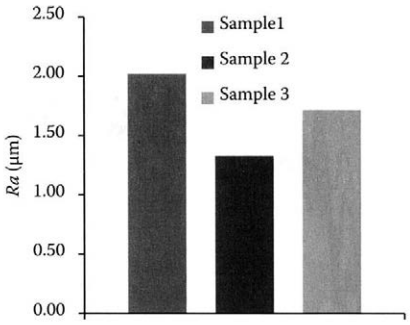

Fig. 7. Dependence of Hardness *Ra* on rotation – dural

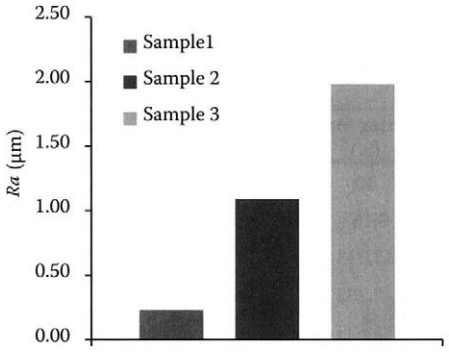

Fig. 8. Dependence of Hardness *Ra* on rotation – leaded bronze

Table 7. Measured values of hardness – leaded bronze

Parameter (μm)	Sample 1	Sample 2	Sample 3
Ra	0.23	1.09	1.98
Rq	0.27	1.34	2.33
Rt	2.6	6.1	10.1
Rv	1.4	5.1	8.2
Rz	0.8	4	6.4
Rp	0.5	1.9	3.2

Table 8. Measured values of hardness – brass

Parameter (μm)	Sample 1	Sample 2	Sample 3
Ra	0.83	0.7	0.95
Rq	1.3	0.88	1.13
Rt	8.3	5.2	5.6
Rv	4.2	3.8	4.5
Rz	2	2.5	3
Rp	1.6	1.4	2.1

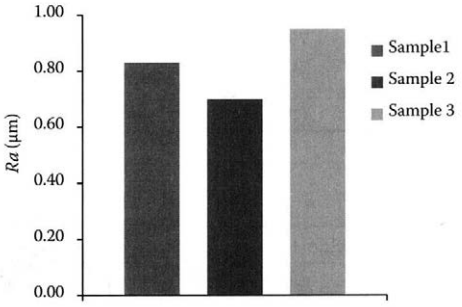

Fig. 9. Dependence of Hardness *Ra* on rotation – brass

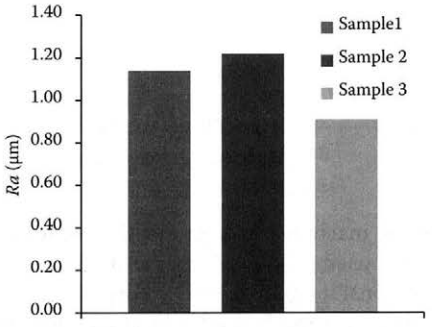

Fig. 10. Dependence of Hardness *Ra* on rotation – copper

Table 9. Measured values of hardness – copper

Parameter (μm)	Sample 1	Sample 2	Sample 3
Ra	1.14	1.22	0.91
Rq	1.49	2.26	1.39
Rt	10.5	17.4	10
Rv	6.4	6.6	4.6
Rz	4.1	4.4	2.7
Rp	3	3.1	2.7

Table 10. Calculated values of ovality

Plane (mm)	Sample 1	Sample 2	Sample 3
Dural			
A-A	16.09	16.09	16.11
B-B	16.13	16.12	16.12
Ovality	0.04	0.03	0.01
Leaded bronze			
A-A	16	16.01	16.01
B-B	16.01	16.02	16.02
Ovality	0.01	0.01	0.01
Brass			
A-A	16.02	16.035	16.02
B-B	16.04	16.04	16.03
Ovality	0.02	0.005	0.01
Copper			
A-A	16.39	16.39	16.257
B-B	16.37	16.355	16.3
Ovality	0.02	0.035	0.043

est deviations were obtained with the lowest cutting speed with the spindle rotation of 85 1/min. A higher stabilisation of the cutting forces was reached by cutting speed increment. Higher values of the cutting forces at a lower rotation could be caused by the mechanism of splinter production, when a higher plastic deformation was occasionally noted. This influenced also the degree of tool dullness and course of temperature. The highest cutting speed of 13.32 m/min caused the most abrupt temperature flow increment, when the resultant temperature flow measured on the spot of the cut increased almost linearly. The temperature was increasing from the beginning of the drilling process approximately evenly and then this trend of the temperature increase gradually deminished with a different cutting speed. The linear course of temperature at the highest rotation was caused by a more intensive production of the friction heat in short time, thus this heat could not be led away by the material quickly enough. The cutting forces and temperature decrement at the end of the drill track was as in all other drilled materials caused by the drilling surface decrement within running out of the drill from the material. The results suggest that with dural, the best values of surface geometry were reached at the rotation of 150 1/min with the cutting speed of .54 m/min. The best values of Hardness Ra = 1.33 μm were also reached by using these parameters. The lowest selected cutting speed of 4.27 m/min with the rotation of 85 1/min was marked in terms of hardness as the most suitable for drilling the leaded bronze sample. The quality of machined surface with Hardness Ra = 0.23 μm and very high geometry precision were reached by the use of these cutting parameters. This hardness was the highest one obtained among all coloured metals examined. The deviation from the set drilling proportion of the hole diameter of 16 mm was 0–10 μm. The cutting speed increment caused a significant hardness increment to 1.98 μm with the rotation of 265 1/min.

The cutting speed of 7.54 m/min with the average spindle rotation of 150 1/min was marked as the most suitable for brass drilling. The best values of ovality and hardness Ra = 0.7 μm were also measured at the cutting speed mentioned.

The best values of the copper samples-in hardness contrast to the other materials-were observed at the highest rotation of 265 1/min with the cutting speed 13.32 m/min. The lowest deviations from the hole drilling diameter set was also reached at the cutting speed mentioned. However, ovality was the worst with these cutting parameters. The lowest ovality of the machined hole was obtained at the lowest rotation (Žitňanský, Kročko 2001; Ružbarský, Tomáš 2006).

CONCLUSIONS

In the paper, the results are described of the drilling of different materials used for the manufacturing of agricultural machines moving parts. These materials include copper, brass, duraluminium and lead bronze. The same parameters were used in the drilling of all materials.

Based on the results achieved, we can conclude that the quality of drilled holes in particular material depends significantly on the cutting speed. Different effects of the cutting speed on the surface roughness and roundness were found. The lowest roughness values were achieved at different cutting speeds as those leading to the best roundness in the case of all materials in research.

References

Anonymous, 2003. Iljin Machinery Co., Ltd. Available at http://www.iljin-mc.co.kr/english/technology/quality.htm?qt=surface (accessed February 03, 2010).

ANONYMOUS, 2007. Dimar Slovakia, Ltd. Available at http://mtf.dattex.net/modules.php?name=Downloads&d_op=getit&lid=28 (accessed April 25, 2009).

AUDY J., 2008. A study of dry machining performance of the TiN, Ti (Al,N) and Ti (C,N) coatings and a type M35 HSS tool substrate material assessed through basic cutting quantities generated when orthogonal turning a Bisalloy 360 grade steel work-piece material. Annals of Faculty Engineering Hunedoara – International Journal of Engineering, 6: 59.

AUDY J., 2009. Study of coatings on experimental thrust and torque in drilling. Annals of Faculty Engineering Hunedoara – International Journal of Engineering, 7: 31–40.

BÁTORA B., VASILKO K., 2000. Obrobené povrchy (Cutting Surfaces). Trenčín, GC – Tech 2000, Inc.: 131.

RUŽBARSKÝ J., TOMÁŠ J., 2006. Some results of the turning of hardened steel without cooling. Acta Avionica, 8: 87–90.

STEPHENSON D.A., AGAPIOU J.S., 2006. Metal Cutting Theory and Practice. Boca Raton, CRC Press.

STN 22 1140, 1977. Vrtáky skrutkové s kužeľovou stopkou. Základné rozmery (Taper shank twist drills. Basic dimensions).

UNTICELL, 2007. Untilcell. Available at http://www.utilcell.com (accessed Fabruary 10, 2010).

ŽITŇANSKÝ J., KROČKO V., 2001. Vplyv podmienok dokončovania predvŕtaných dier na kvalitu vŕtaného povrchu a rozmerovú presnosť (Influence of drilled holes finishing conditions on drilling surface quality and accuracy of size). In: 6th International Scientific Symposium – Quality and Reliability of Machines. Nitra, SPU in Nitra: 101.

ŽITŇANSKÝ J., ŽARNOVSKÝ J., 2010. Effects of material and cutting conditions on the temperature of drilling measured by thermovision technics. Manufacturing Engineering, 9: 34.

Received for publication March 3, 2011
Accepted after corrections October 21, 2011

Corresponding author.

Ing. JAN ŽITŇANSKÝ, Ph.D., Slovak University of Agriculture in Nitra, Faculty of Engineering, Department of Quality and Engineering Technologies, Tr. A. Hlinku 2, 949 76 Nitra, Slovak Republic
phone: + 421 376 414 104, e-mail: jan.zitnansky@uniag.sk

Shadow method for the evaluation of surface created by hydroabrasive dividing of materials

J. Valíček[1], M. Kadnár[2], P. Hlaváček[1], J. Rusnák[2], S. Hloch[3], M. Zeleňák[1], M. Řepka[1], M. Kušnerová[1], J. Kadnár[4]

[1]*Faculty of Mining and Geology, VŠB-Technical University of Ostrava, Ostrava, Czech Republic*
[2]*Faculty of Engineering, Slovak University of Agriculture in Nitra, Nitra, Slovak Republic*
[3]*Faculty of Manufacturing Technologies, Technical University of Košice, Košice, Slovak Republic*
[4]*Faculty of Materials Science and Technology, Slovak University of Technology in Bratislava, Bratislava, Slovak Republic*

Abstract

Valíček J., Kadnár M., Hlaváček P., Rusnák J., Hloch S., Zeleňák M., Řepka M., Kušnerová M., Kadnár J., 2011. **Shadow method for the evaluation of surface created by hydroabrasive dividing of materials**. Res. Agr. Eng., *57 (Special Issue)*: S69–S73.

The contribution deals with the analysis of the optical data obtained from the surfaces generated by hydroabrasive dividing of materials. The samples of different materials were prepared at the Academy of Sciences of the Czech Republic. The comparison of further results performed between the commercial contact profilometer HOMMEL TESTER T8000 and the contactless shadow method developed included its calibration. On the basis of the optical data analysis, the results evaluated especially the height irregularities of the surface topography caused by hydroabrasive cutting planes. The evaluation of the surface topography generated by abrasive waterjet was realised via spectral analysis. The amplitude-frequency analysis of the signals generated on surface topography was mainly realised.

Keyword: disintegration of materials; optical method; roughness; measurements

While the engineering cutting technologies generally make mirror surface reflections, the hydroabrasive dividing of materials makes diffusive surface reflections. The topography of the hydroabrasive generated surfaces records significant diversity in the heights of amplitudes and their waves lengths. Thus, the development of the optical method is focused on the metrological compatibility of optical and mechanical profilometry methods, i.e. the optical method will evaluate the basic parameters of the surface roughness according to the engineering standards. It is the shadow method which was selected from all the methods to realise the experiment because this method is able to fulfil the experimental demands. The experimental results of the commercial contact profilometer HOMMEL TESTER T8000 (Hommewerke GmbH, Villingen-Schwenningen, Germany) were used for further

Supported by Student Grant Competition, Project No. SP2011/78, SP/201058, Czech Science Foundation, Grant No. 101/09/0650, Ministry of Education, Youth and Sports of the Czech Republic, Project No. MSM 6198910016, Regional Research Center of Materials and Technology, Project No. CZ.1.05/2.1.00/01.0040, Institute of Clean Technologies for Extraction and Utilization of Energy Resources, Project No. CZ.1.05/2.1.00/03.0082.

Table 1. Technological parameters of samples

Technological parameter	Value
Liquid pressure (p, MPa)	300
Water orifice diameter (d_o, mm)	0.25
Focusing tube diameter (d_a, mm)	0.8
Focusing tube length (l_a, mm)	76
Abrasive mass flow rate (m_a, g/min)	250
Standoff distance (L, mm)	2
Material thickness (h, mm)	8
Traverse speed (v_p, mm/min)	50, 100, 150, 200
Abrasive size (–, MESH)	80
Abrasive material (–)	Garnet Barton

analysis. The main aim was to use the proposed methodology for measuring and evaluating the surface topography generated by hydroabrasive dividing of materials with the aim of proposing semi-automatic and automatic operations of the surface quality estimation. Thus, it is necessary to process the bank of input and output parameters of hydroabrasive dividing and to propose the criteria for on-line operation (Hashish 1984; Valíček 2007a).

Hydroabrasive dividing of materials

Dividing of materials causes hydroabrasive fission of the material including possible material destruction. The impact of the material particles has elastic-plastic characterisation. In the case of the plastic dominance, the particles can be constrained in the material in the dividing flow as well as in the cutting plane. The dividing effect is then based on the cumulated particles with certain quantity and traverse speed. The size and the shape of the machined particles depend on the amount of the cutting planes and the trajectory of their movement. The parameters which influence the process are: the speed of element, abrasive mass flow rate, wall sharpness, hardness of element, size and shape of element, physical and mechanical properties of work-piece. The material removal then depends on the combination of the factors mentioned. Hashish (1984) reported on the interdependence of the removal size, elements speed, wall sharpness for plastic and brittle materials as well as the hardness and size of the abrasive elements.

The creation of the machined particles is then based on the movement trajectory and the speed. The speed can be divided into translational and rotational parts. Hashish (1984) and other scientists Tichomirov and Guenko (1984), Blickwedel et al. (1990), Zeng and Kim (1990), Guo (1994), Brandt et al. (2000) worked on the scanning of the moves by high speed cameras. Hutchings described and defined two types of rotation for the rotational part of the speed, i.e. rotation in traverse speed and backward rotation towards traverse speed. He observed different behaviour of plastic materials and brittle materials. Brittle materials were plastically changed whereas plastic materials were reinforced. He also explained that the abrasive effect of abrasive water jet (AWJ) is mainly determined by inertial and resistant forces of the abrasive particles and their deformation and disintegration overtake hydrodynamic forces. That explains the abrasive scratch of materials disintegration.

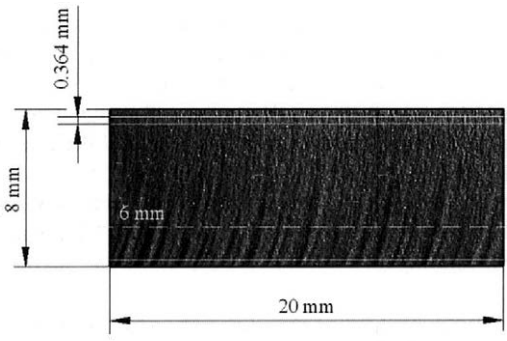

Fig. 1. Illustration of measuring lines on steel sample (ČSN 41 725, 1991)

MATERIAL AND METHODS

Thirty samples of different materials were prepared at the Academy of Sciences of the Czech Republic. The size of each material was 20 × 20 × 8 mm (Fig. 1). The samples were made with PTV–37–60 Pump (PTV, Ltd., Hostivice, Czech Republic) according to the parameters given in Table 1. The traverse speed of the cutting head was the only variable parameter, i.e. 200, 150, 100 and 50 mm/min.

Each material and each side of the samples was measured in 22 measuring lines. Each measuring line provided the information about the signal of the light and shadow by means of a CCD camera (ILC, Bratislava, Slovak Republic) Valíček et al. (2007b).

A laser diode with the performance of W/650 nm was used in the experiment. The shadow visual effect

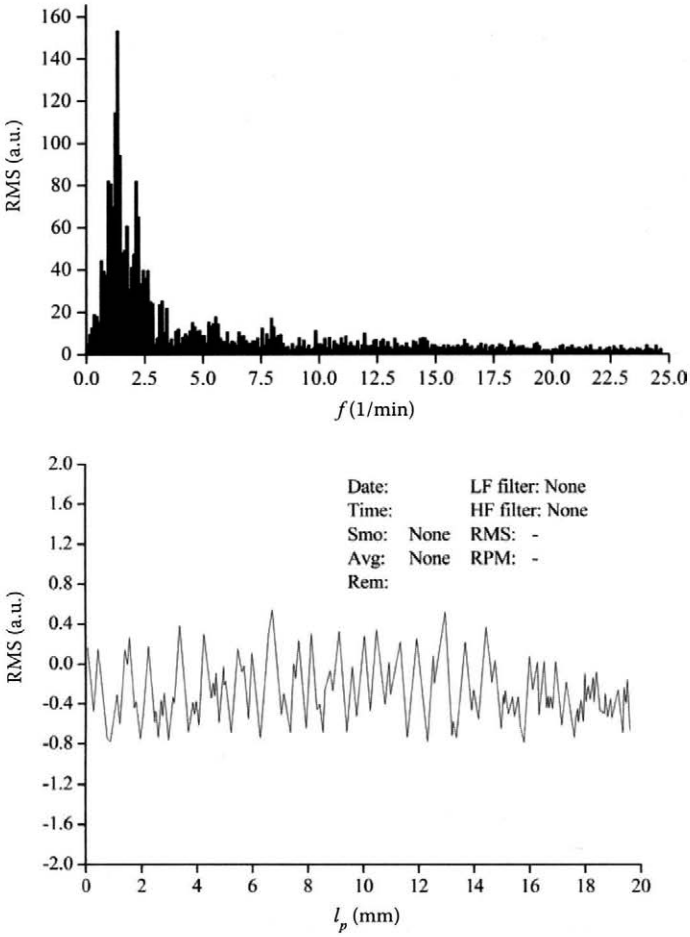

Fig. 2. The signal obtained in sampling the intensity distribution from the surface picture obtained by CCD camera

also depends on the illumination angle. The beam angle allows to view clearly the elevations and depressions of the surface topography which is related to the typical waviness of hydroabrasive dividing of materials. The sample illumination was realised under 15° and the changes were detected by means of a CCD camera with 1,090 × 1,370 pixels.

Fig. 2 illustrates a typical signal obtained by intensity distribution sampling from the surface as gained by the CCD camera.

The signals were processed by Vibroanalyser program (ILC, Bratislava, Slovak Republic). The program transfers the signals via Fourier Transform (FFT) from the time area to the amplitude-frequency spectrum. The spectrums involve the areas in which waviness and roughness are concentrated. That is why the zonal filtration of amplitude-frequency spectrum was realised (Fig. 3), i.e. the spectrum was divided into six frequency zones whereby the selected frequency intervals simulated to contact profilometer cut-off to provide the topography of samples.

RESULTS AND DISCUSION

Results comparison between commercial method and shadow method

The results of the shadow method could be compared with the results of the commercial method. The results of the shadow method measuring could be confronted with the results of the contact profilometer HOMMEL TESTER T8000 according to the amplitude-frequency spectrums. The signal from 6 mm was selected to present the differences between these methods.

Fig. 4 illustrates a twelve times extended cutting plane of hydroabrasive dividing. From the signal, the amplitude-frequency spectrum was recorded.

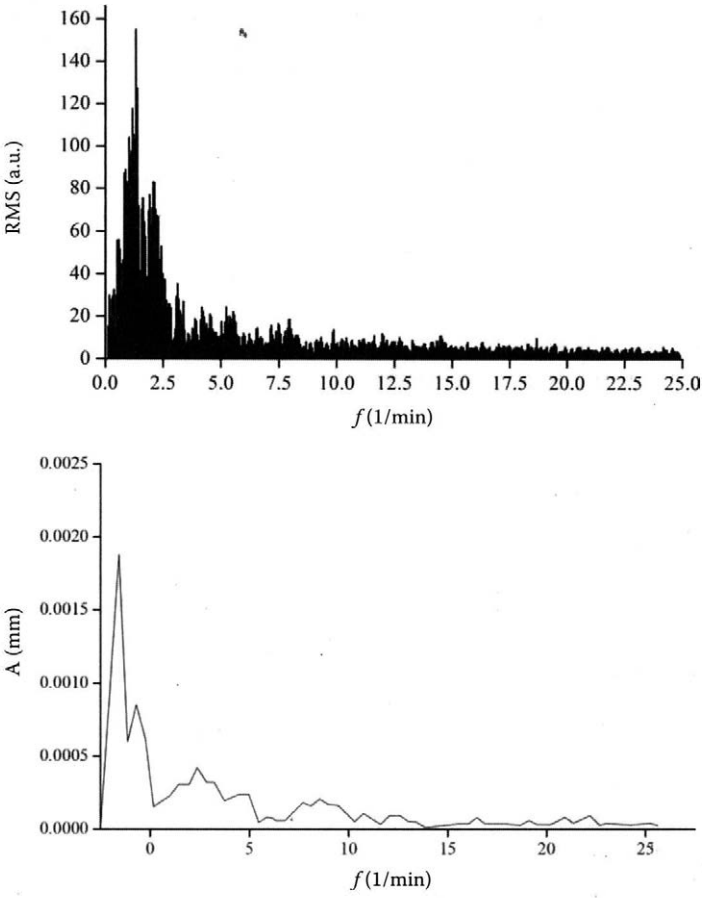

Fig. 3. Amplitude-frequency spectrum of the surface obtained from one representative measured line at 6 mm depth from surface with distinguished frequency bands

The localisation can be seen of low-frequency components with the highest amplitude values from to the frequency band 0–2.5 1/mm definitely corresponding to the waviness of the machined surface. The average value of this zone was approximately 1 l/mm which corresponded to the wave length λ of 1 mm. This can be confirmed directly on the sample and it also allowed a better understanding of the hydroabrasive dividing.

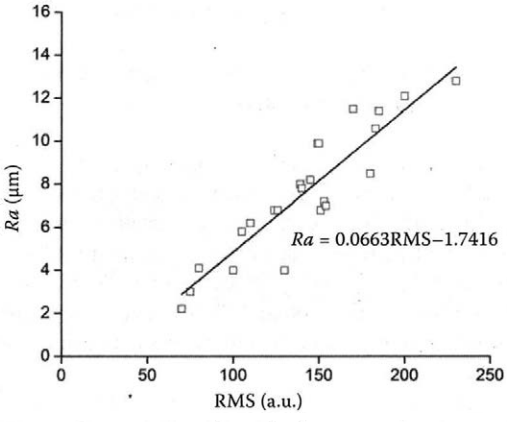

Fig. 4. Comparison of results between a) commercial method and b) shadow method

Calibration of the shadow method by contact profilometer

Based on the results and their confrontation with *Ra* and *Rq* parameters directly detected on the samples of the contact profilometer HOMMEL TESTER T8000, the RMS (Root Mean Square of reflected light intensity) was selected as the appropriate parameter for the surface topography of the samples machined by hydroabrasive dividing. The RMS parameter used in the shadow method enables to detect the fluctuation of the changes developed by the topographical principle of the sample surface.

It has been confirmed that the surfaces generated by hydroabrasive dividing of materials are not stochastic but are mostly periodical with a wide range of high amplitudes and their wave lengths. For the pitches and wave lengths, about 5,000 values of RMS parameters were measured and the calibration of primary signals was realised. After analysing the results (Figs 2 and 3) reached by the shadow method and after the verification with the commercial profilometer HOMMEL TESTER T8000 for steel ČSN 41 17241 (1980) and iron ČSN 42 2712 (1979), the RMS value was 0.05 Ra. The calibration function is shown in Fig. 4.

Acknowledgement

We would also like to thank the Moravian-Silesian Region 01737/2010/RRC for financial support.

References

Blickwedel H., Guo N.S., Haferkamp H., Louis H., 1990. Prediction of abrasive jet cutting efficiency and quality. In: Proceedings 10th International Conference on Jet Cutting Technology. Cranfield, BHRA Fluid Engineering.

Brandt S., Maros Z., Monno M., 2000. AWJ parameters selection – a technical and economical evaluation. In: Proceedings 15th International Conference on Jet Cutting Technology. Cranfield, BHRA Fluid Engineering.

ČSN 41 17241, 1980. Ocel 17 241 Cr-Ni (Steel 17 241 Cr-Ni).

ČSN 41 7251, 1991. Ocel 17 251 Cr-Ni-Si (Steel 17 251 Cr-Ni-Si).

ČSN 42 2712, 1979. Ocel na odlitky 42 2712 manganová (Cast manganese steel 42 2712).

Guo N.S., 1994. Schneidprozess und Schnittqualität beim Wasserabrasiusstrahl – schneiden. Düsseldorf, VDI Verlag: 1–174.

Hashish M., 1984. Modeling study of metal cutting with abrasive waterjets. Journal of Engineering Materials and Technology, *106*: 88–101.

Tichomirov R.A., Guenko V.S., 1984. Hydroabrasive Cutting of Non-metal Materials. New York, The American Society of Mechanical Engineers.

Valíček J., Držík M., Hloch S., Ohlídal M., Lupták M., Gombár M., Radvanská A., Hlaváček P., Páleníková K., 2007a. Experimental analysis of irregularities of metallic surfaces generated by abrasive waterjet. International Journal of Machine Tools and Manufacture, *47*: 1786–1790.

Valíček J., Hloch S., Držík M., Ohlídal M., Mádr V., Lupták M., Radvanská A., 2007b. Raziskave vodno jedkanih površin s svetlobnim zaznavanjem (An investigation of surfaces generated by abrasive waterjet using optical detection). Strojniški vestnik – Journal of Mechanical Engineering, *53*: 224–323.

Zeng J., Kim T.J., 1990. A study of brittle erosion mechanism applied to abrasive waterjet processes. In: Proceedings 10th International Conference on Jet Cutting Technology. Cranfield, BHRA Fluid Engineering.

Received for publication December 7, 2010
Accepted after corrections April 7, 2011

Corresponding author:

doc. Ing. Milan Kadnár, Ph.D., Slovak University of Agriculture in Nitra, Faculty of Engineering, Departnemt of Machine Design, Tr. A. Hlinku 2, 949 76 Nitra , Slovak Republic
phone: + 421 376 414 107, e-mail: milan.kadnar@uniag.sk

Analysis of wear resistent weld materials in laboratory conditions

M. Kotus[1], Z. Andrássyová[1], P. Čičo[1], J. Fries[2], P. Hrabě[3]

[1]*Faculty of Engineering, Slovak University of Agriculture in Nitra, Nitra, Slovak Republic*
[2]*Faculty of Mechanical Engineering, Technical University of Ostrava, Ostrava, Czech Republic*
[3]*Faculty of Engineering, Czech University of Life Sciences Prague, Prague, Czech Republic*

Abstract

Kotus M., Andrássyová Z., Čičo P., Fries J., Hrabě P., 2011. **Analysis of wear resistent weld materials in laboratory conditions**. Res. Agr. Eng., *57 (Special Issue)*: S74–S78.

The aim of the study was the evaluation of the suitability of using filler surfacing materials in abrasion resistant layers according to their material and tribology features. Laboratory analysis of the selected materials consisted of the tests of hardness, microstructure and wear resistance determination. The abrasive wear resistance was defined according to the standard STN 01 5084. On the basis of the results obtained, we can state that using the hard-facing for the background is tenable for the purpose of wear amount decrement where the abrasive wear prevails.

Keywords: abrasive wear; relative resistance; laboratory analysis; abrasion resistant layers; Fluxofilcord 58; Fluxofilcord 59

Material properties can be evaluated from the point of view of abrasive wear resistance by tests in laboratory conditions and on the basis of the results obtained in tests in operational conditions. Common methods of wear amount testing allow determining the relative material wear resistance by several quantitative methods (Kotus, Drahoš 2010).

One of the tribological test methods is the determination of the metal material abrasive wear resistance on a device with grinding fabric according to the standard STN 01 5084 (1973). Relative abrasive wear resistance ($\psi_{abr.}$) is an elemental criterion for the material evaluation in laboratory conditions (Balla 1989).

On the basis of the indicators defined (hardness, microstructure) in laboratory conditions, we can evaluate also the suitability of filler materials for forming abrasion resistant layers, which are abrasive wear resistant (Kotus 2009).

On the basis of the laboratory analysis, the object of this study was the evaluation of mechanical properties of filler materials Fluxofilcord 58 and Fluxofilcord 59 (Air Liquide Welding, Lužianky, Slovak Republic) suitability of their use in abrasion resistant layers formation. The formation of abrasion resistant layers by surfacing with filler materials is a possible way of resistance enhancement in functional machine parts.

MATERIAL AND METHODS

The analysis of the filler materials was done in the laboratories of the Department of Quality and Engineering Technologies, Faculty of Engineering, Slovak University of Agriculture in Nitra. The test

Supported by the Scientific Grant Agency VEGA of the Ministry of Education of the Slovak Republic and the Slovak Academy of Sciences, Grant No. 1/0576/09.

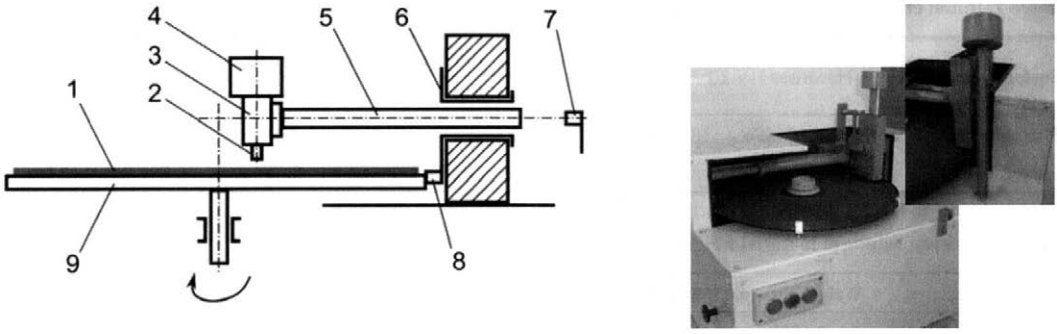

Fig. 1. Test device with grinding fabric
1 – grinding fabric, 2 – sample, 3 – holder, 4 – weight, 5 – moving screw, 6 – rotary matrix, 7 – limit switch, 8 – stopper, 9 – rotary horizontal panel

device (Fig. 1) for the determination of metal material abrasive wear resistance on the grinding fabric meets all conditions defined by the standard STN 01 5084 (1973).

The parameters of the samples, as well as the procedures and conditions which need to be met in the test for reproducible and comparable results, are given in the standard. The comparative sample tested according to the standard STN 41 2014 (1993) was steel 12014.20 with the range of hardness HV = 95 to 105. The weight loss with precision of 1×10^{-4} g was computed from the measured weights of the samples before and after the test. Minimum of four tested samples were obtained from each material. The comparative etalon sample was regularly alternated by the tested material in the order 1-2-1-2-1.

Abrasive wear relative resistance ($\psi_{abr.}$) was calculated by the following adapted equation:

$$\psi_{abr.} = \frac{W_{hE}}{W_h} \quad (1)$$

where:

W_{hE} – average weight loss of etalon sample body (g)

W_h – average weight loss of samples of tested material (g)

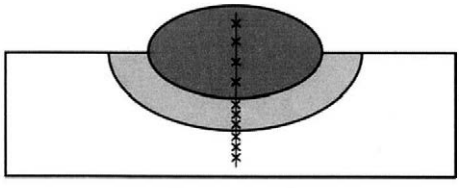

Fig. 2. Scheme of plane and location of hardness measurement HV 10: 4× surfacing metal (SM), 3× heat affected zone (HAZ), 3× parent material (PM)

The set parameters of the test device were the following:

- frictional speed – max. 0.5 m/s
- transverse feed per rev – 3 mm
- diameter of rotary panel – 480 mm
- length of frictional track – 50 m
- amount of contact pressure – 0.32 MPa
- grinding fabric – Globus 100
- sample length – 50 mm with diameter 10 mm

Vickers's method was used for the evaluation of the hardness measurement by crossing the parent material through the heat affected area into the surfacing metal. Vickers's test of hardness is given by the standard STN ISO 6507-1 (2006) using the load of 98 N, this means marking HV 10. The location punctures of the hardness measurement HV 10 are illustrated in Fig. 2. The location punctures were at the distance of 1.25 mm from the surface of the material in the surfacing metal. The distance of the location punctures was 0.50 mm in the heat affected zone as well as in the parent material.

The microstructure of the surfacing metal was evaluated on the basis of the image obtained by measuring chain consisting of microscope Epityp 2 (Carl Zeiss Jena GmbH, Jena, Germany), a camera and a computer. Filler materials Fluxofilcord 58 and Fluxofilcord 59 (ø 1.6 mm) are basic pipe wires for surfacing of resilient and abrasion resistant layers on machine parts. The surfacing metal shows high toughness and impact resistance. They are used for parts of the tools exposed to heavy abrasive wear such as components of dredgers, excavators, grabs, conveyors, drills, jaw crushers.

Chemical composition and hardness HV 10 (given by the producer) of surfacing filler materials are shown in Table 1.

Table 1. Initial chemical composition and hardness HV 10 of the filler materials

Surfacing material	Hardness HV 10	Elemental contents (%)					
		C	Mn	Ni	Cr	Mo	W
Fluxofilcord 58	615–655	0.5	1.5	–	5.5	0.6	–
Fluxofilcord 59	596–675	0.4	1.0	1.0	5.0	0.8	2.0

Table 2. Average values of material weight loss in tests on grinding fabric

Material	Weight loss (g)	Standard deviation (g)	Relative wear resistance ($\Psi_{abr.}$)	Standard deviation (g)
Fluxofilcord 58	0.1783	0.007597	2.10	0.110799
Fluxofilcord 59	0.1698	0.005808	2.21	0.092966
Etalon 12 014.20	0.3750	0.005199	1	–

Welding power source Optipuls 500i W (Air Liquide Welding, Lužianky, Slovak Republic) with stepless welding current and voltage was used for surfacing the samples. MIG surfacing was used as a method of filler material application on the parent material in protective atmosphere of mixed gas [MIG – GMAW – marking 131 according to ČSN EN ISO 4063 (2011)]. The following are the parameters of surfacing: welding voltage U = 26 V, welding current I = 133 A, welding speed 0.30 m/min, wire feed speed 2.0 m/min, shielding gas Ferroline C18 (Messer Tatragas, Šaľa, Slovak Republic) in the amount of 12 l/min.

RESULTS AND DISCUSSION

The weight values measured before and after the test as well as the calculated weight loss and relative wear resistance are shown in Table 2. Graphical evaluation is given in Fig. 3.

The measured values of the hardness of the parent material, heat affected area and surfacing metal are shown in Table 3. Graphical evaluation is given in Fig. 4.

The microstructure reached of the filler materials used is shown in Fig. 5.

The evaluation of the relative abrasive wear resistance shows a greater wear with the hard-facing Fluxofilcord 58. A lower weight loss and thus a lower wear by about 5% were reached with the filler material Fluxofilcord 59.

The wear resistance is not an internal property of the material like e.g. some of its mechanical or physical properties. The comparison of the material hardness and relative resistance shows that the relative resistance increases by the increments of hardness and thus the amount of wear decreases.

The values of hardness of the net overlay corresponded to those specified by the manufacturer of both used filler materials. The surfacing metal hardness decreases towards the parent material

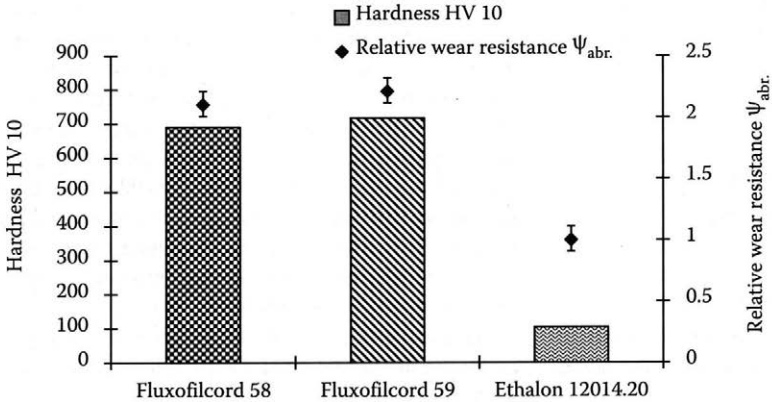

Fig. 3. Hardness HV 10 and relative wear resistance of the materials tested

Table 3. Average values of hardness HV 10 of the materials tested

Material/Hardness HV 10	Surfacing metal				Heat affected area			Parent material		
	1	2	3	4	5	6	7	8	9	10
Fluxofilcord 58	691	670	630	604	340	291	268	195	205	218
Fluxofilcord 59	718	689	702	673	327	284	270	233	214	199

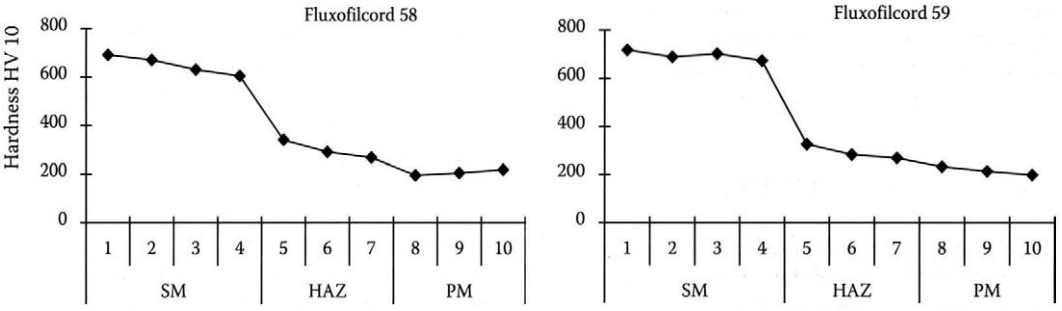

Fig. 4. Behaviour of hardness HV 10 of the materials tested
SM – surfacing metal, HAZ – heat affected zone , PM – parent material

as shown by gradual measurement of hardness. Fluxofilcord 58 caused a more significant decrease of hardness than Fluxofilcorde 59. The difference of the hardness reduction of Fluxofilcord 58 was 87 HV 10 and of Fluxofilcord 59 only 45 HV 10, which is double value.

The comparison of the heat affected area showed lower values of hardness with the material Fluxofilcord 59. The decrease of the hardness values was less significant with this material compared with the parent material. It may have been caused by mixing of the surfacing metal with the parent material. A decrease of hardness was noted also in the final structure of the overlay, which confirmed more significant mixing of the parent material with the surfacing material Fluxofilcord 58.

The most important element, which gives hardness to the material, is carbon. The critical speed of cooling for the creation of martensitic structure decreases by increasing the carbon content. In the terms of the basic effect of elements on the microstructure and properties of an alloy, those creating special carbides such as e.g. Mn, Cr, Mo, are of greater importance. Fluxofilcord 59 contains more wolfram that increases the hardness and abrasion resistance. Apart from wolfram it also contains nickel that does not create carbide, is soluble in the basic matrix and increases the corrosion resistance.

Filler material Fluxofilcord 58 has a fine, pouring structure with a thick netting carbide phase. Segregation of the new phase in space between dendrite was noted with some samples. Filler ma-

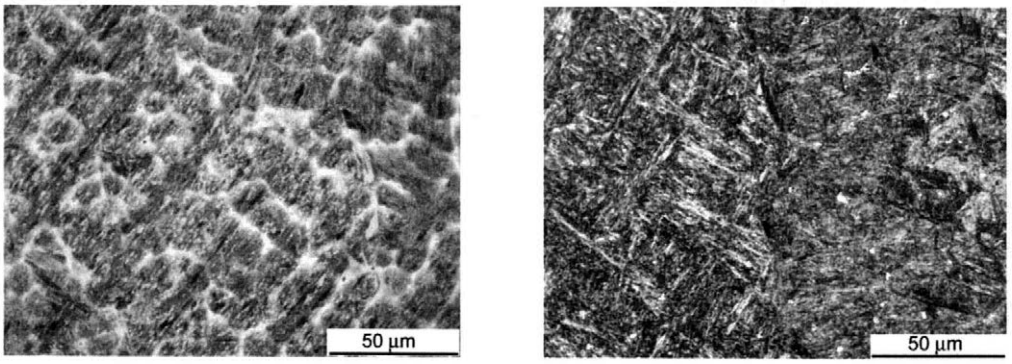

Fig. 5. Microstructure of the filler materials Fluxofilcord 58 (left) and Fluxofilcord 59 (right)

terial Fluxofilcord 59 has a pouring structure with a significantly lower amount of carbide netting. A fine acicular martensitic structure with a combination of primary and secondary carbide accretion is mostly observed here.

The results obtained suggest that the relative wear resistance increases with increasing hardness of the materials tested in defined conditions. However, hardness is not always the decisive factor that affects the wear resistance at the most. An important factor of the wear resistance is also the microstructure of the concrete overlay.

CONCLUSION

The lifetime of agricultural machines is significantly affected by the lifetime of the functional parts of the working tools, which are constantly worn out during the operation e.g. skives, shares, under-slinging skives, seeding base, etc. Their wear and tear adversely affects the quality of the work performance and energy consumption of the machine (Kotus 2007).

Soil as the abrasive background causes an intensive wear and tear by its specific properties and therefore decreases the lifetime of the functional parts of agricultural machines. The application of suitable hardfacing materials on the working surfaces of tools prolongs their lifetime (Hrabě, Chotěborský 2005).

On the basis of the tests carried out, we can state the suitability of the use of selected filler materials, which are resistant in conditions of abrasive wear.

The abrasion resistant materials can be one of the possibilities for surfacing when the wear and tear reduction is to be achieved.

References

Balla J., 1989. Tribológia a tribotechnika (Tribology and Tribotechnics). Nitra, SUA in Nitra: 134.

ČSN EN ISO 4063, 2011. Svařování a příbuzné procesy – Přehled metod a jejich číslování (Welding and allied processes – Nomenclature of processes and reference numbers).

Hrabě, P., Chotěborský, R. 2005. Zvyšování životnosti abrazivně opotřebených strojních částí (Life Cycle Increasing of Abrasive Wear Machine Tools). MM Průmyslové spektrum, 5: 80–81.

Kotus M. 2007. Aplikácia pulzných zváracích zdrojov pri renovácií súčiastok poľnohospodárskych strojov (Application of Pulse Welding Aggregates in Machine Parts Renovation of Agricultural Machines). [Ph.D. Thesis.] Nitra, SUA in Nitra: 201.

Kotus, M. 2009. Tribologické skúšky oteruvzdorných materiálov (Tribological tests of abrasive resistant materials). In: Safety – Quality – Reliability. Košice, The Technical University of Košice: 103–107.

Kotus M., Drahoš Š., 2010. Stanovenie odolnosti proti abrazívnemu opotrebeniu v laboratórnych podmienkach (Determination of abrasive wear resistance in laboratory conditions). In: Quality and Reliability of Technical Systems. Nitra, SUA in Nitra.

STN 01 5084, 1973. Stanovenie odolnosti kovových materiálov proti abrazívnemu opotrebeniu na brúsnom plátne (Determination of metal material resistante against wear by abrasiva cloth).

STN 41 2014, 1993. Ocel 12 014 (Steel 12 014).

STN ISO 6507-1, 2006. Kovové materiály. Vickersova skúška tvrdosti. Časť 1: Skúšobná metóda (ISO 6507-1: 2005) [Metallic materials. Vickers hardness test. Part 1: Test method (ISO 6507-1:2005)].

Tolnai R., Čičo P., 2002. Výber oteruvzdorných materiálov pre špecifické podmienky degradačných procesov (Selection of abrasive wear materials for specific conditions of degradable processes). Acta Mechanica Slovaca, 6: 167–170.

Received for publication December 11, 2010
Accepted after corrections June 6, 2011

Corresponding author:

Ing. Martin Kotus, Ph.D., Slovak University of Agriculture, Faculty of Engineering,
Department of Quality and Engineering Technologies, Tr. A. Hlinku 2, 949 76 Nitra, Slovak Republic.
phone: + 421 376 415 696, e-mail: martin.kotus@uniag.sk

The journal publishes results of basic and applied research from all fields of agricultural engineering. Original scientific papers, short communications, review articles, and selectively book reviews from the disciplines concerned are published in the journal. Papers are published in English (British spelling). The author is fully responsible for the originality of the paper and formal correctness. The paper and its content must not be published previously elsewhere. The Board of Editors decides on the publication of papers, taking into account scientific importance, peer reviews and manuscript originality, quality and length. Standard size of paper (A4 format), type size 12 font, double-space lines, 2.5 cm margins on each edge of the page. **Scientific papers** and **review articles** shall not be longer than 20 standard pages, including tables and figures. **Short communications** should not be longer than 6 standard pages and book reviews should not be longer than 3 standard pages. Manuscripts must be submitted in MS Word text editor to the electronic editorial system (http://www.agriculturejournals.cz/web/rae.htm).

Tables should be placed at the end of the manuscript. Word editor should be used to create tables; each item should be placed into a separate cell. Tables are to be numbered with Arabic numerals in the order in which they are referred to in the text. **Figures**. Figure captions should be placed after the tables. Autotypes should be submitted in TIFF or JPG format in minimal resolution 300 dpi. Graphs should be provided in MS Excel and they should be stored with original data. All graphs and photos should be numbered, continually according to the order in which they are included in the text, using Arabic numerals. **Abbreviations and units**. If any abbreviations are used in a paper, they shall be explained appropriately when they are used in the text for the first time. It is not advisable to use any abbreviations in the paper title or in the abstract. The SI international system of measurement units should be used.

Title page must contain title of paper, complete name(s) of the author(s), the name(s) and address(es) of the institution(s) where the work was done.

Abstract is a short summary of the whole paper (as a single paragraph). It should describe all essential facts of a scientific paper. The abstract should not go to more than 170 words. The abstract is an important part of the paper because it is published and cited in world databases. No references are to be cited. **Keywords** (recommendation 5 words) should be different from words mentioned in the title.

Introduction should outline the main reasons why the research was conducted; describe a brief review of literature consisting of refereed periodicals, journals and books, and the goal of the authors.

Material and Methods. All preliminary material, experiments conducted, their extent, conditions and course should be described in detail in this section. All original procedures that were used for the processing of experimental material and all analytical methods used for evaluation should also be detailed. Data verifying the quality of acquired data should be indicated for the used methods. The whole methodology is only to be described if it is an original one; in other cases it is sufficient to cite the author of the method and to mention any particular differences. Methods of statistical processing including the software used should also be listed in this section.

Results and Discussion. More than one-year results should be published in the paper. The results obtained from the experiments including their statistical evaluation and any commentary should be presented graphically or in tables in this section. Each phenomenon should be commented and explained, using scientific arguments. The author should confront partial results with data published by other authors, whose names and year of publication are to be cited by including them in the text directly, e.g. ... as published by Lowe (1981), Novák and Šídlo (2002) found ..., or citing authors and years of publication in parenthesis (Lowe 1981; Novák, Šídlo 2002; Jakl et al. 2003).

References should be preferably a list of refereed periodicals arranged in alphabetical order according to the surname of the first authors. The surnames and initials of all authors should be followed by the year of publication cited, the original title of the paper (if the cited source is not in English, it should be translated in brackets behind of the original title), the name of the periodical, the relevant volume and page number, in the case of a book or proceedings the title should be followed by the name of the publisher and the place of publication. Names of authors should be separated by commas, not by & or and.

Examples of references in the list:

Journal article: Carter C., Finley W., Fry J., Jackson D., Willis L., 2007. Palm oil market and future supply. European Journal of Lipid Science and Technology, *109*: 307–314.

Monographs: Tullock J., 2005. Growing Hardy Orchids. Portland, Timber Press: 244.

Papers published in collections and proceedings: Lu C., Chandler S.F., 1995. Genetic transformation of *Dianthus caryophyllus*. In: Bajaj Y.P.S. (ed.), Biotechnology in Agriculture and Forestry. Berlin, Heidelberg, Springer-Verlag: 156–170.

Steele W.K., 1996. Large scale production of North American *Cypripedium species*. In: Allen C. (ed.), Proceedings North American Native Terrestrial Orchids Propagation and Production, March 16–17, 1996. Washington: 11–26.

Dissertation: Šimek P., 2001. Hodnocení dřevin a jejich porostů pro pěstební účely v zahradní tvorbě (Evaluating Woody Species and their Communities for Gardening and Landscaping). [Ph.D. Thesis.] Brno, Mendel University in Brno: 1–159.

Internet publications: Weinert M., 2008. International *Cypripedium* forum. Available at: www.cypripedium.de (accessed December 23, 2009).

Contact address should include the postal address, telephone and fax numbers, and e-mail of the corresponding author in English.

Proof-sheets will be sent to the corresponding author by e-mail. Your response, with or without corrections, should be sent within 72 hours.

Offprints: Corresponding author will receive a free "electronic reprint" in Portable Document Format (PDF).

Compliance with these instructions is obligatory for all authors. If a manuscript does not comply with the above requirements, the editorial office will not accept it for a consideration and will return it to the authors without reviewing.

Research in **AGRICULTURAL ENGINEERING**

Volume 57 **2011**

Research in AGRICULTURAL ENGINEERING • Published by the Czech Academy of Agricultural Sciences • Editorial Office: Slezská 7, 120 00 Prague 2, Czech Republic, phone: + 420 227 010 606, fax: + 420 227 010 116, e-mail: rae@cazv.cz •
Distribution: Czech Academy of Agricultural Sciences, Slezská 7, 120 00 Prague 2, Czech Republic, phone: + 420 227 010 427, fax: + 420 227 010 116, e-mail: redakce@cazv.cz